Biological Sciences: Biochemistry, Neuroscience

Na, K-ATPase α3 Is a Death Target of Alzheimer Patient Amyloid-β Assembly

Takayuki Ohnishi[a,b1], Masako Yanazawa[c1], Tomoya Sasahara[a,b], Yasuki Kitamura[c], Hidekazu Hiroaki[d], Yugo Fukazawa[e], Isao Kii[f], Takashi Nishiyama[a,f], Akiyoshi Kakita[g], Hiroyuki Takeda[h], Akihide Takeuchi[f], Yoshie Arai[a,b], Akane Ito[c,2], Hitomi Komura[a,b], Hajime Hirao[i], Kaori Satomura[a,b], Masafumi Inoue[a,b], Shin-ichi Muramatsu[j], Ko Matsui[k], Mari Tada[g], Michio Sato[c,3], Eri Saijo[a,b], Yoshiki Shigemitsu[d], Satoko Sakai[a,b], Yoshitaka Umetsu[d], Natsuko Goda[d], Naomi Takino[b], Hitoshi Takahashi[g], Masatoshi Hagiwara[f], Tatsuya Sawasaki[h], Genji Iwasaki[l], Yu Nakamura[m], Yo-ichi Nabeshima[a], David B. Teplow[n], and Minako Hoshi[a,c,f,4]

[a]Institute of Biomedical Research and Innovation, Foundation for Biomedical Research and Innovation (FBRI), Kobe 650-0047, Japan; [b]TAO Health Life Pharma Co., Ltd. (TAO), Medical Innovation Center in Kyoto University, Kyoto 606-8507, Japan; [c]Mitsubishi Kagaku Institute of Life Sciences (MITILS; dissolved in March 2010); [d]Department of Basic Medicinal Sciences, Graduate School of Pharmaceutical Sciences, Nagoya University, Nagoya 464-8601, Japan;

[e]Department of Histological and Physiological Sciences, Faculty of Medical Science, University of Fukui, Yoshida 910-1193, Japan; [f]Department of Anatomy and Developmental Biology, Graduate School of Medicine, Kyoto University, Kyoto 606-8501, Japan; [g]Department of Pathology, Brain Research Institute, Niigata University, Niigata 951-8585, Japan; [h]Proteo-Science Center, Ehime University, Matsuyama 790-8577, Japan; [i]School of Physical and Mathematical Sciences, Nanyang Technological University, Singapore 637371; [j]Department of Medicine, Jichi Medical University, Shimotsuke 329-0498, Japan; [k]Division of Interdisciplinary Medical Science, Graduate School of Medicine, Tohoku University, Sendai 980-8575, Japan; [l]Faculty of Pharmacy, Takasaki University of Health and Welfare, Takasaki 370-0033, Japan; [m]Department of Neuropsychiatry, Faculty of Medicine, Kagawa University, Kagawa 761-0793, Japan; [n]Department of Neurology, David Geffen School of Medicine, University of California, Los Angeles, CA 90095

[1]T.O. and M.Y. equally contributed to this work.

[2]Present address: Institute of Industrial Science, University of Tokyo, Tokyo 153-8505, Japan.

[3]Present address: Graduate School of Agriculture, Meiji University, Kawasaki 214-8571, Japan.

[4]To whom correspondence should be addressed.

E-mail: hoshi.minako.8w@kyoto-u.ac.jp

Keywords: NMR; computational modeling; abnormal protein-protein interaction in synapse; hyperexcitotoxicity; protein-protein interaction inhibitors

Short title: NAKα3 Is An Alzheimer Neuron Death Target

Abstract

Neurodegeneration correlates with Alzheimer's disease (AD) symptoms, but the molecular identities of pathogenic amyloid β-protein (Aβ) oligomers and their targets leading to neurodegeneration remain unclear. Amylospheroids (ASPD) are AD patient-derived 10-to 15-nm spherical Aβ oligomers that cause selective degeneration of mature neurons. Here, we show that the ASPD target is neuron-specific Na^+/K^+-ATPase α3 subunit (NAKα3). ASPD-binding to NAKα3 impaired NAKα3-specific activity, activated N-type voltage-gated calcium channels, and caused mitochondrial calcium dyshomeostasis, tau abnormalities, and neurodegeneration. NMR and molecular modeling studies suggested that spherical ASPD contain N-terminal-Aβ-derived "thorns" responsible for target binding, which are distinct from low-molecular-weight oligomers and dodecamers. The fourth extracellular loop (Ex4) region of NAKα3 encompassing Asn^{879} and Trp^{880} is essential for ASPD-NAKα3 interaction, because tetrapeptides mimicking this Ex4 region bound to the ASPD surface and blocked ASPD neurotoxicity. Our findings open up new possibilities for knowledge-based design of peptidomimetics that inhibit neurodegeneration in AD by blocking aberrant ASPD-NAKα3 interaction.

Significance statement (up to 120 words understandable for undergraduates)

Alzheimer's disease (AD) involves neuron dysfunction and loss. This brain damage is thought to be caused by a small protein, the amyloid β-protein (Aβ), which forms aggregates that are neurotoxic. This neurotoxicity has been explained by multiple mechanisms. We reveal here a new neurotoxic mechanism that involves the interaction between patient-derived Aβ assemblies termed amylospheroids, and the neuron-specific Na^+/K^+-ATPase α3 subunit. This interaction causes neurodegeneration through pre-synaptic calcium overload, which explains earlier observations that such neuronal hyperactivation is an early indicator of AD-related neurodegeneration. Importantly, amylospheroid concentrations correlate with disease severity and progression in AD patients. Amylospheroid:neuron-specific Na^+/K^+-ATPase α3 subunit interactions may be a useful therapeutic target for AD.

¥body

Alzheimer's disease (AD) brains characteristically display fibrillar and non-fibrillar (oligomeric) protein assemblies composed of the amyloid β-protein (Aβ)(1-6). Aβ has been shown to bind to postsynaptic receptors, such as α7-nicotinic acetylcholine receptor (α7nAChR)(7), receptor for advanced glycation end products (RAGE)(8), receptor tyrosine kinase EPHB2 (9), and cellular prion protein PrP^C (10). These 'Aβ receptors', except for RAGE, have been reported to mediate toxicity of Aβ oligomers through modulating NMDA receptors (NMDAR)(11). Aβ oligomers, including dimers from AD brains (12, 13), dodecamers (Aβ*56) from AD model mice (14), or *in vitro*-generated Aβ-derived diffusible ligands (ADDLs)(15, 16), induce synaptic impairment by affecting NMDAR (11). Thus, NMDAR are a common target for synaptic impairment in AD. However, these oligomers do not cause neuronal death (12, 14). The atomic resolution structures of neurotoxic Aβ oligomers and their *in vivo* targets leading to neuronal death in AD remain unclear (6), even though neuronal death is the central mechanism responsible for symptomatic onset in AD (17).

We previously isolated neurotoxic Aβ oligomers, termed amylospheroids (ASPD), from the brains of AD patient (18-20). ASPD appear in transmission electron microscopic (TEM) images as spheres of diameter ~11.9 ± 1.7 nm (19). ASPD appear to be unique Aβ assemblies, as

determined immunochemically. These structures are recognized strongly by ASPD-specific antibodies (K_d ~pM range), but not with the oligomer-specific polyclonal antiserum A11 (19). ASPD are distinct from Aβ dimers, ADDLs, dodecamers, and other A11-reactive entities (19).

ASPD cause severe degeneration of mature human neurons (19). ASPD levels in the cortices of AD patients correlate well with disease severity (19). In contrast, ASPD-like oligomers were minimally detectable in the brains of transgenic mice expressing human amyloid precursor protein (*APP)*, in which no significant neuronal loss is observed (19). These findings suggest that ASPD are an important effector of neuronal death in AD patients. We sought to elucidate mechanisms of ASPD-induced neurotoxicity. We report here that ASPD interact with the α– subunit of neuron-specific Na^+/K^+-ATPase (NAKα3), resulting in presynaptic calcium overload and neuronal death.

Results

ASPD Bind To NAKα3 In Mature Neurons. ASPD caused degeneration of mature rat hippocampal neurons, but not immature neurons or nonneuronal HEK293 (Fig. 1*A*). ASPD toxicity required binding to mature neurons, because ASPD-specific mouse monoclonal

amylospheroid (mASD)3 antibody blocked binding and toxicity of ASPD (Fig. 1 *A* and *B*). [The K_d for ASPD binding = 5.43 ± 0.27 nM (n = 3; Fig. 1*C*). ASPD concentration was determined using an average ASPD molecular weight of 128 kDa (20). See summary of the characteristics of patient and synthetic ASPD in Table S1. See also *SI* Discussion for updated definition of ASPD.] Blockers of known Aβ receptors (21), including glutamate receptors (NMDA, non-NMDA, and metabotropic types) and voltage-gated sodium channels, did not affect ASPD neurotoxicity (Fig. S1). These findings suggested ASPD exert their toxicity through binding to novel cell-surface molecules specific to mature neurons.

To identify ASPD-binding proteins on mature neurons, Far-Western ligand-binding assays were performed in physiological medium. We used ASPD isolated (19) from the soluble brain extracts of the two AD patients displaying the most severe neurodegeneration and the highest ASPD concentrations among those shown in Fig. 2*A* (Fig. 2*B*). These ASPD were A11-negative (Fig. 2*C*), composed predominantly of $A\beta_{1-42}$ and $A\beta_{1-40}$ (Fig. 2*B* and *D*), had molecular masses of 123 ± 20 kDa (Fig. 2*E*), and appeared as ~11.7 ± 1.6 nm spheres (n = 49) in TEM (Fig. 2*C*), consistent with previous data (18-20). We also used *in vitro*-reconstituted synthetic ASPD, which shares essential characteristics with patient ASPD (19)(Table S1), as an analogue.

Binding of ASPD was detected with ASPD-specific hamster monoclonal (haASD)1 antibody (K_d for ASPD ~0.5 pM (19)). ASPD bound to a 105-kDa band in extracts from mature neurons cultured for 21 days *in vitro* (DIV) (red arrow in Fig. 3*A* Center), but not immature 2 DIV neurons or HEK293 cells. This band was also recognized by synthetic ASPD (Fig. S2*A*, red arrow on the left), indicating that ASPD bind directly to this band, because purified synthetic ASPD contained no protein other than ASPD (19). This band was not detected when we used haASD1 alone or synthetic ASPD presaturated with haASD1 (Fig. S2*B*). Unlike ASPD, freshly dissolved $A\beta_{1\text{-}42}$, which consisted of monomers, dimers, and other low-molecular-weight (LMW) oligomers, did not bind to the 105-kDa band, but bound to 55-kDa and 45-kDa bands, likely corresponding to 54.2 kDa α7nAChR and 40.4 kDa RAGE, respectively (Fig. 3*A,* Left). These findings showed that the 105-kDa band corresponds to ASPD-specific binding proteins present only in mature neurons.

MS and MS/MS analyses of the 105-kDa band (red arrow in Fig. S2*A* Right) identified various NAKα-derived peptides (Table S2). We confirmed that NAKα appeared at 105 kDa (Fig. 3*A,* right). ASPD-binding bands from immature neurons or HEK293 (* in Fig. 3*A* middle and

Fig. S2*A* left) were identified as intracellular proteins (see Fig. S2*A* legend). Thus, NAKα, which has a molecular mass of 112-113 kDa, is likely to be the 105-kDa band entity.

NAKα is an essential catalytic subunit of the NAK pump (Fig. 3*B*), which is responsible for keeping the neuron resting membrane potential at about -70 mV (22). The functional NAK pump also requires β subunit (22)(Fig. 3*B*). In adult brains, NAKα1 is ubiquitously expressed, whereas NAKα3 is expressed exclusively in neurons, and NAKα2 is found in astrocytes (22). We found that NAKα3 was abundant in extracts of mature neurons only (Fig. 3*C*). Western blotting showed that NAKα3 became detectable at 7 DIV and that its levels continued to increase until 21 DIV in our culture (Fig. S2*C*). This developmental increase in NAKα3 level correlated well with that of the 105-kDa band in Far-Western blotting using synthetic ASPD (Fig. S2*B*). To establish whether NAKα3 is the sole ASPD-binding isoform, we performed co-immunoprecipitation experiments. First, NAKα3 in mature neuron extracts was co-immunoprecipitated directly with purified synthetic ASPD using haASD1 antibody (Fig. 3*D*). Second, biotin-labelled ASPD were incubated with mature hippocampal neurons, and MS/MS analysis confirmed that the NAKα3 isoform was selectively co-immunoprecipitated as the 105-kDa band with biotin-labelled ASPD (red arrows in Fig. S2*D*). We then confirmed that

ASPD and NAKα3 were essentially co-localized within the neuropil of mature hippocampal neurons double-stained for synthetic ASPD and NAKα3 (*Inset* in Fig. 3*E* left). Furthermore, surface plasmon resonance spectroscopy (SPR) demonstrated that rat NAKα3 directly bound to synthetic ASPD (K_d = 7.8 ± 2.5 nM, n=3, Fig. 3*F*). The K_d value obtained from this SPR data was almost identical with that obtained from ASPD-binding to mature neurons (Fig. 1*C*, K_d = 5.43 ± 0.27 nM as described above). We confirmed that human and mouse NAKα3 bound directly to synthetic ASPD using SPR (human K_d = 28.6 ± 6.6 nM, n=5; mouse K_d = 4.0 ± 1.9 nM, n=3). Notably, most mature hippocampal neurons were stained for NAKα3, whereas most mature cerebellar neurons were NAKα3-immunonegative (Fig. S2*E*). This finding was consistent with Western blotting showing that the amount of membrane NAKα3 in cerebellar neurons was only ~20% of that in hippocampal neurons (Fig. 3*G* left). Synthetic ASPD bound to NAKα3-immunopositive neurons among hippocampal or cerebellar neurons (Fig. 3*E*) and induced death in those neurons at levels correlating with their membrane NAKα3 amount (Fig. 3*G*). Stable knockout of NAKα3 expression with microRNA (miR)-expressing virus vector decreased NAKα3-expressing neurons to 19.8 ± 14% (n = 3; $p < 0.0001$ compared with the untreated neurons using Scheffé's *post-hoc* test, n = 3) in hippocampal neurons and abolished

ASPD-binding and ASPD-induced neurodegeneration (Fig. 3*H*). These data support the conclusion that NAKα3 is the mature neuron-specific ASPD-binding protein that is linked to ASPD neurotoxicity.

ASPD Impair NAKα3 Activity, Leading To Ca^{2+} Dyshomeostasis And Neuron Death. We next examined the effect of ASPD-binding on NAKα3 activity. As shown in Fig. 4*A*, exposure of membrane preparations from mature hippocampal neurons to 110 nM synthetic ASPD rapidly (~70% in 1 hr) impaired NAKα3-specific activity in those membrane preparations. Overnight treatment of intact mature hippocampal neurons with 140 nM synthetic ASPD caused a >90% decrease in NAKα3-specific activity (Fig. 4*B*).

This NAKα3 impairment should cause a failure in active transport of Na^+ and K^+ ions (Fig. 3*B*). Indeed, we found that cytoplasmic Na^+ levels were increased immediately after exposure of neurons to synthetic ASPD (at the orange arrow in Fig. S3*A*), which reached a maximum after ~18 min (at the yellow arrow in Fig. S3A_3 and A_4; see legends). ASPD-induced impairment of NAKα3 activity thus increased cytoplasmic Na^+ levels and likely induced depolarization in the treated neurons.

This process would lead to an increase in intracellular Ca^{2+} level ($[Ca^{2+}]_i$) through the plasma membrane Na^+/Ca^{2+} exchanger (NCX) or voltage-gated Ca^{2+} channels (VGCC) activated by depolarization (22). We therefore monitored $[Ca^{2+}]_i$ using Fura-PE3AM staining. Vehicle treatments did not affect $[Ca^{2+}]_i$ for at least 2 hrs (Fig. 4*C1* and Fig. S3B_1), but ASPD increased the number of Ca^{2+}-responsive cells dose-dependently (Fig. 4*C2* and Fig. S3B_2~B_4), with a plateau at ~40 nM synthetic ASPD (Fig. 4*D*). The dose-dependent effect of ASPD on the number of Ca^{2+}-responsive cells correlated well with the level of ASPD-binding (Fig. 1*C* left), as well as that of ASPD neurotoxicity (EC_{50} =18 ± 2.4 nM, n = 5), suggesting that ASPD-binding to mature neurons caused increased $[Ca^{2+}]_i$, leading to eventual neuronal death.

Depending on the ASPD concentration, two types of Ca^{2+}-responses were observed (*SI* Discussion for a plausible mechanistic explanation). With 18 nM ASPD, repetitive Ca^{2+} spikes were observed ≈3 min after the treatment (Fig. S3B_2). In this case, $[Ca^{2+}]_i$ increased gradually and led to a sustained increase after 2 hrs (e.g. Fig. S3C_1). With higher concentrations of ASPD (e.g., 42 nM in Fig. 4*C2*), $[Ca^{2+}]_i$ increased ~2 min after the treatment, maintained a sustained increase during 0-40 min, and then rose precipitously before plateauing at ~40-70 min. Much higher concentrations of ASPD accelerated the process, with $[Ca^{2+}]_i$ plateauing earlier (within 1

h; compare 88 nM synthetic ASPD in Fig. S3*B*$_4$ with 42 nM synthetic ASPD in Fig. S3*B*$_3$). Unlike ASPD, 1.4 μM 20-30-nm A$\beta_{1\text{-}42}$ aggregates (TEM in Fig. 4*E*), which were obtained by making a 20-fold concentration and then a 10-fold re-dilution of ASPD (*SI Materials and Methods, Preparation of 20- to 30-nm Aβ aggregates*), were rarely detected by ASPD-specific rabbit polyclonal (rpASD)1 antibody in dot blotting (Fig. 4*E*) and did not cause such a persistent increase in $[Ca^{2+}]_i$ (Fig. 4*C3*), and the neurons remained intact (inset bright-field images in Fig. 4*C3*).

This ASPD-induced increase in $[Ca^{2+}]_i$ required extracellular Ca^{2+}, because it was blocked by addition of EGTA to the medium (Fig. S3*C*$_2$). Furthermore, blockade of $[Ca^{2+}]_i$ overload by chelation with BAPTA-AM suppressed ASPD toxicity (Fig. 5*A*). We then asked which plasma membrane calcium conductors, VGCC or NCX, were involved in ASPD toxicity. Inhibitor effects on ASPD neurotoxicity showed that N-type VGCC were involved in ASPD-induced neuronal death, whereas the other VGCC subtypes and NCX were not involved (Fig. 5*A*). We confirmed that an inhibitor specific to N-type VGCC blocked ASPD-induced $[Ca^{2+}]_i$ increase (Fig. S3*D*$_3$). Notably, N-type VGCC are found primarily at pre-synaptic terminals of neurons (23), consistent with pre-synaptic binding of ASPD (19).

Next, we examined whether the two major intracellular Ca^{2+} stores, mitochondria and endoplasmic reticulum (ER), could be involved in ASPD neurotoxicity. A mitochondrial NCX inhibitor and an inhibitor of mitochondrial permeability transition (MPT) pore opening both blocked ASPD-induced apoptosis, whereas an inhibitor of Ca^{2+} influx in ER (mediated by a Ca^{2+} sensor, STIM1), an IP3 receptor antagonist, or a ryanodine receptor (RyR) antagonist, failed to block ASPD neurotoxicity (Fig. 5*A*). Thus, Ca^{2+} dyshomeostasis in mitochondria was involved in ASPD neurotoxicity, but ER Ca^{2+} stores were not (Fig. 5 *A* and *B*). We found that treatment with both CGP37157 (a mitochondrial NCX inhibitor) and cyclosporin A (an inhibitor of mitochondrial MPT pore opening) inhibited the ASPD-induced sharp $[Ca^{2+}]_i$ increase that followed the initial sustained increase in $[Ca^{2+}]_i$ more strongly than the single treatments (Fig. S3*E*). This finding suggests that mitochondrial NCX and MPT pore opening are both involved in Ca^{2+} release from mitochondria that is linked to ASPD neurotoxicity (see the legend of Fig. S3*E* for more details).

These findings indicate that impairment of NAKα3 activity by ASPD binding increases cytoplasmic Na^+ levels (Fig. S3*A*), activates N-type VGCC, and causes continuous Ca^{2+} influx into cytoplasm. This in turn results in Ca^{2+} overload in mitochondria (observed as the sustained

1 $[Ca^{2+}]_i$ increase) and subsequent Ca^{2+} release from mitochondria through mitochondrial NCX
2 and MPT pore opening (observed as the sharp increase $[Ca^{2+}]_i$), which results in the eventual
3 death of neurons.

4 Previously we have shown involvement of tau protein kinase I/glycogen synthase kinase-3β
5 (TPKI/GSK3β) in ASPD neurotoxicity (18). We also found that tau protein kinase
6 II/cyclin-dependent protein kinase 5 (TPKII/CDK5) was activated after ASPD treatment (Fig. 5
7 *C* and *D*) and tau phosphorylation increased at Ser^{396} and Ser^{404}, which are known to be
8 phosphorylated in AD brains by TPKI/GSK3β/TPKII/CDK5 and TPKII/CDK5, respectively
9 (24)(Fig. 5*E*). Furthermore, tau and microtubule-associated protein 2 (MAP2) were rapidly lost
10 after ASPD treatment (Fig. 5*F*). Tau phosphorylation and loss, together with MAP2 loss, could
11 destabilize microtubules and promote neurodegeneration.

12 Next, time-lapse DIC images of mature neurons after ASPD treatment were taken. Because
13 of osmotic imbalance, neurons started swelling at ~30 min after exposure to 140 nM synthetic
14 ASPD, and cell shrinkage, a ubiquitous feature of apoptosis (25), took place in ~3-5 h (Video S1,
15 Fig. 6*A* and S4*A*). Subsequently, DNA fragmentation became detectable after 5 h (Fig. 6*B*).
16 Scanning electron microscopic (SEM) images clearly showed ASPD-induced neuronal swelling

and shrinkage (Fig. 6*C*). The video showed that the surface of the ASPD-treated neurons became rough within 30 min after the ASPD treatment (Video S1) and holes appeared within 1 h (see arrows in Fig. 6*C*). Similar swelling and shrinkage of neurons were induced by 100 nM ouabain (Video S2, Fig. 6*A* and S4*A*), which selectively blocks rodent NAKα3 activity (26). Unlike ASPD and ouabain, staurosporine, an apoptosis inducer that inhibits multiple kinases, induced shrinkage but not swelling (Video S3, Fig. 6*A* and S4*A*). Vehicle treatment induced neither swelling nor shrinkage (Video S4, Fig. 6*A* and S4*A*). Ouabain also elicited the events triggered by ASPD (summarized in Fig. 5*B*; Fig. S3*F*). Our data are consistent with the conclusion that NAKα3 is a death target for ASPD toxicity. We summarize a possible ASPD-induced sequence of events leading to neuronal death in Fig. 6*A*.

We next examined NAKα3 localization in human brains. In non-clinically demented individual (NCI) cerebrum, punctate staining by anti-NAKα3 antibody surrounded the cell body of pyramidal neurons (arrows in Fig. 6*D* upper left) and diffuse staining was detected on axons and in neuropils. Intense staining was found in basket cells surrounding Purkinje cells in NCI cerebellum (arrows in Fig. 6*D* lower left). NAKα3 localization was consistent with that in adult mouse brain (27).

We found that NAKα3 staining was essentially lost in AD cerebrum, whereas it was not decreased in AD cerebellum (Fig. 6*D* right). Quantitative dot blotting with an ASPD-specific antibody, rpASD1, showed patient ASPD levels in NCI cerebrum, AD cerebrum, and AD cerebellum of 0.7 ± 0.4, 55.7 ± 7.0, and 0.7 ± 0.7 pmol/mg soluble brain extracts, respectively (a representative blot in Fig. 6*D*), suggesting that decreased NAKα3 staining correlated with patient ASPD levels in AD brains. Comparison of quantitative dot blotting results with rpASD1 those with and anti-Aβ antibody 82E1 indicated that patient ASPD accounted for 62 ± 3 % (n =3) of soluble Aβ. Unlike decreased NAKα3 staining, anti-NAKα1 antibody showed diffuse staining throughout NCI and AD cerebrum (Fig. S4*B*). Results of *in situ* hybridization (ISH) of adjacent sections of the same AD or NCI cases with NAKα3 mRNA (*ATP1A3*) or NAKα1 mRNA (*ATP1A1*)(n=3 each) showed the same correlation with the histological data (compare Figs. 6*E* and S4*C* with Figs. 6*D* and S4*B*). With NAKα3 ISH, the signal intensity of *ATP1A3* was clearly lower in layers of pyramidal neurons in the hippocampus in AD compared with that observed in NCI. No obvious differences were detected in the cerebellum between AD and NCI. With NAKα1 ISH, the signal intensity of *ATP1A1* was not changed in both regions between AD and NCI cases. These results are consistent with a previous quantitative ISH study on AD

patients (28) and suggest NAKα3-expressing neurons are preferentially lost in AD-susceptible brain regions where ASPD concentrations are high.

Structural Characteristics of ASPD And Their Target, Ex4 of NAKα3. To examine structural features of ASPD relevant to binding with NAKα3, we acquired solution NMR spectra of ^{15}N-labelled ASPD. Although we detected 39 heteronuclear single quantum coherence (HSQC) signals in the case of freshly dissolved Aβ, we detected 14 of 39 HSQC signals representing peptide backbones of Aβ in ASPD, and these were nearly superimposable on the signals of the $A\beta_{1-13}$, $A\beta_{15-16}$, and $A\beta_{23}$ regions of monomer (Fig. 7*A*). Remaining NMR-invisible amino acids presumably form a magnetically nonequivalent core. In other words, the NMR-visible amino acids, although derived from different Aβ regions, may exist in close proximity to form the ASPD surface (Fig. 7*B*), in accordance with our finding that specific binding of monoclonal mASD3 antibody to ASPD was blocked by pentapeptides covering $A\beta_{2-8}$, $A\beta_{15-19}$, or $A\beta_{19-23}$ (19). Since mASD3 antibody neutralizes ASPD toxicity (19), the NMR-identified ASPD surface is likely involved in binding to NAKα3. The HSQC spectra of ASPD were different from those of precursors of synaptotoxic dodecamers (termed

globulomer)(29) and of LMW oligomers (30). Thus, ASPD appear to be structurally distinct from pre-globulomers and LMW oligomers. This finding is consistent with our finding that ASPD are immunologically distinct from synaptotoxic oligomers (19). We obtained the same HSQC spectra of ASPD in all experiments (n = 3), suggesting that there is one defined structure that is dominant within the ASPD sample. Taken together with our previous immunological data using ASPD-specific antibodies (details in Table S1), this finding supports the notion that ASPD consist of closely related structures. Our recent analysis of ASPD structure using solid-state NMR also supports the notion (31).

The above findings suggest that the unique ASPD surface has a key role in ASPD-NAKα3 interaction. Because protein-protein interaction inhibitors can be designed based on the protein surface region essential for binding, we sought to determine which extracellular region of NAKα3 serves as the ASPD target site. NAKα1 and NAKα3 share 96% sequence identity. Given ASPD's preferential binding to NAKα3, the NAKα3-specific region, either the first extracellular loop (Ex1) or the fourth extracellular loop (Ex4)(Figs. 3*B* and 7*C*), would be the key ASPD target. We found that a chemically synthesized octapeptide from Ex4 (RLNWDDRT) significantly blocked ASPD toxicity, whereas Ex1 peptides neither bound to ASPD, as

determined by SPR (Fig. S5*A*), nor blocked ASPD toxicity (Fig. 7*D*). Scrambled Ex4 peptides failed to block ASPD toxicity (Fig. 7*D*). We confirmed that Ex4 interfered with binding of both patient ASPD and synthetic ASPD to mature hippocampal neurons (Figs. 7*E* and S5*B*), in addition to blocking the subsequent $[Ca^{2+}]_i$ increases (Fig. S3*D4*) and activation of the kinases (Fig. S5*C*). Notably, with 15-min patient ASPD treatment, neurites began to degenerate (Fig. 7*E*, arrowheads). This degeneration was almost completely blocked by Ex4 (Fig. 7*E*). These findings suggest that Ex4 is the main ASPD target site (pink in Fig. 7*C*).

We then planned to develop ASPD-binding peptides with toxicity-neutralizing activity by utilizing phage display (PD) analysis. Three independent screenings of a randomized 12-mer peptide library detected ~21 kinds of ASPD-binding peptides with high His and Trp contents. Among them, many showed similarity to Ex4 of NAKα3. Chemically synthesized PD-identified dodecapeptides (PD2, 50, 68) bound to ASPD (K_d = 5.8-8.9 x 10^{-8} M by SPR). These dodecapeptides, which commonly contain a four-amino-acid sequence (H*NW) similar to Ex4 (RLNW; corresponding to positions 877-880), inhibited ASPD toxicity towards mature neurons as effectively as the Ex4-derived peptide, whereas other peptides containing H**W (lacking NAKα3-specific Asn) were ineffective (Fig. 7*F*). Notably, ASPD-binding tetrapeptide PD2-11

(HFNW) was enough to significantly block binding and neurotoxicity of ASPD (Fig. 7*F* and Fig. S5*B*). These findings suggest that the NAKα3-specific region in Ex4 encompassing residues Asn^{879} and Trp^{880} is essential for ASPD-NAKα3 interaction (Fig. 7 *C* and *G*).

We built a 3D homology model of human NAKα3 based on the pig NAKα1 structure (32), as no crystal structure of human NAKα3 is available. Ex4 appeared to form a cavity and Asn^{879} and Trp^{880} are exposed on the NAKα3 surface, to which ASPD can gain access (Fig. 7*C*). Molecular modeling suggested that the mature NAK pump has a 9.9-nm-wide opening (Fig. S6). Solution atomic force microscopy showed that ASPD are 7.2 ± 2.6 nm in height (20). The maximum number concentration of bound ASPD, calculated from B_{max}, was 14 ± 0.7 pmol of ASPD per milligram of membrane protein (Fig. 1*C*). This concentration was 40% of the concentration of NAKα3 (35.2 ± 10 pmol/mg membrane protein; n=4) that we measured (as shown in Fig. 3*G* using pre-quantified, cell-free synthesized NAKα3 as the quantification standard; for details see *SI* Materials and Methods) and it was ~37-88% of the concentrations found in the literature (16-38 pmol/mg membrane protein)(33, 34). Simple arithmetic calculations thus give an ASPD:NAKα3 ratio ranging from 1:1 to 1:3. However, since past studies have shown that the NAK pump exists predominantly as $(NAK\alpha3)_2$:$(NAK\beta1)_2$ heterotetramer in membranes (35, 36)

and ASPD appeared to bind almost all NAKα3-containing NAK pump in membranes (Fig. 3*E*), we infer, using Occam's razor (37), that the most likely ratio is 1:2, (i.e., 1:1 binding of ASPD with NAKα3 dimer). This inference is consistent with other ASPD binding data (Fig. S6). Because the tetrapeptide segment in Ex4 of NAKα3 is conserved in rodents and humans (Fig. 7*G*), this opens up possibilities for knowledge-based design of inhibitors of neuronal death in AD.

Discussion

Past studies have reported the loss of the NAK pump activity, and the protein itself, in the brains of AD patients (28, 38, 39). In particular, NAKα3 expression, but not NAKα1 expression, is reduced in the frontal cortices of AD patients and this reduction correlates inversely with levels of diffuse plaques in that region (28). No such reduction is observed in the unaffected cerebellum of the same patients (28). NAKα3 activity was reported to decrease in $A\beta_{1\text{-}40}$-treated neuronal cultures (40) and the NAK pump activity was reported to decrease in 17- to 18-mo-old *APP* and *presenilin-1* transgenic mice (41). These previous observations suggest a potential link between Aβ and NAKα3 impairment. However, until now, the question of whether NAKα3 impairment

is the cause or the result of neuronal death has remained unanswered. We present here direct evidence that the neuron-specific α subunit of the NAK pump, NAKα3, is the neuronal death-inducing target of ASPD.

SPR data demonstrated direct binding of ASPD to NAKα3 (Fig. 3*F*). ASPD-binding to NAKα3 impaired rapidly NAKα3-specific NAK pump activity (Fig. 4*A*). Cytoplasmic Ca^{2+} overload was highly correlated with ASPD-binding (compare Figs. 1*C* and 4*D*), which eventually led to mitochondrial defects and neuronal death (Fig. 5*A*), as observed in AD (42). Stable knockout of NAKα3 expression with a microRNA-expressing virus vector decreased NAKα3-expressing neurons and abolished ASPD-binding and ASPD-induced neurodegeneration (Fig. 3*H*). ASPD binding peptides inhibited the ASPD binding to NAKα3 and protected mature neurons from ASPD neurotoxicity (Figs. 7*D-F*, S3*D*$_4$, S5*B*, and S5*C*). In addition to these cell-based data, we found that NAKα3-expressing neurons were lost in AD-susceptible regions such as the cortex and the hippocampus in patients (where ASPD levels were high), but were not lost in the far less affected cerebellum of the same patients (where ASPD levels were low) (Figs. 6 *D, E*, S4*B* and S4*C*). The explanation for these regional differences in ASPD concentrations

must await further experimentation, but these observations further support our conclusion that NAKα3 serves as the specific death-inducing target of ASPD.

Recent studies have shown that Aβ forms numerous structurally distinct oligomers that may contribute differently to disease pathogenesis (6, 19). Aβ receptor/ligand systems may be organized into three categories (Fig. 8, Table S3). The first category involves regulating the CNS concentration of Aβ monomer available for assembly. The second category involves Aβ impairment of synaptic connections by indirectly affecting NMDAR activity (see *SI* Discussion for more details about the first two categories). Post-synaptic Sigma-2/PGRMC1 has been reported to serve as a receptor for 50~75 kDa $A\beta_{1\text{-}42}$ oligomers (43). We report here a third system involving pre-synaptic neurons. Pre-synaptic neuronal Ca^{2+} hyperactivation has been reported to occur near amyloid plaques in AD model mice (44). Interestingly, such hyperactivation of neurons in hippocampus has been associated with the cortical thinning in mild cognitive impairment patients and has been considered to be an early indicator of AD-related neurodegeneration (45). However, the underlying mechanisms were largely unknown. We have previously shown that ASPD co-localize with pre-synaptic Bassoon (19). Among different NAKα subunits, only NAKα3 is present in the pre-synaptic side of neurons (27, 46-48).

Electrophysiological studies have also shown the importance of NAKα3 in the pre-synaptic function (49, 50). Our data are consistent with ASPD binding to pre-synaptic NAKα3 of mature neurons, leading to activation of pre-synaptic N-type VGCC, and eventual death of NAKα3-expressing neurons. Notably, NAKα3 appears as punctate patterns restricted to layers III and V of the neocortex (27), where N-type VGCC are present (51). These layers are particularly vulnerable in AD brains (52). It is an intriguing speculation that the 100-kDa band sometimes observed by Gong *et al.* in ligand overlay assays with ADDLs was NAKα3 (53).

The human NAKα3 gene *ATP1A3* is located on chromosome 19q13.31, an AD linkage region, but at present there are no reports that mutations in *ATP1A3* are linked to AD. The mutation rate in *ATP1A3* is very low in humans (54), suggesting that people with mutations in *ATP1A3* might be at high risk of neurodevelopmental/neuropsychiatric diseases and develop these diseases before they become old. Indeed, genetic studies have shown that mutations in the protein-coding region of *ATP1A3* cause rapid-onset dystonia parkinsonism, alternating hemiplegia of childhood, and cerebellar ataxia, areflexia, pes cavus, optic atrophy, and sensorineural hearing loss syndrome (54). Notably, although a direct linkage of *ATP1A3* mutations to AD is difficult to detect, AD and *ATP1A3*-mutated diseases share features such as

convulsive seizures (derived from hyperactivity of neurons). A recent clinical study of AD patients has revealed that convulsive seizures occurred early in the course of AD, which often began around the same time when symptoms of neurodegeneration first appeared (55). Levetiracetam, which inhibits pre-synaptic calcium channels (56), suppresses neuronal hyperactivation and reverses cognitive deficits in their AD model mice (57). These results are consistent with our findings (Fig. 8) and suggest that hyperactivation of pre-synaptic neurons occurs in AD patients contemporaneously with neurodegeneration.

AD is a progressive disease with risk highly correlated with ageing. As shown in Fig. 2*A*, ASPD are not detectable in brains of most healthy old people, suggesting that accumulation of ASPD may not begin in the very early phase of Aβ accumulation. This notion is consistent with the fact that ASPD are minimally present in the brains of *APP*-overexpressing mice, which accumulate dodecamers and retain the early features of AD development (such as spine loss) but not the features of symptomatic human AD (such as neurodegeneration)(19). These observations suggested to us that formation of ASPD might require an age-related "facilitating factor," in addition to *APP* overexpression. A prospective study of ASPD formation relative to AD development and progression could be of interest. We think this study may be particularly

significant in the light of our prior work showing that ASPD levels correlate with disease severity (19) and the data presented here (see Fig. 2*A*) demonstrating that AD patient ASPD levels correlate with the severity of neurodegeneration based on Braak staging and duration of disease.

Fine structural analysis of ASPD by solution NMR suggests that amino acid residues Ala^{1}-His^{13}, Gln^{15}-Lys^{16}, and Asp^{23} are involved in forming a portion of the ASPD surface, a portion likely involved in NAKα3-binding (Fig. 7*B*). Furthermore, molecular modeling of NAKα3 indicated that the region in Ex4 of NAKα3 encompassing residues Asn^{879} and Trp^{880} is essential for the ASPD-NAKα3 interaction. Indeed, an ASPD-binding tetrapeptide that mimics this Ex4 region blocked ASPD neurotoxicity. Because Asn^{879} is essential for neutralizing ASPD neurotoxicity, we speculate that H-bonding interactions are involved in the ASPD-NAKα3 interaction. Interestingly, in the case of human NAKα2, mutation at this tryptophan (W887R; Trp^{887} in NAKα2 corresponds to Trp^{880} in NAKα3), which is highly conserved among all NAKα isoforms (Fig. 7*G*), leads to complete loss of catalytic activity and causes familial hemiplegic migraine type 2 (58). This suggests the importance of this conserved Trp for native NAKα

function and it may be that ASPD binding to the region containing this Trp causes impairment of NAKα3 function.

Except for the NAKβ subunit and agrin, all other NAKα-binding proteins have been reported to bind to the intracellular region of NAKα (59). Because this NAKβ-binding region is located ten amino acids more C-terminally than Trp^{880} (Fig. 7*G*), the Ex4-mimicking tetrapeptide is unlikely to interfere with the NAKα-NAKβ interaction. In the case of the NAKα2 mutation W887R, loss of NAK pump activity occurs without interfering with the NAKα-NAKβ interaction because the NAK pump containing the NAKα and NAKβ subunits is present at substantial levels in the plasma membrane (58). With respect to agrin, although its binding region in NAKα3 has not been determined, it has been suggested to take the place of NAKβ, and accordingly, it is reasonable to consider that agrin and NAKβ share the same binding region (59). Taken together, these observations suggest that peptidomimetics would not disrupt interactions between NAKα3 and proteins other than ASPD. The Ex4-mimicking tetrapeptide (PD2-11, MW602.6) that inhibits ASPD neurotoxicity is sufficiently small that the molecule could serve as a lead compound for knowledge-based design of peptidomimetics. This class of compounds is expected to offer superior stability and pharmacokinetics compared with anti-Aβ antibodies.

Given the essential functions of the NAK pump in neurons (22), direct modulation of the NAK pump would be a risky approach. We therefore propose a new strategy to treat AD by blocking ASPD-NAKα3 interaction through masking the Aβ oligomer surface with specific peptidomimetics, as illustrated in Fig. S6. In summary, our data support the conclusion that ASPD-NAKα3 interactions is a cellular basis for neuronal loss induced by ASPD and that blocking this interaction could be a useful strategy for AD treatment.

Materials and Methods

Ethics. The Bioethics Committees and the Biosafety Committees of MITILS, Niigata University, Kyoto University, FBRI, and TAO approved experiments using human subjects. The Animal Care and Experimentation Committees of MITILS, Kyoto University,FBRI, and TAP approved animal experiments.

ASPD Preparation. ASPD are neurotoxic, spherical Aβ oligomers of 10-15-nm diameter (measured by TEM) that are recognized by ASPD-specific antibodies (19, 20). Patient ASPD were purified from the 100-kDa retentates of soluble AD brain extracts (devoid of LMW oligomers, prepared as in (19)) by IP using haASD1 ("IP" in *SI* Materials and Methods).

Synthetic ASPD were formed in 50 μM $A\beta_{1-42}$ solution (with or without 2 μM biotinylated $A\beta_{1-40}$) using in-house-prepared highly soluble Aβ peptides (essential for obtaining ASPD; see "Aβ synthesis") in F12 buffer without L-glutamine and phenol red by slowly rotating the solution for ~16 hrs at 4 ˚C (19). The level of $A\beta_{1-42}$-ASPD in this $A\beta_{1-42}$ solution after slow rotation is usually ~30 %. Synthetic ASPD were obtained in the fraction that passed through 0.22-μm filters, but was retained on 100-kDa MWCO filters (Sartorius) (19). ^{15}N-Labelled ASPD were prepared in the same way using purified *E. coli*-expressed ^{15}N-labelled $A\beta_{1-40}$ (60). ASPD quality was confirmed by dot blotting, TEM, amino acid analysis, and toxicity assays (20).

Statistical Analyses. Statistical analysis was performed using StatView®5.0 (SAS Institute Inc.).

Other Methods. Methods for Aβ Synthesis, Preparation of 20- to 30-nm Aβ aggregates, Primary neuronal cultures, ASPD Toxicity, ASPD binding, Immunocytochemistry, MicroRNA of *ATP1A3*, Western and Far-western blotting and MS/MS, Cell-free NAKα3 production, SPR, IP, NAK activity, Ca^{2+} and Na^{+} Imaging, Time-lapse, Dot blotting, TEM, SEM, Human brain pathology and ISH, Glycerol gradient sedimentation, PD, NMR, and Molecular modeling are described in *SI* Materials and Methods.

Online Supporting Information. This includes *SI* Materials and Methods, *SI* Discussions, 6 figures, 3 tables, and 4 videos. Fig. S1 shows that glutamate receptor antagonists did not change ASPD neurotoxicity. Fig. S2 shows data on ASPD interactions with NAKα3, developmental changes in NAKα3 levels, co-immunoprecipitations, and immunostaining. Fig.S3 shows ASPD-induced Na^+ increase, Ca^{2+} overload induced by different concentrations of ASPD, which were abolished by EGTA pretreatment, as well as ouabain-induced Ca^{2+} overload and tau phosphorylation/destabilization. Fig. S4 shows time-lapse shots and immunohistochemical studies of human brains using anti-NAKα1 antibody and ISH. Fig. S5 shows ASPD-binding peptides inhibit ASPD-binding to NAKα3 and other ASPD-induced downstream phenomena. Fig. S6 presents a model of ASPD-NAKα3 interactions and how masking the ASPD surface with specific masking peptides or peptidomimetics could be a new therapeutic strategy.

Acknowledgements. We thank S. Kikuchi, Y. Matsumura, K. Takatsuka for technical assistance, Masatoshi Takeichi and Shigenobu Yonemoto for help in using the TEM instrument, and Dominic Walsh for comments. This work was supported by grants from the Ministry of Health,

Labor and Welfare (Research on Nanotechnical Medical), the Ministry of Education, Culture, Sports, Science and Technology (Grant-in-Aid for Scientific Research B and Grant-in-Aid for Scientific Research on Innovative Areas (Comprehensive Brain Science Network)), the Collaborative Research Project of the Brain Research Institute, Niigata University, Takeda Science Foundation to M.Hoshi, and NIH Grants NS038328 and AG041295 to D.B.T.

Author contributions: H. Hiroaki, Y.F., I.K., D.B.T., and M. Hoshi designed research; T.O., M.Y., T. Sasahara, Y.K., T.N., H. Takeda, A.T., Y.A., A.I., H.K., H. Hirao, K.S., M.I., M.T., M.S., E.S., Y.S., S.S., Y.U., N.G., N.T., and M. Hoshi performed research; T.O., M.Y., T. Sasahara, Y.K., H. Hiroaki, Y.F., I.K., T.N., A.K., H. Takeda, A.T., Y.A., A.I., H.K., H. Hirao, K.S., M.I., S.-i.M., K.M., M.T., M.S., E.S., Y.S., S.S., Y.U., N.G., N.T., H. Takahashi, M. Hagiwara, T. Sawasaki, G.I., Y.N., Y.-i.N., D.B.T., and M. Hoshi analyzed data; and H. Hiroaki, Y.F., I.K., D.B.T., and M. Hoshi wrote the paper.

Conflict of interest statement: M.Hoshi has served as a technical advisor to TAO, a Kyoto University-derived bioventure, with the permission of the conflict-of-interest committee of

Kyoto University. T.Sasahara, Y.A., H.K., K.S., M.I., E.S., S.S., and N.T. are employees of TAO.

References

1. Hardy J & Selkoe DJ (2002) The amyloid hypothesis of Alzheimer's disease: progress and problems on the road to therapeutics. *Science* 297(5580):353-356.
2. Klein WL, Krafft GA, & Finch CE (2001) Targeting small Aβ oligomers: the solution to an Alzheimer's disease conundrum? *Trends Neurosci* 24(4):219-224.
3. Walsh DM & Selkoe DJ (2007) Aβ oligomers - a decade of discovery. *J Neurochem* 101(5):1172-1184.
4. Roychaudhuri R, Yang M, Hoshi MM, & Teplow DB (2009) Amyloid β-protein assembly and Alzheimer disease. *J Biol Chem* 284:4749-4753.
5. Chiti F & Dobson CM (2009) Amyloid formation by globular proteins under native conditions. *Nat Chem Biol* 5(1):15-22.
6. Benilova I, Karran E, & De Strooper B (2012) The toxic Aβ oligomer and Alzheimer's disease: an emperor in need of clothes. *Nat Neurosci* 15(3):349-357.
7. Wang HY*, et al.* (2000) β-Amyloid$_{1-42}$ binds to α7 nicotinic acetylcholine receptor with high affinity. Implications for Alzheimer's disease pathology. *J Biol Chem* 275(8):5626-5632.
8. Yan SD*, et al.* (1996) RAGE and amyloid-β peptide neurotoxicity in Alzheimer's disease. *Nature* 382:685-691.
9. Cissé M*, et al.* (2011) Reversing EphB2 depletion rescues cognitive functions in Alzheimer model. *Nature* 469(7328):47-52.
10. Laurén J, Gimbel DA, Nygaard HB, Gilbert JW, & Strittmatter SM (2009) Cellular prion protein mediates impairment of synaptic plasticity by amyloid-β oligomers. *Nature* 457(7233):1128-1132.
11. Danysz W & Parsons CG (2012) Alzheimer's disease, β-amyloid, glutamate, NMDA receptors and memantine--searching for the connections. *Br J Pharmacol*

167(2):324-352.

12. Shankar GM, *et al.* (2008) Amyloid-β protein dimers isolated directly from Alzheimer's brains impair synaptic plasticity and memory. *Nat Med* 14:837-842.
13. O'Nuallain B, *et al.* (2010) Amyloid β-protein dimers rapidly form stable synaptotoxic protofibrils. *J Neurosci* 30(43):14411-14419.
14. Lesné S, *et al.* (2006) A specific amyloid-β protein assembly in the brain impairs memory. *Nature* 440(7082):352-357.
15. Lambert MP, *et al.* (1998) Diffusible, nonfibrillar ligands derived from $A\beta_{1-42}$ are potent central nervous system neurotoxins. *Proc Natl Acad Sci USA* 95(11):6448-6453.
16. Lacor PN, *et al.* (2007) Aβ oligomer-induced aberrations in synapse composition, shape, and density provide a molecular basis for loss of connectivity in Alzheimer's disease. *J Neurosci* 27(4):796-807.
17. Weiner MW, *et al.* (2012) The Alzheimer's Disease Neuroimaging Initiative: a review of papers published since its inception. *Alzheimer's & Dementia: J Alz Assoc* 8(1 Suppl):S1-S68.
18. Hoshi M, *et al.* (2003) Spherical aggregates of β-amyloid (amylospheroid) show high neurotoxicity and activate tau protein kinase I/glycogen synthase kinase-3β. *Proc Natl Acad Sci USA* 100:6370-6375.
19. Noguchi A, *et al.* (2009) Isolation and characterization of patient-derived, toxic, high mass amyloid β-protein (Aβ) assembly from Alzheimer disease brains. *J Biol Chem* 284(47):32895-32905.
20. Matsumura S, *et al.* (2011) Two distinct amyloid β-protein (Aβ) assembly pathways leading to oligomers and fibrils identified by combined fluorescence correlation spectroscopy, morphology, and toxicity analyses. *J Biol Chem* 286(13):11555-11562.
21. Verret L, *et al.* (2012) Inhibitory interneuron deficit links altered network activity and cognitive dysfunction in Alzheimer model. *Cell* 149(3):708-721.
22. Blanco G & Mercer RW (1998) Isozymes of the Na-K-ATPase: heterogeneity in structure, diversity in function. *Am J Phys* 275(5 Pt 2):F633-F650.
23. Catterall WA & Few AP (2008) Calcium channel regulation and presynaptic plasticity. *Neuron* 59(6):882-901.
24. Yamaguchi H, *et al.* (1996) Preferential labeling of Alzheimer neurofibrillary tangles with antisera for tau protein kinase (TPK) I/glycogen synthase kinase-3β and

cyclin-dependent kinase 5, a component of TPK II. *Acta Neuropathol* 92(3):232-241.

25. Bortner CD & Cidlowski JA (2002) Apoptotic volume decrease and the incredible shrinking cell. *Cell Death Differ* 9(12):1307-1310.
26. O'Brien WJ, Lingrel JB, & Wallick ET (1994) Ouabain binding kinetics of the rat alpha two and alpha three isoforms of the sodium-potassium adenosine triphosphate. *Arch Biochem Biophys* 310(1):32-39.
27. Bøttger P*, et al.* (2011) Distribution of Na/K-ATPase alpha 3 isoform, a sodium-potassium P-type pump associated with rapid-onset of dystonia parkinsonism (RDP) in the adult mouse brain. *J Comp Neurol* 519(2):376-404.
28. Chauhan NB, Lee JM, & Siegel GJ (1997) Na,K-ATPase mRNA levels and plaque load in Alzheimer's disease. *J Mol Neurosci* 9(3):151-166.
29. Yu L*, et al.* (2009) Structural characterization of a soluble amyloid β-peptide oligomer. *Biochem* 48(9):1870-1877.
30. Yamaguchi T, Matsuzaki K, & Hoshino M (2011) Transient formation of intermediate conformational states of amyloid-β peptide revealed by heteronuclear magnetic resonance spectroscopy. *FEBS Lett* 585(7):1097-1102.
31. Parthasarathy S, *et al.* (2015) Structural insight into an Alzheimer's brain-derived spherical assembly of amyloid β by solid-state NMR. *J Am Chem Soc* 137(20): 6480-6483
32. Morth JP*, et al.* (2007) Crystal structure of the sodium-potassium pump. *Nature* 450(7172):1043-1049.
33. Pylova SI, Majkowska J, Hilgier W, Kapuscinski A, & Albrecht J (1989) Rapid decrease of high affinity ouabain binding sites in hippocampal CA1 region following short-term global cerebral ischemia in rat. *Brain Res* 490(1):170-173.
34. Bignotto M & Benedito MA (2006) Repeated electroconvulsive shock induces changes in high-affinity [^{3}H]-ouabain binding to rat striatal membranes. *Neurochem Res* 31(4):515-521.
35. Hayashi Y, Mimura K, Matsui H, & Takagi T (1989) Minimum enzyme unit for Na^+/K^+-ATPase is the αβ-protomer. Determination by low-angle laser light scattering photometry coupled with high-performance gel chromatography for substantially simultaneous measurement of ATPase activity and molecular weight. *Biochim Biophys Acta* 983(2):217-229.

36. Antolovic R, *et al.* (1999) Affinity labelling with MgATP analogues reveals coexisting Na^+ and K^+ forms of the α-subunits of Na^+/K^+-ATPase. *Eur J Biochem* 261(1):181-189.
37. Courtney A & Courtney M (2008) Comments Regarding "On the Nature Of Science". *Physics in Canada* 64(3):7-8.
38. Liguri G, *et al.* (1990) Changes in Na^+,K^+-ATPase, Ca^{2+}-ATPase and some soluble enzymes related to energy metabolism in brains of patients with Alzheimer's disease. *Neurosci Lett* 112(2-3):338-342.
39. Hattori N, *et al.* (1998) CI-ATPase and Na^+/K^+-ATPase activities in Alzheimer's disease brains. *Neurosci Lett* 254(3):141-144.
40. Mark RJ, Hensley K, Butterfield DA, & Mattson MP (1995) Amyloid β-peptide impairs ion-motive ATPase activities: evidence for a role in loss of neuronal Ca^{2+} homeostasis and cell death. *J Neurosci* 15(9):6239-6249.
41. Dickey CA, *et al.* (2005) Dysregulation of Na^+/K^+ ATPase by amyloid in APP+PS1 transgenic mice. *BMC Neurosci* 6:7.
42. Marambaud P, Dreses-Werringloer U, & Vingtdeux V (2009) Calcium signaling in neurodegeneration. *Mol Neurodegener* 4:20.
43. Izzo NJ, *et al.* (2014) Alzheimer's therapeutics targeting amyloid beta 1-42 oligomers II: Sigma-2/PGRMC1 receptors mediate Abeta 42 oligomer binding and synaptotoxicity. *PLoS One* 9(11):e111899.
44. Busche MA, *et al.* (2008) Clusters of hyperactive neurons near amyloid plaques in a mouse model of Alzheimer's disease. *Science* 321(5896):1686-1689.
45. Putcha D, *et al.* (2011) Hippocampal hyperactivation associated with cortical thinning in Alzheimer's disease signature regions in non-demented elderly adults. *J Neurosci* 31(48):17680-17688.
46. McGrail KM, Phillips JM, & Sweadner KJ (1991) Immunofluorescent localization of three Na,K-ATPase isozymes in the rat central nervous system: both neurons and glia can express more than one Na,K-ATPase. *J Neurosci* 11(2):381-391.
47. Pietrini G, Matteoli M, Banker G, & Caplan MJ (1992) Isoforms of the Na,K-ATPase are present in both axons and dendrites of hippocampal neurons in culture. *Proc Natl Acad Sci USA* 89(18):8414-8418.
48. Azarias G, *et al.* (2013) A specific and essential role for Na,K-ATPase α3 in neurons co-expressing α1 and α3. *J Biol Chem* 288(4):2734-2743.

49. Taruno A, Ohmori H, & Kuba H (2012) Inhibition of presynaptic Na^+/K^+-ATPase reduces readily releasable pool size at the avian end-bulb of Held synapse. *Neuroscience research* 72(2):117-128.

50. Kim JH, Sizov I, Dobretsov M, & von Gersdorff H (2007) Presynaptic Ca^{2+} buffers control the strength of a fast post-tetanic hyperpolarization mediated by the α3 Na^+/K^+-ATPase. *Nat Neurosci* 10(2):196-205.

51. Chung YH, Shin C, Park KH, & Cha CI (2000) Immunohistochemical study on the distribution of the voltage-gated calcium channel α_{1B} subunit in the mature rat brain. *Brain Res* 866(1-2):274-280.

52. Bussière T*, et al.* (2003) Progressive degeneration of nonphosphorylated neurofilament protein-enriched pyramidal neurons predicts cognitive impairment in Alzheimer's disease: stereologic analysis of prefrontal cortex area 9. *J Comp Neurol* 463(3):281-302.

53. Gong Y*, et al.* (2003) Alzheimer's disease-affected brain: presence of oligomeric Aβ ligands (ADDLs) suggests a molecular basis for reversible memory loss. *Proc Natl Acad Sci USA* 100(18):10417-10422.

54. Heinzen EL*, et al.* (2014) Distinct neurological disorders with ATP1A3 mutations. *Lancet Neurol* 13(5):503-514.

55. Vossel KA*, et al.* (2013) Seizures and epileptiform activity in the early stages of Alzheimer disease. *JAMA Neurol* 70(9):1158-1166.

56. Vogl C, Mochida S, Wolff C, Whalley BJ, & Stephens GJ (2012) The synaptic vesicle glycoprotein 2A ligand levetiracetam inhibits presynaptic Ca^{2+} channels through an intracellular pathway. *Mol Pharmacol* 82(2):199-208.

57. Sanchez PE*, et al.* (2012) Levetiracetam suppresses neuronal network dysfunction and reverses synaptic and cognitive deficits in an Alzheimer's disease model. *Proc Natl Acad Sci U S A* 109(42):E2895-2903.

58. Koenderink JB*, et al.* (2005) Na,K-ATPase mutations in familial hemiplegic migraine lead to functional inactivation. *Biochim Biophys Acta* 1669(1):61-68.

59. Reinhard L, Tidow H, Clausen MJ, & Nissen P (2013) Na^+,K^+-ATPase as a docking station: protein-protein complexes of the Na^+,K^+-ATPase. *Cell Mol Life Sci* 70(2):205-222.

60. Hiroaki H, Umetsu Y, Nabeshima Y, Hoshi M, & Kohda D (2011) A simplified recipe for assigning amide NMR signals using combinatorial ^{14}N amino acid inverse-labeling. *J*

Struct Funct Genomics 12(3):167-174.

61. Kolansky DM, Brines ML, Gilmore-Hebert M, & Benz EJ, Jr. (1992) The A2 isoform of rat Na^+,K^+-adenosine triphosphatase is active and exhibits high ouabain affinity when expressed in transfected fibroblasts. *FEBS Lett* 303(2-3):147-153.
62. Blanco G, Xie ZJ, & Mercer RW (1993) Functional expression of the α2 and α 3 isoforms of the Na,K-ATPase in baculovirus-infected insect cells. *Proc Natl Acad Sci U S A* 90(5):1824-1828.
63. Blanco G, Sanchez G, & Mercer RW (1995) Comparison of the enzymatic properties of the Na,K-ATPase α3β1 and α3β2 isozymes. *Biochem* 34(31):9897-9903.
64. Takatsuka K, Ishii TM, & Ohmori H (2005) A novel Ca^{2+} indicator protein using FRET and calpain-sensitive linker. *Biochem Biophys Res Commun* 336(1):316-323.
65. Nozawa A*, et al.* (2011) Production and partial purification of membrane proteins using a liposome-supplemented wheat cell-free translation system. *BMC Biotech* 11:35.
66. Kaiser L*, et al.* (2008) Efficient cell-free production of olfactory receptors: detergent optimization, structure, and ligand binding analyses. *Proc Natl Acad Sci U S A* 105(41):15726-15731.
67. Gill SC & von Hippel PH (1989) Calculation of protein extinction coefficients from amino acid sequence data. *Anal Biochem* 182(2):319-326.
68. Braak H, Alafuzoff I, Arzberger T, Kretzschmar H, & Del Tredici K (2006) Staging of Alzheimer disease-associated neurofibrillary pathology using paraffin sections and immunocytochemistry. *Acta Neuropathol* 112(4):389-404.
69. Delaglio F*, et al.* (1995) NMRPipe: a multidimensional spectral processing system based on UNIX pipes. *J Biomol NMR* 6(3):277-293.
70. Hou L & Zagorski MG (2006) NMR reveals anomalous copper(II) binding to the amyloid Aβ peptide of Alzheimer's disease. *J Am Chem Soc* 128(29):9260-9261.
71. Gunter TE, Yule DI, Gunter KK, Eliseev RA, & Salter JD (2004) Calcium and mitochondria. *FEBS Lett* 567(1):96-102.
72. Doczi J*, et al.* (2011) Complex contribution of cyclophilin D to Ca^{2+}-induced permeability transition in brain mitochondria, with relation to the bioenergetic state. *J Biol Chem* 286(8):6345-6353.
73. Deane R*, et al.* (2012) A multimodal RAGE-specific inhibitor reduces amyloid β-mediated brain disorder in a mouse model of Alzheimer disease. *J Clin Invest*

122(4):1377-1392.

74. Deroo S*, et al.* (2015) Chemical Cross-Linking/Mass Spectrometry Maps the Amyloid β Peptide Binding Region on Both Apolipoprotein E Domains. *ACS Chem Biol*. *in press*

75. Yamauchi K*, et al.* (1999) Higher avidity binding of apolipoprotein (E-AII) complex than of apolipoprotein E monomer to β-amyloid. *J Neurosci Res* 58(2):301-307.

76. Snyder EM*, et al.* (2005) Regulation of NMDA receptor trafficking by amyloid-β. *Nat Neurosci* 8(8):1051-1058.

77. Um JW*, et al.* (2012) Alzheimer amyloid-β oligomer bound to postsynaptic prion protein activates Fyn to impair neurons. *Nat Neurosci* 15(9):1227-1235.

78. Huang Y & Mahley RW (2014) Apolipoprotein E: Structure and function in lipid metabolism, neurobiology, and Alzheimer's diseases. *Neurobiol Dis* 72PA:3-12.

79. Um JW & Strittmatter SM. (2013) Amyloid-β induced signaling by cellular prion protein and Fyn kinase in Alzheimer disease. *Prion*. 7(1):37-41.

80. Yan SS, *et al* (2012) RAGE is a key cellular target for Abeta-induced perturbation in Alzheimer's disease. *Front Biosci*. 1(4):240-50.

81. Parri HR, Hernandez CM & Dineley KT. (2011) Research update: Alpha7 nicotinic acetylcholine receptor mechanisms in Alzheimer's disease. *Biochem Pharmacol.* 82(8):931-42.

82. Decker H*, et al.* (2010) N-methyl-D-aspartate receptors are required for synaptic targeting of Alzheimer's toxic amyloid-β peptide oligomers. *J Neurochem* 115(6):1520-1529.

Figure Legends

Fig. 1. Mature Neuron-Specific Binding And Toxicity of ASPD. (*A*) ASPD neurotoxicity was determined by measuring apoptotic DNA fragmentation in HEK293 cells, 2 DIV immature or 19 DIV mature rat hippocampal neurons after overnight treatment with 140 nM synthetic ASPD, with or without 2-hr pretreatment of ASPD with each antibody (0.1 mg/ml for ASPD-specific

mASD3 antibody; 0.4 mg/ml for $A\beta_{3-8}$ antibody 6E10) (mean ± SD; *, $p < 0.001$ Games-Howell *post-hoc* test, n = 6). The antibody remained during overnight incubation with ASPD. As shown previously (19), mASD3 inhibited ASPD-induced neuronal death, but 6E10, targeting $A\beta_{3-8}$, did not. ASPD concentration is expressed in terms of the average ASPD mass 128 kDa (20). (*B*) Cells were treated for 30 min with 140 nM synthetic ASPD as in *A*. Images are representative of ASPD binding detected by mASD3 (red). Green represents anti-actin for HEK293 or anti-MAP2 for neurons. Neuronal 2D images were made from the z stack to show neurites (19). Neurons (19-27 DIV) gave essentially the same results as to binding and toxicity of ASPD. (*C*) Binding of synthetic ASPD was performed as in *B*, quantified (10), and shown as ASPD concentrations in 400 µL/well. Scatchard analysis gave K_d = 5.43 ± 0.27 nM (n=3). B_{max} of ASPD binding was 8.00 ± 1.0 nM for 30 min, from which the maximum level of ASPD binding was calculated to be 14 ± 0.7 pmol of ASPD/mg membrane protein.

Fig. 2. Characterization of AD Patient-Derived ASPD. (*A*) Levels of ASPD in soluble extracts of the cerebral cortex are shown according to disease duration and the level of neurodegeneration (see "Human brain pathology and ISH" in *SI* Materials and Methods; reanalysis of the samples

used in (19)). ASPD are undetectable in most of the age-matched non-clinically impaired (NCI) cases, but are present even in the very early AD cases. ASPD levels in patients increase markedly in parallel with the severity and progression of the disease. The 100-kDa retentates of the extracts from the two patients containing the highest level of ASPD were used for isolation of patient ASPD in this study. In a severe AD patient 20 years after onset, ASPD levels were very low, likely because such widespread neuronal death already had occurred. (*B-D*) Synthetic ASPD and patient ASPD (see above in *A*) were purified by immunoprecipitation (IP) using ASPD-specific haASD1 antibody as in (19). Soluble extracts from NCI brains and normal mouse IgG were used as controls for patient extracts and haASD1 antibody, respectively. Silver staining in *B*, dot blotting (*SI* Materials and Methods) along with a TEM image of negatively stained patient ASPD (see "TEM" for particle analysis) in *C*, and MALDI-TOF/MS analyses in *D* were performed (19). Representative data are shown. In the silver-stained gels, a band corresponding to $A\beta_{1\text{-}42}$ or $A\beta_{1\text{-}40}$ (red asterisk) was detected only in haASD1-immunoislated patient ASPD. Consistently, in MS of patient ASPD, significant peaks corresponding to $A\beta_{1\text{-}40}$ (4331.3 Da, centroid) and $A\beta_{1\text{-}42}$ (4515.5 Da, centroid) were reproducibly detected. Less intense peaks at lower mass than $A\beta_{1\text{-}40}$ (e.g. see "*" in *D* lower left) were occasionally, but not reproducibly,

detected. The mass of the peak (3319.9 Da, centroid) is consistent with that of [pyroglutamyl-$A\beta_{11-42}$ + H]$^+$. Peaks at higher mass than $A\beta_{40}$ or $A\beta_{42}$ monomer were not detected (right). These showed that $A\beta_{1-40}$ and $A\beta_{1-42}$ are the predominant components of patient ASPD. (*E*) Fractionation of patient ASPD (~16 pmol) in a 15-30% linear glycerol gradient (see "Glycerol gradient sedimentation" in *SI* Materials and Methods) (18). Protein standards (aldolase, 158 kDa; catalase, 232 kDa; ferritin, 440 kDa; and thyroglobulin, 669 kDa) were centrifuged at the same time as a reference and used for molecular mass determination (upper panel). Fractions were collected and immediately assayed for neurotoxicity (lower panel) (18). One unit of toxicity induces apoptosis in 1% of cells (see "Glycerol gradient sedimentation"). Data were obtained from three independent experiments and normalized to Aβ concentration (mean ± SD; Scheffé's *post-hoc* test, *, $p < 0.0001$ compared with vehicle alone). Inset shows a representative TEM image of the sample recovered in fraction 2 (≈11.6 ± 2.2 nm spheres; n = 54).

Fig. 3. Patient ASPD Bind To NAKα3. (*A*) Far-western blotting of RIPA extracts (15 μg/lane) was done using 6.6 nM patient ASPD (Center; detected with ASPD-specific haASD1 antibody) or 100 nM freshly dissolved $A\beta_{1-42}$ containing monomers and dimers (left; detected with anti-Aβ

antibody 6E10). Bands marked an asterisk represent intracellular proteins (legend of Figure S2*A*). Western blotting with anti-NAKα3 antibody (excised from *D*) showed the mass of NAKα3 (right). Red arrow indicates a 105-kDa mature neuron-specific ASPD-binding protein, NAKα3. (*B*) Schematic representation of NAK αβ and its function. (*C*) Western blotting of RIPA extracts (used in *A*). (*D*) Co-immunoprecipitation (CoIP) of NAKα3 with 250 nM synthetic ASPD. (*E*) Representative Z-stack images of 27 DIV hippocampal or 22 DIV cerebellar neurons, or HEK293, treated with 13 nM synthetic ASPD for 15 min. ASPD-binding sites (red) on neuropil co-localize with anti-NAKα3 staining (green)(high-power view in *Inset*; see "Immunocytochemistry" in *SI* Materials and Methods). (*F*) Direct interaction between ASPD on the tip and rat NAKα3 in micelles using SPR (K_d = 7.8 ± 2.5 nM, n=3). NAKα3-binding to the tip without ASPD was subtracted as background. NAKβ1 did not interact with ASPD in the AlphaScreen system. (*G*) Rat hippocampal (19-20 DIV) or cerebellar (23 DIV) neurons were treated overnight with 110 nM ASPD. ASPD neurotoxicity was determined as in Fig. 1*A* and normalized to 0.2 μM staurosporine toxicity. NAKα3 levels in membrane fractions of these neurons before ASPD treatment were determined by Western blotting. Mean ± SD; *, $p = 0.002$; **, $p < 0.0001$ compared with hippocampal neurons, n = 3~4 by Scheffé's *post-hoc* test. (*H*)

Representative images of 27 DIV hippocampal neurons, with or without selective knockout of NAKα3 (see "miR of *ATP1A3*" in *SI* Materials and Methods), treated with 13 nM synthetic ASPD for 15 min. ASPD-binding sites (red) and anti-NAKα3 staining (green) were detected as in *E*. ASPD neurotoxicity was assayed as in Fig. 1*A* (mean ± SD; Scheffé's *post-hoc* test, *, $p <$ 0.0001 compared with vehicle alone, n = 3).

Fig. 4. ASPD Impair NAK Activity And Cause Ca^{2+} Dyshomeostasis. (*A*) Membrane fraction of 25-26 DIV hippocampal neurons (30 μg/assay) was incubated with 110 nM synthetic ASPD and NAKα3-specific ATPase activity (K_d = 45 nM for ouabain (61-63)) was determined by subtracting the 100 nM-ouabain-sensitive activity from overall Mg^{2+}-ATPase activity (46). Mean ± SD; *, Scheffé's *post-hoc* test $p < 0.0001$ compared with 0 hr, n = 4. (*B*) NAKα3-specific ATPase activity of 25-26 DIV hippocampal neurons treated overnight with 140 nM synthetic ASPD was determined as in *A*. Mean ± SD; *, $p < 0.0001$ Scheffé's *post-hoc* test, n = 3. (*C*) Representative $[Ca^{2+}]_i$ changes of cell bodies of 19-20 DIV hippocampal neurons after treatment with each sample using Fura-PE3AM. The ratio of responsive cells was obtained as in *D*. 20-30-nm $A\beta_{1-42}$ aggregates were obtained by concentration and re-dilution processes (see

"Preparation of 20-30-nm Aβ aggregates" in *SI* Materials and Methods). For treatment with ASPD, the circulating buffer was replaced with the buffer containing ASPD. After the replacement, it took ≈110 sec until the ASPD-containing fluid reached the assay chamber (at the orange arrow) and it took ≈17.5 min until all the solution in the assay chamber was replaced by the ASPD solution (at the yellow arrow). Treatment with 20-30-nm $A\beta_{1-42}$ aggregates was done similarly. (*D*) The ratio of neurons that exhibited repetitive Ca^{2+} spikes or reached a saturated $[Ca^{2+}]_i$ within 2 hrs after the treatment was calculated from $[Ca^{2+}]_i$ data from three independent experiments. Mean ± SD; *, $p < 0.0001$ Scheffé's *post-hoc* test. (*E*) TEM images and dot blotting of the samples used in *C*.

Fig. 5. Downstream Signals Leading To Neuronal Death After ASPD Binding To NAKα3. (*A*) Inhibitor effect on 140 nM synthetic ASPD neurotoxicity examined as in Fig. 1*A*. (*B*) Schematic illustration of the mechanism of ASPD-induced neurodegeneration revealed in this study. (*C*) p25 generation from p35, a neuron-specific TPKII/CDK5 activator, after 110 nM synthetic ASPD treatment (right; representative Western blot). Data were normalized to actin and presented relative to total p35 and p25 amount at time 0. Mean ± SD; *, $p < 0.02$ compared with

data at time 0 (Scheffé's *post-hoc* test, n = 4~6). (*D*) TPKI/GSK3β activation as shown by phospho-Tyr^{216} increase and phospho-Ser^{9} decrease after 110 nM synthetic ASPD treatment (right; representative Western blot). Data were normalized to total TPKI/GSK3β and presented relative to each phospho-protein amount at time 0. Mean ± SD; *, $p < 0.002$ compared with data at time 0 (Scheffé's *post-hoc* test, n = 4~6). (*E*) Time-dependent increases in tau phosphorylation after 110 nM synthetic ASPD treatment. Data were normalized to total tau and presented relative to each phospho-protein amount at time 0. Vehicle controls are shown as inverted triangles in black for pSer^{396} and white for pSer^{404} (Mean ± SD; *, $p < 0.0001$ compared with data at time 0 (Scheffé's *post-hoc* test, n = 3~4). (*F*) Time-dependent decreases in MAP2 and tau after 110 nM synthetic ASPD treatment (right; representative Western blot). Data were normalized to actin and presented relative to each protein amount at time 0. Mean ± SD; *, $p < 0.002$ compared with data at time 0 (Scheffé's *post-hoc* test, n = 4~6).

Fig. 6. ASPD Effects On NAKα3-Expressing Neurons In Rat Neurons And Human Brains. (*A*) Representative time-lapse images of mature rat hippocampal neurons treated with each reagent (see Videos S1-4). (*B*) Time-dependent increase in apoptotic DNA fragmentation (determined as

in Fig. 1*A*) induced by 140 nM synthetic ASPD. (*C*) SEM showed the surface and morphology of mature rat hippocampal neurons treated with 35 nM synthetic ASPD. (*D*), (*E*) Immunohistochemical studies using anti-NAKα1 or anti-NAKα3 antibody on 4-μm paraffin-embedded sections in *D* and ISH analyses using probes for *ATP1A1* and *ATP1A3* on 10-μm paraffin-embedded sections in *E*. Soluble extracts were obtained from these brains and amounts of patient ASPD (representative blots in *D*) and Aβ in the extracts were determined by dot blotting as 429 ± 50 and 695 ± 104 (μg/g brain, n = 3), respectively.

Fig. 7. Structural Basis For ASPD Binding To NAKα3. (*A*) ^{1}H-^{15}N HSQC spectra of ~350 nM ^{15}N-ASPD and ~100 μM ^{15}N-$A\beta_{1-40}$ monomers in 0.5x PBS (supplemented with 5% (vol/vol) D_2O) were recorded at 298K on a 600 MHz Bruker *AVANCE*-III spectrometer equipped with a cryogenic TCI probe. (*B*) Schematic diagram of the NMR-derived ASPD surface. (*C*) A three-dimensional homology model of human NAKα3 was constructed using the Prime program (Schrödinger) based on the structure of pig NAKα1 (32) as a template (PDB code 3B8E). (*D*) The effect of each NAKα3-derived Ex1, Ex4, or scrambled Ex4 peptides on 140 nM synthetic ASPD neurotoxicity was examined as in Fig. 1*A*. Mean ± SD; Scheffé's *post-hoc* test, *, $p <$

0.001 compared with vehicle, n = 3. (*E*) Representative Z-stack images of 26 DIV hippocampal neurons, after 15 min treatment with 7 nM patient ASPD (immunoisolated from the patient extracts as in Fig. 2*B*), with or without 30-min pretreatment with Ex4 (20 μM in final concentration). IP eluates of NCI brain extracts, in which ASPD were not detected by dot blotting, were used as a control. ASPD-binding sites (red) and anti-NAKα3 staining (green) were detected as in Fig. 3*E*. (*F*) The effect of each Ex4-mimicking ASPD-binding peptides on 140 nM synthetic ASPD neurotoxicity. All peptides used here contained a free N-terminal amino group and a carboxylic acid at the C-terminus. Mean ± SD; Scheffé's *post-hoc* test, *, $p < 0.001$ compared with vehicle, n = 3. (*G*) Alignment of Ex4 regions.

Fig. 8. Major Aβ ligand/receptor systems previously detected and the system discovered in this work (see Table S3).

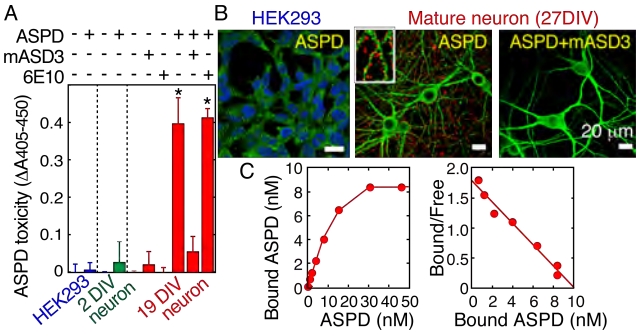
A
ASPD
mASD3
6E10
ASPD toxicity (ΔA405-450)
HEK293
2 DIV neuron
19 DIV neuron
B
HEK293
Mature neuron (27DIV)
ASPD
ASPD
ASPD+mASD3
20 μm
C
Bound ASPD (nM)
ASPD (nM)
Bound/Free
Bound ASPD (nM)

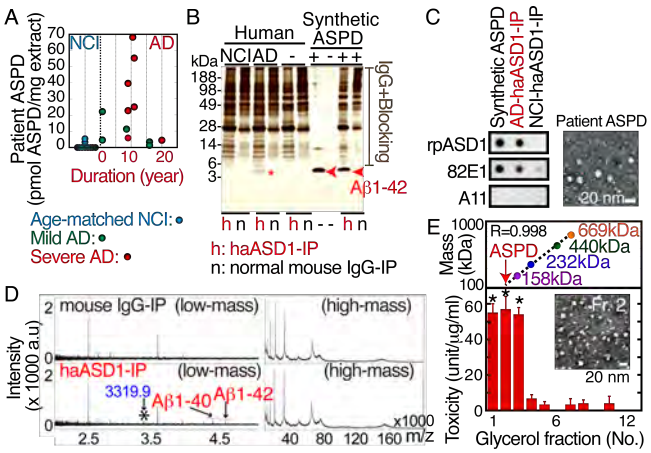
A
Patient ASPD (pmol ASPD/mg extract)
NCI
AD
Duration (year)
Age-matched NCI:
Mild AD:
Severe AD:
B
Human
Synthetic ASPD
NCI AD - + - + +
kDa
188
98
49
28
14
6
3
IgG+Blocking
Aβ1-42
h n h n h n - - h n
h: haASD1-IP
n: normal mouse IgG-IP
C
Synthetic ASPD
AD-haASD1-IP
NCI-haASD1-IP
rpASD1
82E1
A11
Patient ASPD
20 nm
D
mouse IgG-IP (low-mass)
(high-mass)
haASD1-IP
3319.9
Aβ1-40
Aβ1-42
Intensity (x 1000 a.u)
x1000
m/z
E
Mass (kDa)
R=0.998
669kDa
ASPD
440kDa
232kDa
158kDa
Fr. 2
20 nm
Toxicity (unit/μg/ml)
Glycerol fraction (No.)

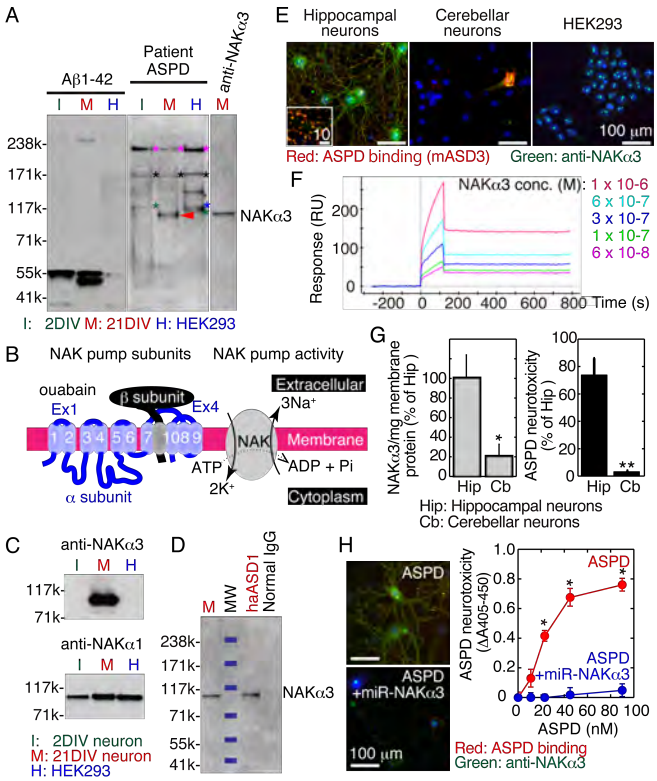
A
Aβ1-42
Patient ASPD
anti-NAKα3
I M H I M H M
238k-
171k-
117k-
71k-
55k-
41k-
NAKα3
I: 2DIV M: 21DIV H: HEK293
B
NAK pump subunits
NAK pump activity
ouabain
β subunit
Ex1
Ex4
1 2 3 4 5 6 7 10 8 9
α subunit
NAK
Extracellular
3Na+
Membrane
ATP
ADP + Pi
2K+
Cytoplasm
C
anti-NAKα3
I M H
117k-
71k-
anti-NAKα1
I M H
117k-
71k-
I: 2DIV neuron
M: 21DIV neuron
H: HEK293
D
M MW haASD1 Normal IgG
238k-
171k-
117k-
71k-
55k-
41k-
NAKα3
E
Hippocampal neurons
Cerebellar neurons
HEK293
10
100 μm
Red: ASPD binding (mASD3) Green: anti-NAKα3
F
NAKα3 conc. (M): 1 x 10-6
6 x 10-7
3 x 10-7
1 x 10-7
6 x 10-8
Response (RU)
200
100
0
-200 0 200 400 600 800 Time (s)
G
NAKα3/mg membrane protein (% of Hip)
100
80
60
40
20
0
Hip Cb
ASPD neurotoxicity (% of Hip)
100
80
60
40
20
0
Hip Cb
**
Hip: Hippocampal neurons
Cb: Cerebellar neurons
H
ASPD
ASPD +miR-NAKα3
100 μm
ASPD neurotoxicity (ΔA405-450)
1.0
0.8
0.6
0.4
0.2
0
0 20 40 60 80 100
ASPD (nM)
ASPD
ASPD +miR-NAKα3
Red: ASPD binding
Green: anti-NAKα3

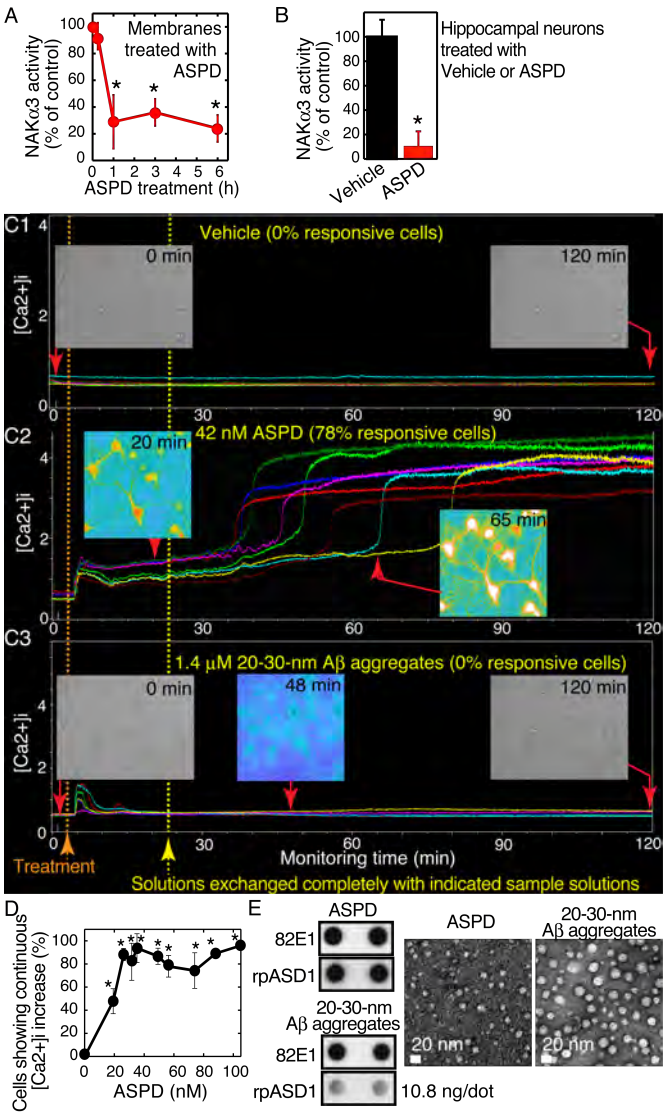
A
Membranes treated with ASPD
NAKα3 activity (% of control)
ASPD treatment (h)
B
Hippocampal neurons treated with Vehicle or ASPD
NAKα3 activity (% of control)
Vehicle
ASPD
C1
Vehicle (0% responsive cells)
0 min
120 min
[Ca2+]i
C2
42 nM ASPD (78% responsive cells)
20 min
65 min
C3
1.4 μM 20-30-nm Aβ aggregates (0% responsive cells)
0 min
48 min
120 min
Treatment
Monitoring time (min)
Solutions exchanged completely with indicated sample solutions
D
Cells showing continuous [Ca2+]i increase (%)
ASPD (nM)
E
ASPD
82E1
rpASD1
20-30-nm Aβ aggregates
82E1
rpASD1
10.8 ng/dot
ASPD
20-30-nm Aβ aggregates
20 nm
20 nm

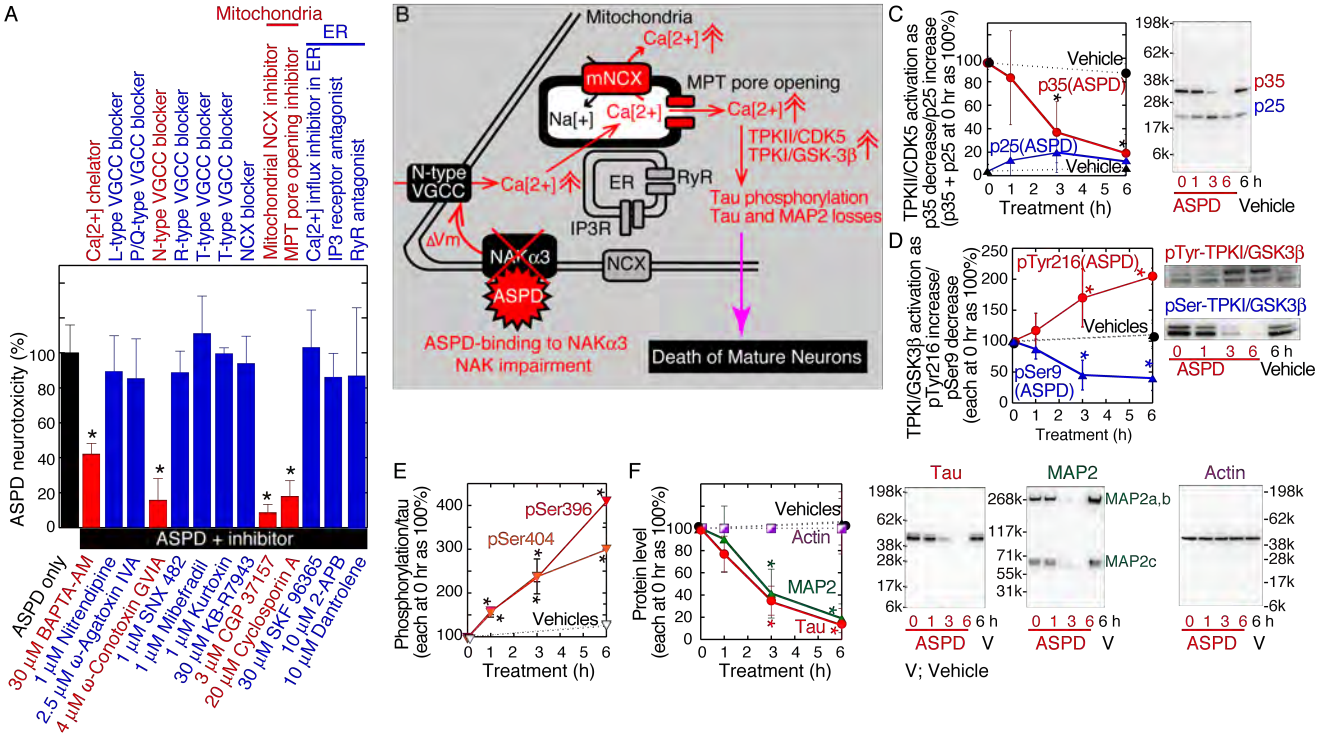
A
Mitochondria
ER
Ca[2+] chelator
L-type VGCC blocker
P/Q-type VGCC blocker
N-type VGCC blocker
R-type VGCC blocker
T-type VGCC blocker
T-type VGCC blocker
NCX blocker
Mitochondrial NCX inhibitor
MPT pore opening inhibitor
Ca[2+] influx inhibitor in ER
IP3 receptor antagonist
RyR antagonist
ASPD neurotoxicity (%)
ASPD + inhibitor
ASPD only
30 μM BAPTA-AM
1 μM Nitrendipine
2.5 μM ω-Agatoxin IVA
4 μM ω-Conotoxin GVIA
1 μM SNX 482
1 μM Mibefradil
1 μM Kurtoxin
30 μM KB-R7943
3 μM CGP 37157
20 μM Cyclosporin A
30 μM SKF 96365
10 μM 2-APB
10 μM Dantrolene
B
Mitochondria
Ca[2+]
mNCX
MPT pore opening
Na[+]
Ca[2+]
Ca[2+]
TPKII/CDK5
TPKI/GSK-3β
N-type VGCC
Ca[2+]
ER
RyR
IP3R
Tau phosphorylation
Tau and MAP2 losses
ΔVm
NAKα3
NCX
ASPD
ASPD-binding to NAKα3
NAK impairment
Death of Mature Neurons
C
TPKII/CDK5 activation as p35 decrease/p25 increase (p35 + p25 at 0 hr as 100%)
Vehicle
p35(ASPD)
p25(ASPD)
Vehicle
Treatment (h)
p35
p25
0 1 3 6 6 h
ASPD Vehicle
D
TPKI/GSK3β activation as pTyr216 increase/ pSer9 decrease (each at 0 hr as 100%)
pTyr216(ASPD)
Vehicles
pSer9 (ASPD)
Treatment (h)
pTyr-TPKI/GSK3β
pSer-TPKI/GSK3β
0 1 3 6 6 h
ASPD Vehicle
E
Phosphorylation/tau (each at 0 hr as 100%)
pSer396
pSer404
Vehicles
Treatment (h)
F
Protein level (each at 0 hr as 100%)
Vehicles
Actin
MAP2
Tau
Treatment (h)
Tau
MAP2
Actin
MAP2a,b
MAP2c
0 1 3 6 6 h
ASPD V
V; Vehicle

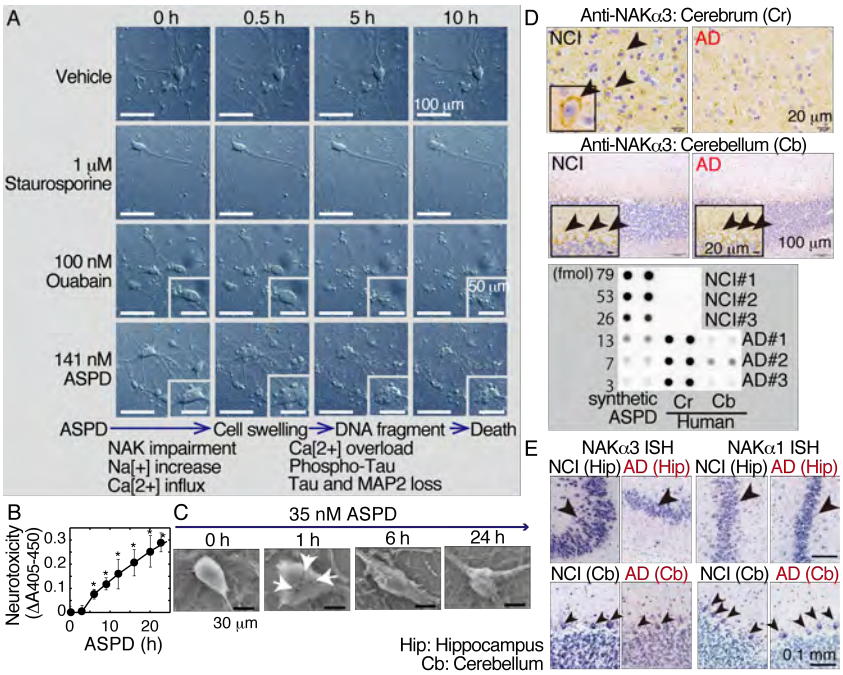
A
0 h
0.5 h
5 h
10 h
Vehicle
1 μM Staurosporine
100 nM Ouabain
141 nM ASPD
100 μm
50 μm
ASPD → Cell swelling → DNA fragment → Death
NAK impairment
Na[+] increase
Ca[2+] influx
Ca[2+] overload
Phospho-Tau
Tau and MAP2 loss
B
Neurotoxicity (ΔA405-450)
0.3
0.2
0.1
0
0
10
20
ASPD (h)
C
35 nM ASPD
0 h
1 h
6 h
24 h
30 μm
D
Anti-NAKα3: Cerebrum (Cr)
NCI
AD
20 μm
Anti-NAKα3: Cerebellum (Cb)
NCI
AD
20 μm
100 μm
(fmol) 79
53
26
13
7
3
NCI#1
NCI#2
NCI#3
AD#1
AD#2
AD#3
synthetic ASPD
Cr
Cb
Human
E
NAKα3 ISH
NAKα1 ISH
NCI (Hip)
AD (Hip)
NCI (Hip)
AD (Hip)
NCI (Cb)
AD (Cb)
NCI (Cb)
AD (Cb)
0.1 mm
Hip: Hippocampus
Cb: Cerebellum

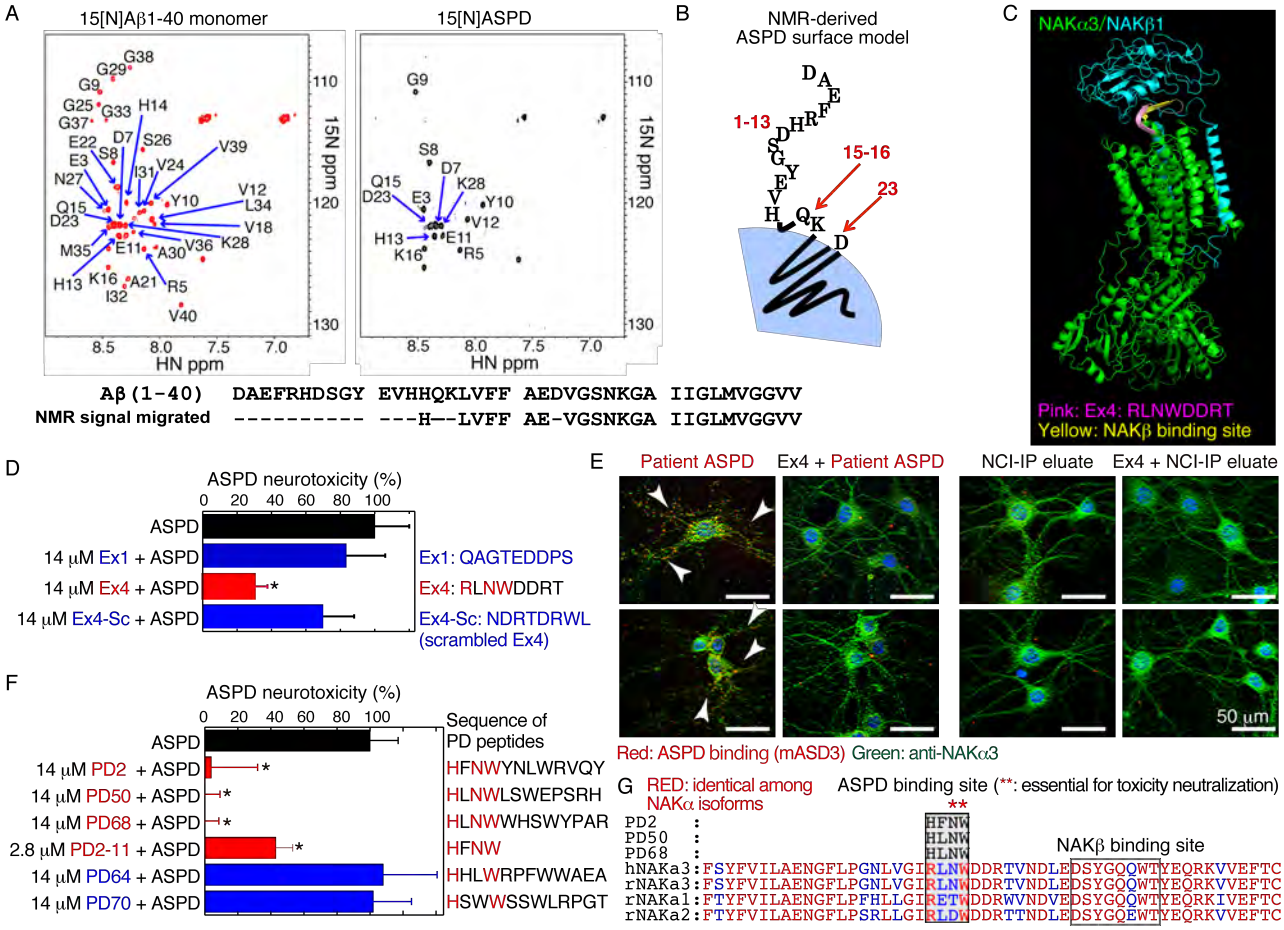
A
15[N]Aβ1-40 monomer
15[N]ASPD
15N ppm
HN ppm
Aβ(1-40) DAEFRHDSGY EVHHQKLVFF AEDVGSNKGA IIGLMVGGVV
NMR signal migrated ---------- ---H--LVFF AE-VGSNKGA IIGLMVGGVV
B
NMR-derived
ASPD surface model
1-13
15-16
23
C
NAKα3/NAKβ1
Pink: Ex4: RLNWDDRT
Yellow: NAKβ binding site
D
ASPD neurotoxicity (%)
ASPD
14 μM Ex1 + ASPD
14 μM Ex4 + ASPD
14 μM Ex4-Sc + ASPD
Ex1: QAGTEDDPS
Ex4: RLNWDDRT
Ex4-Sc: NDRTDRWL
(scrambled Ex4)
E
Patient ASPD
Ex4 + Patient ASPD
NCI-IP eluate
Ex4 + NCI-IP eluate
50 μm
Red: ASPD binding (mASD3) Green: anti-NAKα3
F
ASPD neurotoxicity (%)
Sequence of
PD peptides
ASPD
14 μM PD2 + ASPD
14 μM PD50 + ASPD
14 μM PD68 + ASPD
2.8 μM PD2-11 + ASPD
14 μM PD64 + ASPD
14 μM PD70 + ASPD
HFNWYNLWRVQY
HLNWLSWEPSRH
HLNWWHSWYPAR
HFNW
HHLWRPFWWAEA
HSWWSSWLRPGT
G
RED: identical among
NAKα isoforms
ASPD binding site (**: essential for toxicity neutralization)
NAKβ binding site
PD2 :
PD50 :
PD68 :
hNAKa3:FSYFVILAENGFLPGNLVGIRLNWDDRTVNDLEDSYGQQWTYEQRKVVEFTC
rNAKa3:FSYFVILAENGFLPGNLVGIRLNWDDRTVNDLEDSYGQQWTYEQRKVVEFTC
rNAKa1:FTYFVILAENGFLPFHLLGIRETWDDRWVNDVEDSYGQQWTYEQRKIVEFTC
rNAKa2:FTYFVILAENGFLPSRLLGIRLDWDDRTTNDLEDSYGQEWTYEQRKVVEFTC

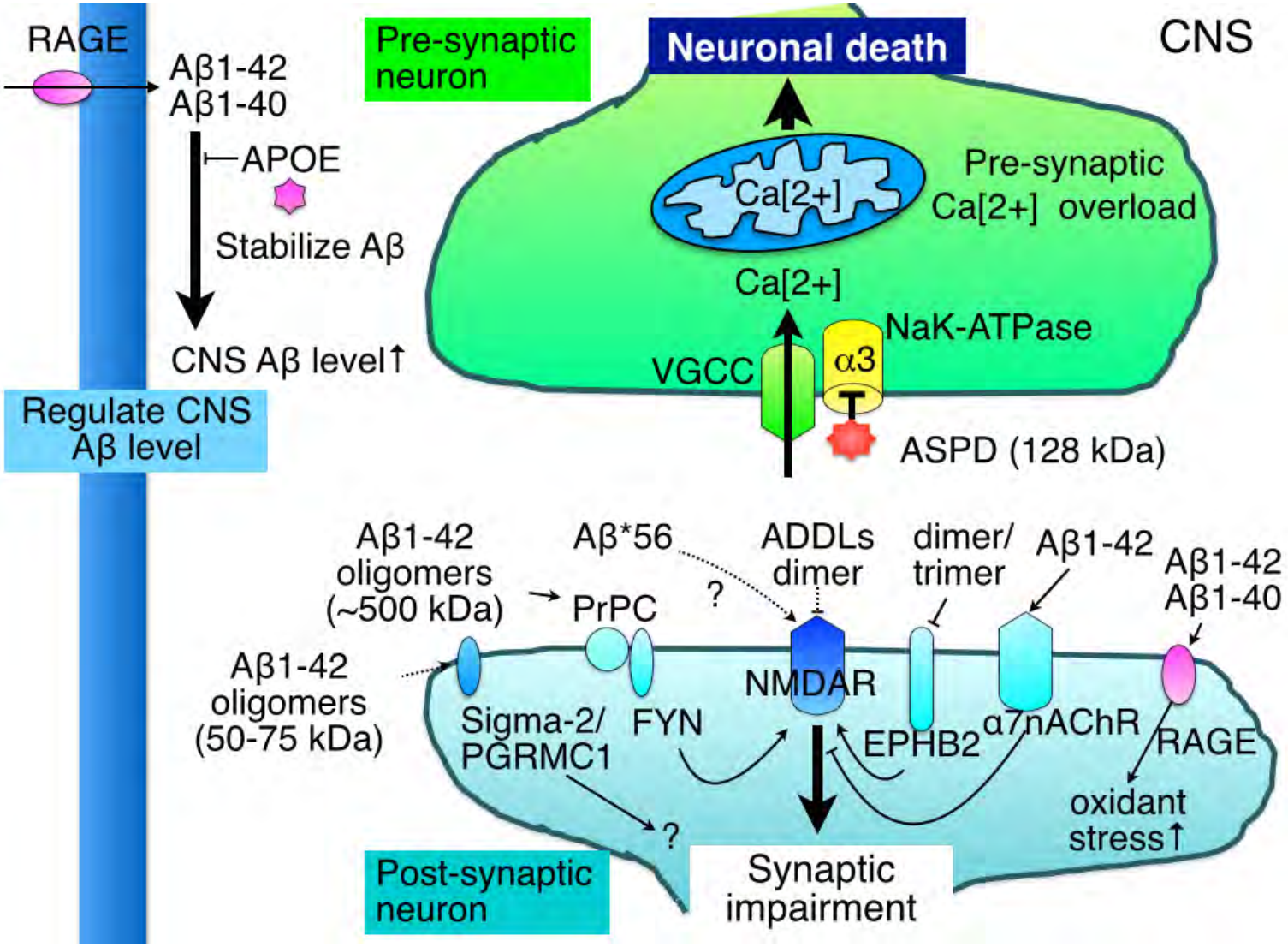
RAGE
Aβ1-42
Aβ1-40
APOE
Stabilize Aβ
CNS Aβ level↑
Regulate CNS Aβ level
Pre-synaptic neuron
Neuronal death
CNS
Ca[2+]
Pre-synaptic Ca[2+] overload
Ca[2+]
NaK-ATPase
VGCC
α3
ASPD (128 kDa)
Aβ1-42 oligomers (~500 kDa)
Aβ*56
ADDLs dimer
dimer/ trimer
Aβ1-42
Aβ1-42 Aβ1-40
PrPC
?
Aβ1-42 oligomers (50-75 kDa)
NMDAR
Sigma-2/ PGRMC1
FYN
EPHB2
α7nAChR
RAGE
oxidant stress↑
?
Post-synaptic neuron
Synaptic impairment

Supporting Information

Na,K-ATPaseα3 Is a Death Target of Alzheimer Patient Amyloid-β Assembly

Takayuki Ohnishi, Masako Yanazawa, Tomoya Sasahara, Yasuki Kitamura, Hidekazu Hiroaki, Yugo Fukazawa, Isao Kii, Takashi Nishiyama, Akiyoshi Kakita, Hiroyuki Takeda, Akihide Takeuchi, Yoshie Arai, Akane Ito, Hitomi Komura, Hajime Hirao, Kaori Satomura, Masafumi Inoue, Shin-ichi Muramatsu, Ko Matsui, Mari Tada, Michio Sato, Eri Saijo, Yoshiki Shigemitsu, Satoko Sakai, Yoshitaka Umetsu, Natsuko Goda, Naomi Takino, Hitoshi Takahashi, Masatoshi Hagiwara, Tatsuya Sawasaki, Genji Iwasaki, Yu Nakamura, Yo-ichi Nabeshima, David B. Teplow, and Minako Hoshi

SI Materials and Methods

Aβ synthesis. Highly soluble $A\beta_{1-42}$ and biotinylated $A\beta_{1-40}$ peptides were in-house synthesized and purified as described below. For $A\beta_{1-42}$, peptides were synthesized on an Applied Biosystems model 433A peptide synthesizer by solid-phase *N*-(9-fluorenyl)methoxycarbonyl (Fmoc) chemistry using Fmoc-Ala-NovaSyn-TGA resin (0.19 mmol/g; Novabiochem) (>75% yield), and were cleaved and deprotected in a solution containing phenol (0.15 g), trifluoroacetic acid (TFA, 1.65 ml), Milli Q water (0.05 ml), thioanisole (0.1 ml), and ethanedithiol (0.05 ml) (2 ml/200 mg resin). Crude peptides were precipitated by adding 30 ml of ice-cold diethyl ether, and the precipitates were washed twice, air-dried for 20 min, further dried in a vacuum for 1 hr, then competely dissolved in a solution containing 0.1% (vol/vol) TFA and 30% (vol/vol) acetonitrile (ACN) on ice, and lyophilized. The $A\beta_{1-42}$ peptides were purified by ZORBAX 300 Extend-C18 (21.2 mm × 250 mm, 5 μm, Agilent) reversed-phase chromatography using linear gradient separation (8-32 % (vol/vol) ACN in 70 mM NH_4OH). The purified peptides were immediately lyophilized, redissolved in a solution containing 0.1% (vol/vol) TFA and 30% (vol/vol) ACN on ice (~150 μM), lyophilized again, and kept at -30 ˚C until used. On average, 40-80 mg of purified $A\beta_{1-42}$ peptide was obtained in the 0.1 mmol scale synthesis. For biotinylated $A\beta_{1-40}$, the peptides were synthesized as described above, except for the use of pre-loaded Fmoc-Val-NovaSyn-TGA resin (0.21 mmol/g; Novabiochem) (>85% yield), and were labelled at the N-terminus with N-(D-biotinyloxy)succinimide. Crude peptides were obtained as described above. Biotinylated $A\beta_{1-40}$ peptides were first purified by Inertsil CN-3 (10 × 150 mm, 5μm) reversed-phase chromatography using a linear gradient separation (8-80 % (vol/vol) ACN in 0.1% (vol/vol) TFA), followed by ZORBAX 300 Extend-C18 as described above. Analytical HPLC, quantitative amino acid analysis, and matrix-assisted laser desorption/ionization time of flight/mass spectrometry (MALDI-TOF/MS) confirmed the purity of the peptides.

Before ASPD preparation, $A\beta_{1-42}$ (with or without 1/25 biotinylated $A\beta_{1-40}$) was completely dissolved in 1,1,1,3,3,3-hexafluoro-2-propanol (HFIP for HPLC; Kanto Chemical Co., Inc.) at 80-100 μM by incubating the peptide solution overnight at 4 ˚C and for another 3 hrs at 37 ˚C, and finally lyophilized (~40 nmol/tube). The $A\beta_{1-42}$ concentration in this step must be kept below 100 μM in order to maintain the monomeric state. This step was repeated three times. The lyophilized peptide was kept at -30 ˚C. We had long used HFIP from Sigma-Aldrich for lyophilization, and we recently found that this usually contained ~1.3 mM bis(2-ethylhexyl)phthalate (DEHP). This means that solutions of peptide lyophilized in Sigma-Aldrich HFIP usually contained ~0.65 mM DEHP when the final peptide concentration was 50 μM. Therefore, when we used HFIP in which DEHP was undetectable, we added DEHP (0.65 mM final

concentration; Tokyo Chemical Industry Co., Ltd.) when the lyophilized peptide was initially dissolved in anhydrous dimethyl sulfoxide (Sigma-Aldrich) in order to ensure consistency with our previous conditions (18-20).

Preparation of 20- to 30-nm Aβ aggregates. First, synthetic ASPD were prepared from 50 μM $A\beta_{1-42}$ and the flow-through fraction of 0.22-μm filters was obtained as usual. Then, the flow-through fraction was concentrated (to ~1/20 volume) by recovering highly condensed retentates of Sartorius 100-kDa MWCO filters. These concentrated retentates were immediately diluted ~10 times with 0.5x Dulbecco's phosphate-buffered saline without calcium and magnesium (PBS(-)). The Aβ aggregates thus produced were usually much larger than ASPD (mostly 20-30 nm in diameter), and showed low reactivity with ASPD-specific antibodies.

Primary neuronal cultures. Primary rat hippocampal cultures were prepared from embryonic day 17 pups and plated into 0.02% (w/v) polyethyleneimine (PEI; Sigma-Aldrich P3143)-coated wells at a density of 4.6×10^4 cells/cm^2 (Flexiperm), 4.3×10^4 cells/cm^2 (48-well plates), or 3.6×10^4 cells/cm^2 (Celldesk®; Sumitomo Bakelite) in neurobasal medium containing B27 supplement and 2.5 μM L-glutamine (18-20). After 3 days, half of the medium was replaced once a week with the above media additionally containing 10% (vol/vol) astrocyte-derived conditioned medium (ACM, Sumitomo Bakelite). Primary rat cerebellar neuronal cultures were prepared from embryonic day 20 pups essentially as reported (64) with some modifications. Briefly, cerebella, free of meninges and blood vessels, were prepared, cut into small pieces, and incubated in Ca^{2+}-Mg^{2+}-free Hanks' balanced salt solution (HBS; Invitrogen) containing 1% (wt/vol) trypsin (Invitrogen) and 0.05% (wt/vol) DNase I (Sigma-Aldrich) for 6 min at 37 ˚C. The pieces were washed three times with HBS, and tissues were dissociated by trituration with a fire-polished Pasteur pipette in HBS containing 0.05% (wt/vol) DNase I and 12 mM $MgSO_4$. Cells were collected by centrifugation for 5 min at 1000 × *g* at room temperature (r.t.), resuspended in culture medium containing basal medium Eagle (BME) (Sigma-Aldrich B9638) containing 10% (vol/vol) equine serum (HyClone) supplemented with 1 mg/ml bovine serum albumin (BSA; Sigma-Aldrich A3156), 10 μg/ml insulin (Sigma-Aldrich I1882), 0.1 nM L-thyroxine (Sigma-Aldrich T0397), 100 μg/ml transferrin (Sigma-Aldrich T1283), 1 μg/ml trypsin inhibitor, aprotinin (Sigma-Aldrich A1153), 30 nM selenium (Sigma-Aldrich S9133), 0.25% (wt/vol) glucose (Sigma-Aldrich G7021), 0.21% (wt/vol) $NaHCO_3$ (Sigma-Aldrich S5761), and 100 U/ml penicillin and 100 μg/ml streptomycin (Gibco 15140-122), and plated into 0.01% (wt/vol) poly-$_D$-lysine (Sigma-Aldrich P6407)-coated 48-well plates (Corning

CellBIND®) at a density of 2.5×10^5 cells/cm^2. After 48 hrs, the culture medium was completely changed to serum-free culture medium additionally containing 10 μM Ara-C. Thereafter, the medium was completely replaced twice a week with the above serum-free culture medium containing 10 μM Ara-C and the cells were grown in a 10% CO_2 atmosphere until ~23 DIV.

ASPD Toxicity. Toxicity was quantified by estimating apoptotic DNA fragmentation (Cell Death Detection ELISA^{plus}, Roche Diagnostics)(19) and was expressed as absorbance difference ($\Delta A_{405-450}$). To examine toxicity neutralization by ASPD-specific mASD3 antibody or inhibitors, neurons were preincubated for 2 hrs with mASD3 or for 30 min with each inhibitor before ASPD treatment**.** Inhibitors used are; tetrodotoxin (TTX), D-(-)-2-amino-5-phosphonopentanoic acid (D-APV), LY341495, nitrendipine, mibefradil dihydrochloride, KB-R7943 mesylate, CGP 37157, 2-APB, and SKF 96365 hydrochloride from Tocris; (+)-MK-801 maleate (MK801) from Calbiochem; 6,7-dinitroquinoxaline-2,3-dione (DNQX), and (RS)-α-methyl-4-carboxyphenylglycine (MCPG) from ALEXIS; ω-agatoxin IVA, *ω*-conotoxin GVIA, kurotoxin, and SNX 482 from Peptide Institute; cyclosporin A, dantrolene, and BAPTA-AM from Merck Millipore.

ASPD binding. Rat primary hippocampal neuronal cultures (19 DIV) were incubated with synthetic ASPD (400 μL/each well) for 30 min at 37 ˚C. After extensive washing with PBS at 37 ˚C, the cells were fixed and stained with rpASD1 (1.25 μg/ml), essentially as described under "Immunocytochemistry". Unbound ASPD in the medium were estimated by dot blotting (19, 20). Bound alkaline phosphatase was visualized by nitro blue tetrazolium/5-bromo-4-chloro-3-indolyl phosphate reaction (Pierce) in the presence of 1 mM levamisole and quantified by measuring the absorbance at 405 nm after solubilization (10).

Immunocytochemistry. Cells were rinsed with PBS at 37 °C, either fixed with 1% (wt/v**ol**) paraformaldehyde (PFA) in 0.1 M sodium acetate buffer, pH 6.0, for 20 min at 37 °C (for NAKα2 and NAKα3 staining), or fixed with 2% (wt/vol) PFA in PBS/neurobasal media (1:1) for 20 min at 37 °C and then with 4% (wt/vol) PFA in PBS for another 20 min at 37 °C (for other staining), and rinsed three times with PBS. The fixed cells were treated with 1 mg/ml $NaBH_4$ for 20 min at room temperature (r.t.), rinsed three times with PBS, permeabilized with 0.2% (vol/vol) Triton X-100 for 5 min at r.t., and rinsed three times with PBS. The cells were then pretreated with PBS containing 3% (wt/vol) BSA (Sigma-Aldrich) and 10% (vol/vol) normal goat serum (NGS) (IBL Co., Ltd.) for 45 min at r.t., and incubated overnight

with a primary antibody against ASPD (1.25 μg/ml rpASD1 or 0.51 μg/ml mASD3), MAP2 (2 μg/ml; mouse monoclonal HM-2, Sigma M4403), actin (1:250; mouse monoclonal clone C4, Millipore MAB1501R), NAKα2 (1:100; rabbit polyclonal, Upstate 07-674), or NAKα3 (0.4 μg/ml; rabbit polyclonal, Santa Cruz sc-16051-R) at 4 °C. After three washes with PBS, the cells were incubated with a highly cross-adsorbed secondary antibody in PBS containing 3% (wt/vol) BSA and 10% (vol/vol) NGS (1:1000; Alexa Fluor 568 anti-rabbit IgG, 1:1000; Alexa Fluor 488 anti-mouse IgG; Molecular Probes) for approximately 90 min at r.t. The cells were rinsed three times with PBS and mounted with Prolong Gold anti-fade reagent (Invitrogen). Fluorescence images were acquired using a cooled CCD camera CoolSNAP HQ (Roper Scientific) on a Zeiss inverted microscope Axiovert 200M with MetaMorph imaging software (Molecular Device Corp.) with laser intensity and signal detection settings held constant (19). Neuronal images were collected at 0.4 μm intervals to create a stack in the z-axis and a 2D rendering was made from the z stack to show neurites that would otherwise be out of focus (19).

To elucidate the specificity of anti-NAKα3 antibodies, NAKα3 expression was selectively knocked down in rat primary hippocampal neuronal cultures by infection at 5 DIV with AAV-miR-*ATP1A3* vector that contained an antisense sequence for rat *ATP1A3* and an enhanced *GFP* sequence (see "MicroRNA (miR) of *ATP1A3*" below) at the virus titer of 1×10^4 particle/cell for 5 days. The cultures were maintained in virus-free medium for another 15-20 days before experiments, with half of the medium replaced once a week (see "Primary neuronal cultures"). NAKα3 protein level, determined by Western blotting, was decreased to 19.8% of that of the mock control at 19-20 DIV, while NAKα1 protein level was not decreased (increased to 233%), by the AAV-miR-*ATP1A3* treatment. Consistent with this large decrease in NAKα3 protein level, little NAKα3 staining was observed and almost all the neurons infected by AAV-miR-*ATP1A3* vector (judged from GFP expression) died, except for a huge cell, also transfected with AAV-miR-*ATP1A3* vector, yet which was heavily stained by anti-NAKα3 antibodies and remained alive. Unlike the other mature hippocampal neurons, this AAV-miR-*ATP1A3* vector-resistant huge cell showed high levels of NAKα2 and MAP2, suggesting that it is likely to have immature neuronal characteristics. These results strongly suggest that AAV-miR-*ATP1A3* vector-resistant NAKα3 staining reflects cross-reactivity of anti-NAKα3 antibodies with NAKα2. We confirmed that the anti-NAKα2 antibody used here did not cross-react with NAKα3 in Western blotting. Consistent with this, ASPD did not bind to this AAV-miR-*ATP1A3* vector-resistant huge cell. As a result, as shown in Fig. 3*E*, punctate signals for ASPD and for NAKα3 were detected on neuropil and were almost exclusively co-localized with each other under the established staining conditions. Within z-stack image sets obtained from specimens prepared according to this protocol, we carefully examined whether these punctate signals

occurred on the plasma membrane or intracellularly and confirmed that individual puncta co-stained for ASPD and NAKα3 appeared to lie on the neuronal surface. In hippocampal neurons, NAKα3-staining was also observed diffusely and strongly in the soma, which was likely to reflect intracellular NAKα3 expression in ER. Binding of anti-NAKα3 antibody to nucleolus-like structures in the nuclei was observed occasionally in both NAKα3-expressing mature hippocampal neurons and NAKα3-non-expressing HEK293 cells (see Western blot in Fig. 3*C*), indicating non-specific binding of the antibody. Thus, it is reasonable that NAKα3-staining on the soma or the nucleolus-like structures did not co-localize with ASPD signals. Taking these results together, we conclude that ASPD and NAKα3 essentially co-localize on the neuronal surface, in particular on neuropil (see Fig. 3*E* Inset).

MicroRNA (miR) of *ATP1A3*. For the selective knockout of rat *ATP1A3* expression, miR-*ATP1A3* vector expressing an antisense sequence for rat *ATP1A3* (TTTACTGTGTGTCAGACCCTG) was generated based on murine miR-155 using the Invitrogen BLOCK-iT^{TM} system. As a control, miR-Mock vector containing Mock sequence (TATTGCGTCTGTACACTCACC) was produced. The above miR sequence was inserted into an expression cassette in which a human cytomegalovirus immediate-early promoter was followed by an enhanced *GFP* sequence, either miR-*ATP1A3* or miR-Mock vector, woodchuck hepatitis virus posttranscriptional regulatory element (nucleotides 1093-1684, GenBank accession number J04514), and simian virus 40 polyadenylation signal sequence. This expression cassette was inserted between the inverted terminal repeats of the AAV3 genome. This miR-expressing AAV3 vector was introduced into HEK293 cells with two helper plasmids, pAAV-2R1C (harboring the AAV2 rep and AAV1 cap genes) and pHelper (harboring *E2A*, *E4*, and *VA1* genes of the adenovirus genome; Agilent Technologies), using the calcium phosphate co-precipitation method. AAV particles (AAV-miR-*ATP1A3* vector or AAV-miR-Mock vector) were harvested and purified by two-sequential continuous CsCl gradient ultracentrifugation. Vector titers were determined by quantitative PCR of the DNase-I-treated vector stocks and estimated at 10^{12}-10^{13} vector genome.

Western and Far-Western Blotting and MS/MS. Whole-cell RIPA extracts (2 DIV or 19-25 DIV of rat primary neuronal cultures or HEK293 cells, 10 or 15 μg/lane) were separated under denaturing conditions on reducing NuPAGE 3-8% Tris-Acetate gels (Invitrogen) and bands were transferred onto 0.45 μm or 0.2 μm nitrocellulose membranes. For the detection of tau- or GSK3β-phosphorylation and p35/25, whole-cell RIPA extracts were obtained using PhosSTOP (Roche Diagnostics) and were separated under

denaturing conditions on reducing NuPAGE 12% Bis-Tris gels (Invitrogen). Bands were transferred onto 0.2 μm nitrocellulose membranes.

For western blotting, the membranes were blocked with 5% (wt/vol) skim milk for 1 h at r.t. and probed with a primary antibody against NAKα1 (0.1 μg/ml, US Biological A4000-52), NAKα2 (1/2,000; Upstate 07-674), NAKα3 (1 μg/ml, Santa Cruz sc16052), actin (1:500, Millipore MAB1501R), MAP2 (1:2000, Sigma M4403; 1:1000, Millipore AB5622), tau (1:1000, Millipore 577801 or Merck Millipore MAB2239), phospho-tau (Ser^{396}, 1:1000, Invitrogen 44752G; Ser^{404}, 1:1000, Sigma-Aldrich T7444-1VL), p35/25 (1:1000, Cell Signaling 2680), GSK3β (1:5000, Santa Cruz sc-9166), or phospho-GSK3β (Ser^{9}, 1:5000, Biosource 44-600G; Tyr^{216}, 1:5000, Millipore 05-413). Bands were detected with SuperSignal West Femto chemiluminescent substrates (Pierce) and quantified using a LAS-1000 Plus or LAS-4000 Mini (18).

For Far-western blotting, the membranes were blocked with 5% (wt/vol) skim milk for 1 h at r.t., washed three times with ice-cold F12 buffer without L-glutamine and phenol red, and incubated with either AD patient-derived ASPD (6.6 nM) or the purified synthetic ASPD (3.5 nM) as a ligand for 3 hrs at 4 °C. They were probed with haASD1 antibody (0.02 μg/ml) overnight at 4 °C, washed with TBS-T and incubated with highly cross-adsorbed anti-hamster antibody (1:5000) (Zymed Laboratories) for 1 h at r.t. Immunoreactions were detected and quantitated as described above (18). Far-western blotting was also performed using freshly dissolved $Aβ_{1-42}$ (100 nM) as a ligand, which was detected with anti-Aβ N-terminal antibody 6E10 (0.1 μg/ml) as described above.

For MS/MS analysis, the samples separated on NuPAGE gels were silver-stained using Silver Quest Silver Staining kit (Invitrogen). Silver-stained bands were excised, destained, and in-gel digested with trypsin. The proteins were reduced with 25 mM NH_4HCO_3-50% (vol/vol) acetonitrile and digested with trypsin (10 μg/ml) at 37 °C overnight. The tryptic peptides were recovered from the gel slices by incubating twice in 50% (vol/vol) acetonitrile-0.1% (vol/vol) trifluoroacetic acid at r.t. for 20 min and then by incubating in 100% (vol/vol) acetonitrile at r.t. for 5 min. At each incubation, the supernate was harvested and pooled. The pooled peptide extracts were desalted, evaporated to dryness, and subjected to MS/MS analysis (Bruker Ultraflex III MALDI-TOF/TOF mass spectrometer). Spectra were collected from 400 shots per spectrum over an m/z range of 1000–5000 and calibrated by 7-point internal calibration (m/z 1046.5418, 1296.6848, 1347.7354, 1619.8223, 2093.0862, 2465.1983, and 3147.4710). Monoisotopic peptide masses were assigned and used for Swiss-Prot primary sequence database searches with BioTools 3.1 software (Bruker-Daltonics) and the MASCOT search engine (Matrix Science). Search parameters were set as follows: a maximum allowed peptide mass error of 50 ppm and consideration of 1

incomplete cleavage per peptide. The known peptide masses of keratins, internal standards, and trypsin were excluded. For MS/MS, the most intense precursor ions with a signal/noise ratio of >25 were selected after exclusion of the common background signal.

Cell-free NAKα3 Production. NAKα3 protein for SPR analysis and for use as standards for quantifying neuronal NAKα3 was synthesized with the wheat germ cell-free protein synthesis system in the presence of asolectin liposomes (65). *ATP1A3* ORF DNA was cloned into pEU-E01-MCS vector, which was used as a template for *in vitro* transcription. Translation reaction was performed using the lipid bilayer method. A reaction mixture (25 µl) containing 10 µl (60 OD) of WEPRO7240 wheat germ extract (Cell-Free Sciences), 10 µl of mRNA, 40 µg/ml creatine kinase, and 10 mg/ml asolectin liposomes (65), was overlaid with 125 µl of SUB-AMIX SGC solution (Cell-Free Sciences) in flat-bottomed 96-well titer-plates. The reaction was performed for 16 hrs at 26 ˚C. To quantify NAKα3 levels, radiolabelled and unlabelled NAKα3 proteins were simultaneously prepared, except for addition of [^{14}C]leucine to both the upper and bottom layers in translation reaction of radiolabelled NAKα3. Each NAKα3/liposome complex was purified by centrifugation at 20,000 × *g* for 10 min at 4 ˚C and then resuspended into HEPES-buffered saline (HBS). This procedure was repeated 3 times. A portion of the purified (~60 %) ^{14}C-labelled NAKα3 was spotted on 3MM filter paper and ^{14}C-decay was measured by liquid scintillation (Hitachi-Aloka Medical). Based on the [^{14}C]leucine level of radiolabelled NAKα3, the concentration of simultaneously prepared unlabeled NAKα3 was accurately determined and used as a standard for quantifying neuronal NAKα3 levels in Western blotting. For SPR analysis, NAKα3 micelles were prepared as described below with the cell-free protein synthesis system. Large-scale translation was conducted by the dialysis method. Five-hundred µl of reaction mixture (60 OD of WEPRO7240 wheat germ extract, 125 µl of mRNA, 40 µg/ml creatine kinase, and 10 mg/ml asolectin liposomes) was prepared in a Thermo Scientific 10K MWCO Slide-A-Lyzer dialysis device, and the dialysis cup was immersed in 3.5 ml of dialysis solution (SUB-AMIX SGC, Cell-Free Sciences). The reaction was performed for 24 hrs at 15 ˚C. The NAKα3/liposome complex was purified by centrifugation and resuspension in HBS as described above. The purified pellet was suspended in 300 µl of a solubilization solution (200 mM HEPES-NaOH, pH 8.0, 750 mM NaCl, 4% (wt/vol) n-dodecyl-β-D-maltoside, 10% (vol/vol) glycerol, and 1 mM dithiothreitol). The suspension was sonicated using Branson Sonifier model 450 Advanced Cell Disrupters for 15 min at 20 ˚C, and centrifuged at 14,000 × *g* for 15 min at 4 ˚C. The supernate containing solubilized NAKα3 was collected and loaded on a Superdex 200 10/300 24-mL SEC column (GE Healthcare) for further purification (66). The concentration of the purified NAKα3

micelles was determined from the absorbance at 280 nm using an extinction coefficient of 94770 (67).

SPR. SPR was performed on a ProteOn XPR36 Protein Interaction Array System (BIO-RAD) with standard system software. About 900 RU (resonance units) of C-terminally biotinylated PD peptide was immobilized on the GLC chip, on which NeutrAvidin had been pre-coupled, according to the manufacturer's instructions. Association and dissociation of ASPD with each PD peptide were measured at 25 ˚C as a function of time (sensorgram). To examine direct interaction between ASPD and NAKα3, synthetic ASPD were diluted with a sodium acetate immobilization buffer (pH 4.5) and immobilized on the intermediate binding capacity-sensor chip GLM according to the manufacturer's instructions (~1600 RU of ASPD). Association and dissociation of ASPD with purified NAKα3 micelles (see "Cell-free Protein Production of NAKα3") were monitored as described above. Langmuir with Mass Transfer determined kinetic parameters in ProteOn Manager software (version 3.1).

Immunoprecipitation (IP). IP with haASD1 was performed using either an Immunocapturing Kit 100 MB-IAC Prot G (Bruker Daltonics 233794) or a Protein Capturing Kit MB-CovAC-Select (Bruker Daltonics 254733) as described previously using 3% (wt/vol) BSA (Sigma A7030) to suppress non-specific binding (19, 20). We confirmed that ASPD retained their structure and toxicity by means of TEM, dot blotting, and toxicity studies (19, 20). The ASPD amount was determined using dot blotting (19, 20). CoIP experiments were performed essentially as described above except that extracts were preincubated with ASPD (250 nM) for 30 min at r.t.

For Figs. 2 and 7, in order to remove other Aβ oligomers less than 100 kDa in mass, soluble extracts from AD or NCI brains were concentrated approximately 16 times using 100-kDa molecular mass cut off filters (Sartorius) (19, 20). IP was performed using N-hydroxysuccinimide (NHS)-Activated Magnetic Beads (Thermo Scientific), according to the manufacturer's instructions, except that BSA was used to suppress nonspecific binding. ASPD-specific haASD1 antibody or normal mouse IgG was coupled to NHS-magnetic beads. In order to remove nonspecific binding proteins to haASD1, pre-absorption of AD and NCI samples was performed with mouse IgG-coupled beads before antigen-antibody complex reaction. After a final washing step of the IP, the captured immunocomplex was separated by SDS-PAGE. The magnetic beads were resuspended in 20 μl of SDS-loading buffer without reducing agent and the beads were heated at 70 ˚C for 10 minutes. The beads were then removed and the supernatant was collected for SDS-PAGE under denaturing conditions on non-reducing NuPAGE 12% Bis-Tris gels (Life Technologies) in MES buffer. Then, silver staining was performed using SilverQuest Silver Staining kit

(Life Technologies), according to the manufacturer's instructions.

Rat primary hippocampal neuronal cultures (21 DIV) were washed twice with PBS at 37 ˚C, incubated with 10 nM streptavidin in PBS for 15 min at 37 ˚C, washed twice with F12 without L-glutamine and phenol red at 37 ˚C, and incubated with 53 nM biotinylated ASPD in F12 without L-glutamine and phenol for 30 min at 37 ˚C. After three washes with F12 without L-glutamine and phenol at 37 ˚C, the cells were extracted using 1% (wt/vol) n-octyl-β-D-thioglucopyranoside for 30 min on ice, and the lysate was centrifuged for 30 min at 16,000 × *g* at 4 ˚C. The biotinylated ASPD-ASPD binding protein complexes in the supernate were isolated using streptavidin magnetic beads (Promega) according to the manufacturer's protocol. The samples were separated on NuPAGE gels and silver-stained using SilverQuest Silver Staining kit (Invitrogen).

NAK activity. ATPase activities in membrane fractions were determined as described (40) with some modifications. Briefly, after vehicle or synthetic ASPD treatment, mature rat primary neuronal cultures (25-26 DIV) were extracted using 300 μl of lysis solution (20 mM Tris-HCl pH 7.5, 0.6 mM EGTA, 0.1 mM PMSF). The lysate was homogenized once using a Potter-Elvehjem homogenizer, and the homogenate was centrifuged for 5 min at 1,500 × *g*. The supernate was further centrifuged for 45 min at 120,000 × *g* at 4 °C. The pellet was suspended on ice in a buffer (20 mM Tris-HCl pH 7.5 and 0.1 mM EGTA), and the suspension was used as the membrane fraction. ATPase activities were determined using the membrane fraction (20-30 μg/assay) in 90 μl of a buffer (18 mM Tris-HCl pH 7.5, 80 mM NaCl, 15 mM KCl, 3 mM $MgCI_2$ and 0.1 mM EGTA) with or without ouabain at different concentrations (40). The level of inorganic phosphate was quantified as ATPase activity using MicroMolar Phosphate Assay Reagent (Profoldin**)**. The absorbance at 655 nm was measured and converted to the activity value by linear regression using a standard curve of phosphate ion standard solution (Wako). Since rodent NAKα3 is extremely sensitive to ouabain (IC_{50}=1.6 nM) (26), the activity of the rodent NAKα3 was determined by subtracting the ouabain-sensitive (100 nM) activity from the overall Mg^{2+}-ATPase activity (40).

Ca^{2+} and Na^{+} imaging. Primary rat hippocampal cultures (19-24 DIV) on Celldesk were washed with HSS buffer (5.4 mM KCl, 130 mM NaCl, 1 mM $CaCl_2$, 0.6 mM $MgCl_2$, 5.5 mM glucose, and 20 mM HEPES, pH 7.3) and loaded with 4 μM Fura-PE3AM (TEFLABs; a leakage-resistant Fura-2AM derivative that is retained in cells for hours) for 45 min at 37°C. The cells were mounted in the chamber where HSS buffer was perfused by a peristaltic pump at 37 ˚C. ASPD and other reagents were added to the perfusion line. Images were captured and processed using Metafluor software (Molecular Devices)

with a CCD camera (Hamamatsu Photonics ImagEM Model C9100-13) coupled to an Olympus IX70 microscope (Olympus). The cells were excited at 340 and 380 nm via a Lambda DG-5 light source (Sutter Instrument Co.) and emission at 500 nm was captured every 2 sec. The absorbance ratio at 340/380 nm is shown. In the case of sodium (Na^+) imaging, cultures were loaded with a Na^+ indicator, 2 μM Asante Na TRIUM Green TM-2AM (ANG-2AM) (K_d = 20 mM; excitation 488-517 nm; emission 540 nm; TEFLABs) for 30 min at 37 °C. Na^+ imaging was performed in essentially the same way as Ca^{2+} imaging, except that the cells were excited at 470-495 nm and emission at 510-550 nm was captured using an Olympus NIBA filter set. In our system, as described above, HSS buffer was circulated. The treatment of neurons with ASPD or other reagents was initiated by changing the circulating HSS buffer to HSS buffer containing ASPD or the sample reagent. After the buffer change, it usually took ~110 sec for HSS buffer containing ASPD or the sample to reach the assay chamber, and by ~17.5 min the solution in the assay chamber was completely replaced with HSS buffer containing ASPD or the sample.

Time-lapse. Confocal images of the culture in a thermostatic chamber (37 ˚C, 5% CO_2) were taken with a 20x objective for 24 hrs (6 images/hr) using a confocal laser microscope system A1 and NIS-Elements C software (Nikon). The time of cell swelling or shrinkage was quantified based on the time of each shot.

Dot blotting. Dot blotting was performed as described (19, 20) using 40 ng/ml ASPD-specific rpASD1 antibody in 5% skim milk with membrane boiling, 1/5000 anti-pan-oligomer A11 antibody (StressMark Biosciences Inc.) in 5% skim milk without membrane boiling, and 12.5 ng/ml anti-Aβ N-terminal 82E1 antibody in 10% skim milk without membrane boiling. Immunoreactions were detected with SuperSignal West Femto chemiluminescent substrates (Pierce) and quantified using a LAS-1000 Plus or LAS-4000 Mini (19, 20). In the case of synthetic ASPD, amounts were determined by quantitative amino acid analysis using a Waters AccQ-Tag system, according to the manufacturer's protocol, as in (19). In the case of patient ASPD, amounts of ASPD or Aβ in samples were obtained from a standard curve generated from serial dilutions of synthetic ASPD, the concentration of which was pre-determined as described above (see 19). The linear range of the assay is 0.3 – 3000 nM in equivalents.

TEM. Samples were negatively stained with 4% (wt/vol) uranyl acetate solution on carbon or elastic carbon-coated Formvar grids and then immediately analyzed at 100 kV (19, 20). ASPD images were captured at a direct magnification of 200,000 and the size of each spherical assembly was determined at the equator (19).

SEM. Rat primary hippocampal neuronal cultures (20 DIV on Aclar films from Nisshin EM Co., Ltd) were treated for the indicated time with 35 nM synthetic ASPD, fixed with 4% (wt/vol) paraformaldehyde, 0.005% (vol/vol) glutaraldehyde, 15% (vol/vol) saturated picric acid, 0.1% (wt/vol) tannic acid, and 1% (w/v) sucrose in 0.1 M phosphate buffer pH 7.4 for 20 min at 37 ˚C, and dehydrated through a 50, 70, 80, 90, 95, and 100% (vol/vol) ethanol series. After replacement of ethanol with 100% (vol/vol) *tert*-butyl alcohol, the samples were dried using a Hitachi freeze dryer ES-2030. The dried specimens were sputter-coated with osmium. The surface and morphology of the cells were examined by scanning electron microscopy (SEM) using a Hitachi model S-4500 field emission electron microscope operating at 15 kV.

Human brain pathology and ISH. We examined 5 clinicopathologically confirmed AD cases (as in (19)) and 5 control cases, among which samples with well-preserved RNA were used for the study. The cases used for this purpose were as follows (patient number, age, gender, disease duration, post-mortem (p.m.) sampling time, brain weight): AD patients (AD1, 86 yr, female, 23 yr duration, 4 hr p.m., 995 g; AD2, 100 yr, female, 6 yr duration, 3 hr p.m., 935 g; AD3, 87 yr, female, 9 yr duration, 3 hr p.m., 1000 g) and NCI cases (NC1, 76 yr, male, no AD symptoms, 3 hr p.m., 1220 g; NC2, 82 yr, male, no AD symptoms, 2 hr p.m., 1170 g; NC3, 79 yr, female, no AD symptoms, 3 hr p.m., 1100 g). Paraffin-embedded 4-μm sections of formalin-fixed brains were pretreated with microwaves for 30 min in 10 mM citrate buffer (pH 6.0), and treated with 0.3% (vol/vol) H_2O_2-methanol for 30 min followed by incubation with normal goat serum for 30 min at r.t. These sections were incubated overnight at 4 °C with primary antibodies against NAKα1 (US Biological A4000-52, 1:300) and NAKα3 (US Biological A4000-65c, 1:300), followed by incubation for 1 hr at r.t. with appropriate biotinylated secondary antibodies. Immunoreactivities were detected by the avidin-biotin-peroxidase complex method using a Vectastain ABC kit (Vector). The chromogen reaction was developed with diaminobenzidine/H_2O_2 solution. Counterstaining was carried out with Mayer's hematoxylin. Sections were viewed by using a light microscope (Olympus AX80T) and images were captured with a digital camera (Olympus DP70). It is well known that the distribution patterns of neurofibrillary tangles and of senile plaques in AD brains develop in a predictable sequence (68). We assessed the overall pathology of the AD brains according to the Consortium to Establish a Registry for Alzheimer's Disease (CERAD) criteria. Since severity of neuronal degeneration usually appears to be associated with the cellular burden, we evaluated it according to the staging system of neurofibrillary pathology by using a phosphorylation-specific anti-tau antibody

(clone AT8)(68). We considered the cases with stages III/IV and V/VI neurofibrillary pathology as corresponding to "moderate" and "severe" degeneration, respectively.

ISH was performed on paraffin sections with some modifications. Briefly, 10-μm sections were made from frontal cortex, cornu ammonis, and cerebellum. The digoxigenin-labelled riboprobes for *ATP1A1* (3189-3741 of human *ATP1A1* cDNA; accession number NM_000701.7) and *ATP1A3* (2882-3573 of human *ATP1A3* cDNA; accession number NM_001256213.1) were used and visualized with the Tyramide Signal Amplification (TSA) Biotin System (NEL700; Perkin-Elmer) according to the manufacturer's protocol. After ISH staining, the sections were counterstained using Methyl Green (Vector Laboratory). Bright-field images were acquired using a Nikon Eclipse E600 microscope with a Nikon DS-Ri1 CCD camera and NIS-Elements Microscope Imaging Software (Nikon Instrument Inc.).

Glycerol gradient sedimentation. Patient ASPD (~16 pmol in a volume of 0.2 ml) was layered on top of a 4 ml 15-30% (vol/vol) linear glycerol gradient in a Beckman Coulter 344057 tube. The tube was centrifuged in a Beckman Coulter SW55Ti rotor at 86,000 × *g* for 16 h at 4 °C. Fractions (0.35 ml each) were collected from the bottom of the tube. Fraction numbering begins with #1, which corresponds to the top 0.35 ml of fluid in the tube (the last fraction actually collected). Fractions were immediately dot-blotted to quantify Aβ content (see "Dot blotting"). Antibody 82E1 was used for Aβ and antibody rpASD1 was used for ASPD. Aliquots of selected fractions then were used in toxicity assays and for TEM. Standards (158 kDa, aldolase, 1 mg; 232 kDa, catalase, 0.3 mg; 440 kDa, ferritin, 4 mg; and 669 kDa, thyroglobulin, 0.5 mg) were centrifuged at the same time as were the ASPD, but in a separate tube, and used to determine the molecular mass of the ASPD fractions. Collected fractions of standard proteins were separated by SDS-PAGE using Novex 10-20 % Tricine gels and stained with a Colloidal Blue Staining Kit (Life Technologies). Densitometric analysis of each band was performed using an LAS-1000 Plus and the mobility shift of each standard protein thus determined was used to construct a standard curve of molecular mass versus relative mobility. Toxicity assays measured apoptotic cell death using propidium iodide and Hoechst 33258 (18). Briefly, after 24 h treatment, 19-22 DIV mature hippocampal neurons were gently rinsed and exposed for 30 min to 5 μM propidium iodide in a buffer (130 mM NaCl, 5.4 mM KCl, 5.5 mM glucose, 20 mM HEPES, pH 7.3, 2 mM $CaCl_2$) at 37 ˚C. Dye uptake was measured using a fluorescence microscope (Axiovert 200M, Zeiss) with a computer-assisted cooled CCD camera unit (CoolSNAP HQ, Roper Scientific) using band-pass filters appropriate for each probe, and analyzed with MetaMorph imaging software (Universal Imaging Corp., West Chester, PA, USA). Cells with shrunken or fragmented nuclear staining were counted as dead cells. The total cell number was assessed

by 1 μg/ml Hoechst 33258 nuclear staining after 10% formalin fixation. At least 400 cells were selected randomly from eight different fields. Data were expressed as the apoptotic ratio with respect to the total cell number. One unit is defined as the activity causing apoptosis in 1% of cells (determined by Hoechst 33258 staining)(18).

PD. A randomized 12-mer peptide library presented on M13 phages (Ph.D.^{TM}-12 phage display library kit; New England Biolabs) was used for screening against ASPD immobilized on an 8-well strip (compatible with a 96-well plate) (Mitsubishi Chemical Medience Corp.) (19). BSA-only-immobilized 8-well strips were also used. Biopanning was performed according to the manufacturer's instructions. Briefly, the phages were incubated in the synthetic ASPD-immobilized wells for 1 hr at 25 °C. To remove phages with low affinity to ASPD, the wells were washed ten times with TBS-T. Bound phage was eluted in 0.2 M glycine-HCl buffer (pH 2.2) and immediately neutralized with Tris. The mixture was then incubated in the BSA-only-immobilized wells four times to subtract non-specific binders. Finally, the phage was transfected into *E. coli*, amplified, and recovered. After the third round of this biopanning processes, the phage was cloned and sequenced using an ABI Prism^{TM} 310 genetic analyzer (Applied Biosystems).

NMR. ^{1}H-^{15}N HSQC spectra of both monomeric ^{15}N-A$\beta_{1\text{-}40}$ and ^{15}N-ASPD were recorded at 298 K on a 600 MHz Bruker *AVANCE*-III spectrometer equipped with a cryogenic TCI probe. Approximately 100 μM ^{15}N-A$\beta_{1\text{-}40}$ and 350 nM ^{15}N-ASPD in 0.5 x PBS (supplemented with 5% D_2O) were used. 128 and 512 scans were accumulated, respectively. The data were processed and analyzed with NMRPipe (69) and Sparky. ^{15}N-A$\beta_{1\text{-}40}$ backbone signal assignments were taken from the literature (70).

Molecular modeling. A three-dimensional homology model of human NAKα3 was constructed using the Prime program (Schrödinger). The structure of pig NAKα1 (32) was selected as a template (PDB code 3B8E). To further refine the model, all the coordinates of the hydrogen atoms and heavy atoms of side chains and main chains except backbone C and N atoms were optimized with the Merck Molecular Force Field (MMFF) using the MacroModel program (Schrödinger). During the optimization, an implicit water solvent model was employed, and a van der Waals cut-off of 8 Å and an electrostatic cut-off of 20 Å were used. Finally, the model was appended with the β and γ subunits of pig NAK (PDB code 3KDP) (32) by superimposing the α subunits on these subunits. The homology model was visualized by the program PyMOL (Schrödinger).

SI Discussion of definition of ASPD

In Hoshi *et al.* (18), two fractions of soluble Aβ aggregates were obtained from the slowly rotated Aβ solutions after glycerol gradient sedimentation: (1) non-toxic aggregates of mass ~60 kDa and diameter <10 nm by TEM (termed "non-toxic ASPD"); and (2) toxic aggregates of mass ~346 kDa and diameter 10-25 nm in TEM (termed "toxic ASPD"). Solution AFM studies have shown that these aggregates both have a height/width ratio of 1 (Fig. 2C of (18)), suggesting they are spheres. We thus refer to them as such. Structure-activity studies demonstrated that the 10-15-nm spheres were the toxic entities within the population of 10-25 nm structures (18). However, all spheres were considered ASPD at that time because we did not know whether any difference, other than size, existed between non-toxic and toxic spheres. In subsequent studies by Noguchi *et al.* (19), toxic ASPD were used as immunogens to produce ASPD-specific antibodies, which reacted robustly with 10-15 nm spheres but very weakly with Aβ monomers, dimers, or fibrils (Fig. 1B in (19)). These antibodies detected the toxic 10-15-nm ASPD, but not the non-toxic, smaller spheres or the non-toxic, larger spheres >15 nm in diameter (19). Furthermore, these antibodies selectively immunoisolated only the neurotoxic 10-15-nm spheres (Fig. 2B and C of Matsumura *et al.* (20)). Therefore, on the basis of neurotoxic activity and immunoreactivity, as well as size, we conclude that the 10-15-nm spheres are distinct from the spheres of diameter <10 nm and those of diameter >15 nm. These new data enable us to make our definition of ASPD more specific: namely ASPD are **"neurotoxic, spherical Aβ oligomers of 10-15-nm diameter (measured by TEM) that are recognized by ASPD-specific antibodies."** Additional details follow.

By using ASPD-specific antibodies, we found that ASPD were recovered in soluble fractions of patients' brains, but not from insoluble fractions, after treatment with 2% SDS or 70% formic acid [Figure S3 in Noguchi et al., (19)]. We selectively isolated 10-15-nm ASPD by a combination of 100-kDa retention and immunoprecipitation using ASPD-specific antibodies (purity >95%) [Figure 2G, H, I in Noguchi et al., (19)] and showed that the purified AD patient-derived ASPD were composed predominantly of $A\beta_{1-40}$ and $A\beta_{1-42}$ (by means of mass spectrometry) and were directly toxic to human mature neurons [Figure 2J, K in Noguchi et al., (19)]. We have thus proved that ASPD are present in AD patients' brains and we have defined the diameter, mass, and neurotoxicity of ASPD (Table S1).

To monitor ASPD formation *in vitro*, as well as to determine ASPD mass more accurately than with the glycerol gradient sedimentation analysis, we have developed a highly sensitive monitoring method using fluorescence correlation spectroscopy (FCS) combined with TEM and toxicity assays (20). With this method, we showed that the mass of 10-25 nm $A\beta_{1-42}$ aggregates containing predominantly

ASPD-sized, 10-15-nm spheres as major species is 330 ± 58 kDa (Fig. 1B 16.5 h in (20)), in good agreement with the result (~346 kDa) of the sedimentation assay in (18). As described above, from these ASPD-containing aggregates, we selectively immunoisolated pure (97%) 10-15-nm ASPD using the ASPD-specific antibody haASD1. This isolation procedure did not affect ASPD structure or neurotoxicity as described in (19). The 10-15-nm spheres were found to have a molecular mass of 128 ± 44 kDa (Fig. 2C in (20)).

To identify the receptor mediating toxicity of ASPD, in this work we used ASPD immunoisolated with the haASD1 antibody from the soluble brain extracts of the two AD patients displaying the most severe neurodegeneration and the highest ASPD concentrations among those shown in Fig. 2*A*. Importantly, these two patients were the same patients from whom we previously purified patient ASPD and characterized them in comparison with synthetic ASPD (19).. To confirm the mass of patient ASPD used in this work, we performed glycerol gradient sedimentation because we cannot apply our FCS method to patient ASPD. In our previous work (18), thyroglobulin (669 kDa) and ferritin (440 kDa), two marker proteins, both were recovered in the bottom-most fraction of the gradient. To enable resolution of assemblies in this mass size range, in the current work, we centrifuged the sample in a Beckman Coulter SW55Ti rotor, instead of the TLS55 rotor we originally used, which allowed us to resolve thyroglobulin and ferritin within two distinct fractions. Note that our ASPD preparation method involves initial filtration through a 100-kDa MWCO filter, which eliminates the smaller (<10 nm) non-toxic aggregates, which pass through filters. Our higher resolution glycerol gradient system yields 10-15 nm spheres (i.e., synthetic ASPD) in fractions 1-3, centered at ~120 kDa in mass (as described in the text in (19)), while larger spheres were recovered in fractions 4-5. Patient ASPD were similarly recovered in fractions 1-3, centered at fraction 2, and of ~120 kDa in mass (Fig. 2*E*). In Parthasarathy *et al.* (31), we compared the size of synthetic ASPD and that of patient ASPD in TEM images using Image J software. The analysis indicated identical diameters, within experimental error, for synthetic ASPD (11.0 ± 2.1 nm; n = 65) and patient ASPD (10.9 ± 1.7 nm; n = 34). These data collectively indicated that synthetic ASPD and patient ASPD are essentially identical in size and in mass.

With respect to the methods of preparation of ASPD, in the case of $A\beta_{1\text{-}40}$, ASPD are prepared from 350 μM $A\beta_{1\text{-}40}$ solution in 0.5x PBS (-) by slowly rotating the solution for 5-7 days at 37 ˚C (as described in (18)) or from 50 μM Aβ1-40 solution in 0.5x PBS (-) by slowly rotating the solution for 5-7 days at 4 ˚C (used in (20)). In either protocol, the level of $A\beta_{1\text{-}40}$-ASPD is maximally ~8%. In the case of $A\beta_{1\text{-}42}$, ASPD are formed in 50 μM $A\beta_{1\text{-}42}$ solution in F12 buffer without L-glutamine and phenol red by slowly rotating the solution for ~16 hrs at 4 ˚C as shown in (19, 20) and the current study, except for the

fluorescence-based study using FCS. Since FCS is highly sensitive to fluorescent materials, we used F12 buffer without riboflavin, L-glutamine, and phenol red in order to eliminate the fluorescent background. The level of $A\beta_{1-42}$-ASPD in the $A\beta_{1-42}$ solution after slow rotation is usually ~30 %. In addition to immunoisolation using ASPD-specific haASD1 antibody as described in (19, 20), synthetic ASPD are obtained by means of two-step filtration, in the fraction that passed through 0.22-μm filters, but was retained on 100-kDa MWCO filters (Sartorius), as described in (19). Synthetic ASPD were prepared every week and the quality was confirmed by dot blotting, TEM, amino acid analysis, and toxicity assays using 19-27 DIV hippocampal neurons. In this work, we also confirmed the *K*d of ASPD-specific rpASD1 antibody for synthetic ASPD each week using SPR. Patient ASPD were isolated by a combination of 100-kDa retention and immunoprecipitation using ASPD-specific antibodies (see "Immunoprecipitation (IP)" in *SI* Materials and Methods and "Human Brain Extracts" in Additional Experimental Procedures in Supplemental Data of Noguchi *et al.* (19). Patient ASPD are very stable, and our isolation procedures are highly reproducible, as evidenced by our ability to obtain essentially the same amounts of ASPD in multiple independent extractions and fractionations over time from the same patient's brain.

Discussion for a Plausible Mechanistic Explanation for Two Types of Ca^{2+}-Responses Induced by ASPD. Mitochondria have been considered to act as a spatial Ca^{2+} buffer by: (*i*) taking up excess cytoplasmic Ca^{2+} mainly through the rapid mode of calcium uptake (the RaM) and partly through the uniporter; or (*ii*) releasing Ca^{2+} mainly through the Na^{+}-dependent mechanism in neurons, to maintain cytoplasmic Ca^{2+} levels (71). At high ASPD concentrations (more than 40 nm), severe NAK impairment causes high levels of Ca^{2+} influx from VGCC, which will result in inactivation of the RaM. As a result, only the uniporter remains to sequester excess cytoplasmic Ca^{2+}. The capacity of the uniporter to do so is limited, which allows the initial sustained increase of cytoplasmic Ca^{2+} levels observed at high ASPD concentrations (Fig. 4C2). At low ASPD concentrations, because of moderate levels of Ca^{2+} influx from VGCC, both the RaM and the uniporter can take excess cytoplasmic Ca^{2+} into mitochondria and as a result cytoplasmic Ca^{2+} levels will increase transiently and then decrease rapidly, as observed. In either case (high or low ASPD), in spite of the presence of the mitochondrial Na^{+}/Ca^{2+} exchanger that releases excessive mitochondrial Ca^{2+}, owing to continuous Ca^{2+} influx from outside, mitochondrial Ca^{2+} levels will continue to increase and sooner or later will reach abnormal levels. Since levels of Ca^{2+} influx from outside will correlate with levels of VGCC activation, i.e. levels of NAK impairment, higher concentrations of ASPD will cause mitochondria to reach the abnormal Ca^{2+} level earlier. That would

explain why cytoplasmic Ca^{2+} levels did not plateau within two hrs in the case of 18 nM ASPD treatment. In either case (high or low ASPD), eventual prolonged Ca^{2+} overload in mitochondria has been reported to cause the mitochondrial permeability transition pore (MPT) to open (72). This mitochondrial calcium-induced calcium release through MPT opening as well as the mitochondrial Na^{+}/Ca^{2+} exchanger both cause the sharp Ca^{2+} increase after the initial sustained increase (Fig. S3*E*), leading to neuronal death induced by ASPD.

SI Discussion for the first and second categories shown in Fig. 8

The first system involves regulating the CNS concentration of Aβ monomer available for assembly. Whereas RAGE transports $A\beta_{1\text{-}40}$ or $A\beta_{1\text{-}42}$ into the CNS and increases brain Aβ levels (73), APOE stabilizes $A\beta_{1\text{-}40}$ or $A\beta_{1\text{-}42}$ through its binding, and as a result reduces brain Aβ levels available for assembly (74). The binding of APOE4 to $A\beta_{1\text{-}42}$ is slightly weaker than that of APOE3 (75), which could be the reason why APOE4 increases the risk for AD onset.

The second system involves post-synaptic neurons. Here, Aβ impairs synaptic connections by indirectly affecting NMDAR activity. $A\beta_{1\text{-}42}$ activates post-synaptic α7nAChR leading to NMDAR internalization (76). Binding of dimers/trimers to EPHB2 induces degradation of EPHB2 by proteasomes. Loss of EPHB2 has been reported to reduce cell-surface NR1 subunit of NMDAR and impair NMDAR-mediated synaptic connections in *APP* transgenic mice (9). Binding of Aβ oligomers larger than 500 kDa to PrP^{C} has been shown to activate FYN kinase, induce phosphorylation of the NR2B subunit of NMDAR, and facilitate a transient overexpression of NMDAR on the cell surface, leading to spine loss (77). Although ADDLs have been reported to co-immunoprecipitate with NMDR-containing synaptosomes (16), at present NMDAR is unlikely to be a direct target for Aβ. Recently, post-synaptic Sigma-2/PGRMC1 has been reported to serve as a receptor for 50~75 kDa $A\beta_{1\text{-}42}$ oligomers (43). It would be interesting in the future to examine whether $A\beta_{1\text{-}42}$ oligomers directly bind to Sigma-2/PGRMC1, and if so, how the $A\beta_{1\text{-}42}$ oligomers-Sigma-2/PGRMC1 interaction affects neuronal function.

AD is a progressive disease with risk highly correlated with ageing and with pathology that may vary due to micro-environmental and genetic differences among patients. Different receptor/ligand systems, as discussed above, thus may act synergistically or in a stage-dependent manner to contribute to AD pathogenesis.

SI FIGURE LEGENDS

Fig. S1. Effects of antagonists on ASPD neurotoxicity (DNA fragmentation) towards mature rat primary neuronal cultures (19 Day-In-Vitro (DIV)). Toxicity of synthetic ASPD (176 nM) towards mature neurons was blocked specifically by 2-hr pretreatment with 0.1 mg/ml ASPD-specific antibody mASD3, but not with the same concentration of another ASPD-specific antibody, haASD1, that detects a different epitope in ASPD, as we have shown previously (19). The antibody remained present during the overnight incubation with ASPD. This ASPD toxicity (176 nM) was unchanged by treatments with 1 μM TTX (a potent sodium channel blocker), or glutamate receptor antagonists (10 μM APV or MK801 for NMDA receptors, 100 μM DNQX for non-NMDA kainate or α-amino-3-hydroxy-5-methyl-4-isoxazole propionic acid (AMPA) receptors, 500 μM MCPG for metabotropic glutamate receptors (I/II), and 50 μM LY341495 for metabotropic glutamate receptors (II)). Mean ± SD; *, $p < 0.001$ Scheffé's *post-hoc* test, n = 3.

Fig. S2. Developmental NAKα3 expression and its binding to synthetic ASPD. (*A*) Representative TEM of negatively stained synthetic ASPD is shown on top. Representative Far-western blotting using 3.5 nM synthetic ASPD (left) and a silver-stained gel used for the Far-western blotting (right) are shown. Binding was detected using anti-ASPD antibody haASD1. RIPA extracts (15 μg/lane) of 2 DIV immature rat neurons (lane I) or 21 DIV mature rat neurons (lane M), or HEK293 cells (lane H) were used. Red arrows indicate a 105-kDa mature neuron-specific ASPD binding protein, NAKα3. MS/MS analysis of the other ASPD-detected bands, derived from immature neurons or HEK293, showed that these bands contained intracellular proteins such as α-spectrin2 (pink* at ~238 kDa), an uncharacterized protein (black* at ~171 kDa), heat shock protein gp96 (green* at ~110 kDa), and eukaryotic translational elongation factor 2 (blue* at ~110 kDa) (Fig. 3*A* and Fig. S2*A*). Postsynaptic Aβ receptors such as 35 kDa PrP^c, 40.4 kDa RAGE, 54.2 kDa α7nAChR, NMDAR (~100 kDa NR1 and 165 kDa NR2 subunits), 108 kDa EPHB2, were not detected among the ASPD-binding bands using MS/MS analysis. (*B*) Representative Far-western blotting using 3.5 nM synthetic ASPD detected by haASD1 antibody (left), 3.5 nM synthetic ASPD presaturated with 100 nM (equimolar in terms of $Aβ_{1-42}$ monomer concentration) haASD1 (middle), and haASD1 alone (right). RIPA extracts (15 μg/lane) were used. Red arrows indicate a 105-kDa mature neuron-specific ASPD binding protein, NAKα3. Asterisks have the same meaning as in *A*. (*C*) Developmental changes in the levels of NAKα3 and MAP2 were analyzed by Western blotting (representative blotting on the right). Data were normalized to actin and shown relative to each protein amount at 2 DIV. Mean ± SD; *, $p < 0.008$ compared with data at time 0 (Scheffé's *post-hoc* test, n = 3).

(*D*) Using biotin-labelled ASPD as a ligand, NAKα3 (red arrows) was co-immunoisolated from living mature neurons (see text). Far-western blotting using biotin-labelled ASPD is shown on the right. (*E*) Representative Z-stack images of 27 DIV hippocampal or 22 DIV cerebellar neurons, treated with 13 nM synthetic ASPD for 15 min were obtained as in Fig. 3*E*. The images showed anti-MAP2 (red) and anti-NAKα3 (green) staining.

Fig. S3. Representative Na^+ and Ca^{2+} imaging data. (*A*) Cytoplasmic Na^+ levels of mature rat hippocampal neuronal cultures (20-24 DIV), treated with vehicle (A_1), 300 nM ouabain (A_2), synthetic ASPD (38 nM in A_3, 59 nM in A_4), or 100 μM NMDA (A_5), were measured using a Na^+ indicator, ANG-2AM (TEFLABs) (see "Ca^{2+} and Na^+ imaging" in *SI* Materials and Methods). The treatment of neurons with ASPD or other reagents was initiated by changing the circulating HSS buffer to HSS buffer containing ASPD or the sample reagent. After the buffer change, it usually took ~110 sec for HSS buffer containing ASPD or the sample to reach the assay chamber (at the orange arrow) and at ~17.5 min the solution in the assay chamber was completely replaced with HSS buffer containing ASPD or the sample (at the yellow arrow). Treatment of neurons with 300 nM ouabain, which corresponds to 52 nM synthetic ASPD based on the average K_d values of ASPD (7.8 nM) and ouabain (45 nM (61-63)) for rat NAKα3, elicited a Na^+ increase similar to that induced by ASPD.

(*B*) Intracellular free Ca^{2+} level ($[Ca^{2+}]_i$) of cell bodies of mature rat hippocampal neurons (19-20 DIV), treated with vehicle, 18 nM, 42 nM, or 88 nM synthetic ASPD (at the orange arrow; see text in *A*), was measured using a leakage-resistant Ca^{2+} indicator, Fura-PE3AM (TEFLABs) (see "Ca^{2+} and Na^+ imaging" in *SI* Materials and Methods). The absorbance ratio at 340/380 nm is shown. The ratio of responsive cells was obtained as in Fig. 4*D*. Ca^{2+} levels were stable during vehicle treatment over 2 hrs, but increased transiently upon brief exposure to 100 μM glutamate, proving that the neurons remained responsive. With 18 nM ASPD, neurons showed repetitive Ca^{2+} spikes starting at the time of ASPD treatment. Higher concentrations of ASPD persistently increased $[Ca^{2+}]_i$, which showed a sudden rise to plateau levels. Higher concentrations of ASPD appeared to accelerate the process: with 35 nM ASPD, the initial Ca^{2+} response was transient, but a sustained increase was seen after 2-hr treatment (Fig S3C_1), whereas with 88 nM ASPD, $[Ca^{2+}]_i$ usually reached a plateau within 1 hr. Note that the data of 42 nM ASPD is also shown in Fig. 4*C2*.

(*C*) C_1, 35 nM synthetic ASPD caused repeated transient increases in $[Ca^{2+}]_i$ of neurons, leading to a sustained increase after 2-hr treatment. C_2, EGTA inhibited ASPD-induced increase in $[Ca^{2+}]_i$ of mature neurons (see text).

(*D*) $[Ca^{2+}]_i$ was monitored as described in *B* in mature rat hippocampal neurons (19 DIV) treated with 16 nM synthetic ASPD, with or without preincubation with 4 μM ω-conotoxin (N-type VGCC specific inhibitor) or 20 μM peptides derived from the 4th extracellular loop (Ex4) of NAKα3 (see Fig. 7 *C*-*G*). The inhibitor was present while neurons were labelled with Fura-PE3AM for 40 min and was also present during the ASPD treatment. The peptides were preincubated with ASPD for 60 min on ice and were also present during the ASPD treatment.

(*E*) $[Ca^{2+}]_i$ changes of rat hippocampal neurons (24 DIV), treated with 50~80 nM synthetic ASPD, with or without 40-min preincubation with 20 μM cyclosporin A (an inhibitor of MPT pore opening) and/or 3 μM CGP37157 (a mitochondrial NCX inhibitor), were monitored as in *B*. The inhibitors were present while neurons were labelled with Fura-PE3AM and were also present during the ASPD treatment. Representative data are shown in E_1. Quantification of the data from three independent experiments (Mean ± SD) is shown in E_2. In the case of ASPD-treated neurons, the second sharp Ca^{2+} rise was seen almost exclusively after the initial sustained $[Ca^{2+}]_i$ increase. As shown in Fig. S3E_2, treatment of neurons with cyclosporin A, CGP37157, or both did not affect this initial sustained $[Ca^{2+}]_i$ increase in terms of the responsive cell number and the response level (=$[Ca^{2+}]_i$ Δ[first peak height-baseline]). In contrast, treatment of neurons with these inhibitors markedly impaired the ASPD-induced second sharp $[Ca^{2+}]_i$ rise in terms of both the responsive cell number and the response level (=$[Ca^{2+}]_i$ Δ[second peak height-first peak height])(*, $p < 0.001$; **, $p < 0.0001$ compared with ASPD alone using the Scheffé's *post-hoc* test, n = 3). In ASPD-treated neurons, the second sharp $[Ca^{2+}]_i$ rise, once it occurred, was saturated without decline, but in the presence of MPT pore opening inhibitor (cyclosporin A), the number of neurons showing this sharp $[Ca^{2+}]_i$ rise was markedly decreased, or, if the sharp $[Ca^{2+}]_i$ rise occurred, it gradually declined (not saturated) to the initial sustained level after it had reached the peak (Fig. S3E_1). The mitochondrial NCX inhibitor strongly inhibited occurrence of the sharp $[Ca^{2+}]_i$ rise, and a gradual increase of $[Ca^{2+}]_i$ was seen, instead of the sharp $[Ca^{2+}]_i$ rise, after the initial sustained $[Ca^{2+}]_i$ increase (Fig. S3E_1). Treatment with both cyclosporin A and CGP37157 appeared to inhibit the ASPD-induced second sharp $[Ca^{2+}]_i{}^+$ rise more potently than the single treatments. These results suggest that mitochondrial NCX and MPT pore openings are both involved in ASPD neurotoxicity.

(*F*) Effects of 100, 300, and 500 nM ouabain, which correspond to 17, 52, and 87 nM ASPD, respectively, based on the average K_d values of ASPD (7.8 nM) and ouabain (45 nM (61-63)) for rat NAKα3. Ouabain elicited the same phenomena triggered by ASPD, including increases in $[Ca^{2+}]_i$, activation of CDK5, increase in the Tyr^{216} phosphorylated active form of TPKI/GSK3β, tau phosphorylation/destabilization, and MAP2 destabilization, except for decrease in the Ser^9

phosphorylated inactive form of TPKI/GSK3β (see Figs. S3*B* and 5*C*-*F*). The reason for the difference in the case of Ser^9 is not clear at present. These data further support the conclusion that ASPD-induced NAKα3 impairment is the main cause of these phenomena. Mean ± SD; *, $p < 0.02$ Scheffé's *post-hoc* test, n = 3.

Fig. S4. Time lapse images of ASPD-treated neurons and human studies. (*A*) Representative time-lapse images of mature rat hippocampal neurons treated with each reagent (see Videos S1-4). (*B*) Immunohistochemical studies of non-clinically demented individual (NCI) and Alzheimer's disease (AD) brains using anti- NAKα1 (see text). Bar = 50 μm (*C*) ISH analyses using probes for *ATP1A3* (NAKα3) and *ATP1A1* (NAKα1) on 10-μm paraffin-embedded adjacent sections.

Fig. S5. ASPD-binding peptides inhibit both ASPD binding to NAKα3 and other ASPD-induced downstream phenomena. (*A*) SPR analyses were performed as in Fig. 3*F*. Ex4 of NAKα3 bound to synthetic ASPD, but Ex1 did not. Representative data are shown. (*B*) Inhibition of synthetic ASPD (50 nM) binding to mature hippocampal neurons by the peptides (20 μM). ASPD-binding sites (red) and anti-NAKα3 staining (green) were detected as in Fig. 3*E*. (*C*) Activation of TPKII/CDK5 and TPKI/GSK3β was determined by Western blotting as shown in Fig. 5*C* and 5*D*, respectively. Ex4 peptides were treated as in Fig. S3*D*. ASPD-binding Ex4 peptides (final concentration 20 μM) significantly inhibited activation of these tau-phosphorylating kinases induced by 6-hr treatment with 35 nM synthetic ASPD. Mean ± SD; *, $p = 0.011$ for TPKII/CDK5; 0.050 for pTyr216; 0.028 for pSer9 by Scheffé's *post-hoc* test, n = 3.

Fig. S6. Interference with aberrant ASPD-NAKα3 interaction by masking the Aβ oligomer surface with specific masking peptides or peptidomimetics. ASPD (7.2 ± 2.6 nm in diameter) bind and cause death of mature neurons. Molecular modeling suggests that the mature heterotetrameric NAK pump forms a 9.9 nm-wide opening. This diameter is similar to that of *in situ* ASPD (7.2 ± 2.6 nm in diameter) and the Ex4 region, which is essential for the ASPD-NAKα3 interaction, is on the edge of the opening. Based on these data, we present a possible model of ASPD-NAKα3 interaction (left). Given the essential functions of the NAK pump in neurons, direct modulation of the NAK pump would be a risky approach. We propose a new strategy to interfere with the aberrant ASPD-NAKα3 interaction by masking the Aβ oligomer surface with specific masking peptides or peptidomimetics (right).

Video Legends

Video S1. Primary rat hippocampal mature neurons (19-25 DIV) were imaged at intervals of 10 min for 11 h (see "Time-lapse" in *SI* Materials and Methods) after the administration of 141 nM ASPD at 20x magnification. The time-lapse videos were shortened (1 sec = 20 msec).

Video S2. Primary rat hippocampal mature neurons (19-25 DIV), treated with 100 nM ouabain, were imaged as in Video S1 at 20x magnification.

Video S3. Primary rat hippocampal mature neurons (19-25 DIV), treated with 1 μM staurosporine, were imaged as in Video S1 at 20x magnification.

Video S4. Primary rat hippocampal mature neurons (19-25 DIV), treated with vehicle, were imaged as in Video S1 at 20x magnification.

Table S1 Summary of the Characteristics of ASPD Reported Previously (18-20) And Found in this Work

	Synthetic ASPD	AD patient-derived native ASPD
Source	▪ Synthetic $A\beta_{1-40}$ or $A\beta_{1-42}$ ▪ Identified as the most toxic entities either in $A\beta_{1-40}$ solutions (50 μM in 0.5x PBS(-), slowly rotated for 5-7 d at 4°C) or in $A\beta_{1-42}$ solutions (50 μM in 0.5x PBS(-) or F12 media without L-glutamine and phenol red, slowly rotated for 14-16 h at 4°C) ▪ Obtained by two-step filtrations as the 100-kDa retentates of the 0.22-μm filtrates ▪ Purified (~97%) by immunoprecipitation using ASPD-specific haASD1 or mASD3 antibody	▪ Hippocampus or cerebral cortex of AD patients (not cerebellum cortex of AD patients) ▪ Increase with the disease severity and duration, along with the increase in neurodegeneration† ▪ Ultracentrifuge supernatant of the extracts of AD brains, homogenized in F12 media without L-glutamine and phenol red (no detergents) ▪ Purified (>95%) by immunoprecipitation using ASPD-specific haASD1 or mASD3 antibody from the 100-kDa retentates of the above supernatant ▪ $A\beta_{1-40}$ and $A\beta_{1-42}$ are detected as major components by MS analysis and by silver staining†
Size of active components	▪ 10- to 15-nm spheres in TEM (11.8 ± 2.1 nm; n = 94)* ▪ Complete spheres y/x = 0.982 (n = 100; in TEM) height/diameter = 1.0 (n = 100; solution AFM) ▪ ASPD mass peak is ~120 kDa in 15-30% glycerol gradient sedimentation assays (slightly smaller than 158-kDa aldolase). ▪ ASPD (purified (97%) using ASPD-specific haASD1 antibody) is 128 ± 44 kDa in mass (FCS) ~30 ± 10 mers (using 4.5 kDa for $A\beta_{1-42}$) 7.2 ± 2.6 nm in height (solution AFM)	▪ 10- to 15-nm spheres in TEM (11.9 ± 1.7 nm; n = 108) * ▪ ASPD mass peak is 123 ± 20 kDa (n = 3)(slightly smaller than 158-kDa aldolase) in 15-30% glycerol gradient sedimentation assays†. ▪ The size of ASPD is estimated to be 128 ± 44 kDa in mass 28~30 ± 10 mers (using 4.3 kDa for $A\beta_{1-40}$ and 4.5 kDa for $A\beta_{1-42}$) based on FCS analysis of synthetic ASPD
Structural characteristics	▪ Originate from trimer ▪ A11-negative in dot blotting ▪ ASPD-specific antibodies (rpASD1, mASD3, haASD1, etc.)-positive in dot blotting ▪ Immunoprecipitated by haASD1 or mASD3 antibody, but not by 6E10	▪ A11-negative in dot blotting† ▪ ASPD-specific antibodies (rpASD1, mASD3, haASD1, etc.)-positive in dot blotting ▪ Immunoprecipitated by haASD1 or mASD3 antibody, but not by 6E10 ▪ Bind to a 105-kDa band in mature

	▪ Solution NMR analysis indicated the presence of one defined structure in the ASPD sample and determined the amino acid sequences exposed on the ASPD surface†, which are consistent with the previous epitope map of ASPD obtained by ASPD-specific antibodies. ▪ Bind to a 105-kDa band in mature neurons in Far-western ligand binding assay†	neurons in Far-Western ligand binding assay†
Biological effects	▪ Activate both TPKI/GSK-3β and TPKII/CDK5 and increase tau phosphorylations† ▪ NMDAR independent neuronal cell death of mature neurons ▪ Nontoxic against non-neuronal cells or immature neurons (human, monkey, and rat origins) ▪ Toxicity is neutralized by ASPD-specific antibodies (rpASD1 and mASD3) but not by 6E10 or 82E1 antibody. ▪ Impair NAKα3 activity in mature neurons† ▪ Activate N-type voltage gated calcium channels and cause mitochondrial calcium dyshomeostasis† ▪ Induce loss of tau and MAP2†	▪ Cause neuronal cell death of mature neurons ▪ Nontoxic to non-neuronal cells or immature neurons (human) ▪ Toxicity is neutralized by ASPD-specific mASD3 antibody. ▪ Colocalize with NAKα3 and this binding is inhibited by ASPD-binding peptides†

*Calculated from the data in Noguchi et al. JBC 2009

†Data from the current work

Table S2 Summary of the MS/MS analysis of ~105 kDa bands in Fig. S2*A*

Sample	MS hit	MS hit peak	MS/MS peak	MS/MS protein	Mass	pI
2 DIV	-	-	1081	heat shock protein gp96†	92713	4.72
	-	-	2030	heat shock protein gp96†	92713	4.72
21 DIV	NAKα3	776				
		1030				
		1158				
		1268				
		1284				
		1296				
		1055				
		1619	1619	NAKα1, -2, -3	111664	5.26
		1659	1659	NAKα3	111664	5.26
		1158				
		1431				
		1490				
		1766				
		1829	1829	NAKα1, -2, -3	111664	5.26
		1867				
		1236				
		2505				
		2464				
		2480				
		2505				
		2866				
		2882				
		1442				
	-	-	1501	adaptor-related protein complex 2 β1 subunit†	105625	5.19
	-	-	1709	dynamin I*	95867	6.32
	-	-	1400	hexokinase I*	102342	6.29
	-	-	1081	heat shock protein gp96†	92713	4.72
HEK	-	-	1799	eukaryotic translation elongation factor 2†	95277	6.41
	-	-	2220	eukaryotic translation elongation factor 2†	95277	6.41
	-	-	1081	heat shock protein gp96†	92713	4.76

The MALDI-TOF/MS analyses of three independent experiments are shown. In each sample, the results are shown in high hit score order. NAKα3 is the only protein that was detected by MS analysis, and this was confirmed by further MS/MS analyses. Proteins that were not detected by MS are considered insignificant.

*; detected only in one run only by MS/MS (without MS hit)

†; detected only by MS/MS (without MS hit)

Table S3 Summary of the representative Aβ ligand/target systems

Target	Target character	Ligand	Binding mode	Mechanism
Sigma-2/ PGRMC1 (43)	▪ 21.6 kDa* ▪ Heme-binding protein, co-purified with progesterone binding proteins in liver ▪ Possible roles in cell survival and apoptosis ▪ High expression in liver and kidney, lower expression in lung, brain, in humans (. expression in liver, lung, e.g., kidney, and brain in rodents) ▪ Post-synaptic localization in neurons	Aβ1-42 oligomers (50-75 kDa mixtures)	▪ K_d = 518 nM for neuronal cultures（using Aβ1-42 oligomers） ▪ PGRMC1 siRNA reduced oligomer binding to neurons.	▪ PGRMC1 levels increased ~30% after 48 h oligomer treatment. ▪ Aβ1-42 oligomers facilitate membrane trafficking (MTT assay), which is inhibited by small compounds that inhibit oligomer binding to neurons.
APOE (78)	▪ 34.2 kDa glycoprotein* ▪ A major component of very low-density lipoproteins (VLDLs). VLDLs maintain normal levels of cholesterol and triglyceride in systemic tissues by carrying these lipids from the liver. ▪ E2, E3, E4 isoforms (E4 as a risk factor for AD) ▪ High expression in liver and in astrocytes in brains	Aβ1-40 Aβ1-42	▪ Direct binding of purified APOE to Aβ on the microplate. ▪ K_d = 48.1 nM for E2; 63.7 nM for E3; 75.9 nM for E4 (using Aβ1-42) ▪ 1:1 binding ▪ Lys16 of Aβ binds to Lys72, 75, 95, 143, 157 and 242 of APOE.	▪ Binding of APOE to Aβ prevents formation of Aβ fibrils. APOE stabilizes extracellular Aβ monomers and may reduce the extracellular Aβ concentration of Aβ monomers available for fibril formation.
PrP^C (10, 79)	▪ 35-36 kDa* ▪ GPI-anchored protein ▪ PrP^C's physiological function is a complex issue that requires further studies. ▪ Ubiquitous expression. Greater expression in CNS, spinal cord, and thymus, less in the other tissues. ▪ Localization in synaptic connections and in astrocyte in brains.	Aβ1-42 oligomers (~500 kDa in SEC)	▪ Direct binding of purified PrP^C and Aβ1-42 oligomers using SPR ▪ K_d = 50~100 nM for neuron cultures (using Aβ1-42 oligomers); K_d = 71 nM with EPR spectroscopy ▪ PrP^C 23-27, 92-110 are both critical for binding to Aβ1-42 oligomers.	▪ Post-synaptic PrP^C mediates activity of certain type of Aβ oligomers (mitochondria dysfunction, reactive oxygen species production, Ca^{2+} influx and LTP suppression). ▪ Binding of Aβ oligomers activates FYN kinase, induce phosphorylation of NR2B subunit of NMDAR, and facilitate transient overexpression of NMDAR on the surface, leading to spine loss.
RAGE sRAGE (80)	▪ 40.6 kDa* ▪ Multi-ligand receptor of the IgG superfamily (several ligands known including Aβ) ▪ Expression in the blood-brain barrier (BBB), glia, microglia, and neurons ▪ Post-synaptic localization in neurons	Aβ1-40 Aβ1-42	▪ Direct binding of ^{125}I-Aβ to purified RAGE on the microplate ▪ K_d = 55 nM for rat neuronal cultures（using Aβ1-40）	▪ RAGE mediates Aβ transport across BBB into CNS. ▪ RAGE inhibitors markedly reduced Aβ40 and Aβ42 levels in brain and normalized cognitive performance in aged *APP^{swe}* mice. ▪ RAGE mediates Aβ-induced oxidant stress in neurons and activation of microglia.
α7nAChR (81)	▪ Homopentamer (54.1 kDa)* ▪ Neuronal nicotinic AChR ▪ Abundant pre- and post-synaptic distributions	Aβ1-42	▪ Direct binding of Aβ1-42 to purifid α7nAChR by co-immunoprecipitation ▪ K_d ~ pM and nM ranges for α7nAChR-expressing N-MC cell membrane (using Aβ1-42 monomers) ▪ N-terminal domain of α7nAChR is involved in binding.	<u>Neuroprotective Effects:</u> ▪ Aβ1-42 monomers activate pre- and post-synaptic α7nAChR, promote calcium influx, enhance neurotransmitter release, and trigger protective signals such as ERK. <u>Pathologic Effects:</u> ▪ Aβ1-42 activates post-synaptic α7nAChR, promotes NMDAR internalization. ▪ ADDLs inactivate α7nAChR, impair LTP probably through

				NMDAR.
EPHB2 (9)	▪ 108.1 kDa* ▪ EPH B2-type receptor tyrosine kinase ▪ Pre- and post-synaptic distributions	Aβ1-42 oligomers Dimers/trimers	▪ Direct binding of Aβ1-42 oligomers to purified EPHB2-Fc chimaera by co-immunoprecipitation ▪ K_d undetermined ▪ Fibronectin type III repeats domain of EPHB2 is involved in binding.	▪ Dimers/trimers induce degradation of EPHB2 by the proteasome in neuronal cultures. ▪ Loss of EPHB2 reduce surface NR1 of NMDAR and impairs NMDAR-mediated synaptic connections in h*APP* mice.
NMDAR (12, 16, 82)	▪ Heterodimer (97.3 kDa for NR1; 132.3-165.2 kDa for NR2A, B, C, D)* ▪ Post-synaptic localization	ADDLs (3~24-mers mixtures)	▪ Synaptosomes (containing PSD95, NR1 and NR2A/2B) and ADDLs were co-immunoprecipitated by anti-ADDL antibody. ▪ Knockdown of NR1 with its anti-sense reduced ADDL binding to neurons.	▪ Morphology change and loss of spines are induced by ADDLs and dimers through NMDAR.
NAKα3 (current work)	▪ 111.7 kDa* ▪ Neuron-specific catalytic subunit of NAK pump ▪ Mainly pre-synaptic localization	ASPD (128 kDa on average)	▪ Direct binding of ASPD to recombinant human NAKα3 by SPR ▪ K_d = 28.6 nM (using NAKα3 by SPR) ▪ 1:1 binding of ASPD to $(NAK\alpha3)_2(NAK\beta1)_2$ heterotetramer ▪ RLNW motif in extracellular loop 4 is involved in binding.	▪ ASPD directly bind to NAKα3, impair its activity, which activate N-type VGCC and induce calcium dyshomeostasis in cytoplasm and mitochondria, induce tau phosphorylation and loss, and degenerate mature neurons. ▪ Tetrapeptides inhibit ASPD binding and protect neurons from ASPD-induced death.

*Human protein's mass value is shown.

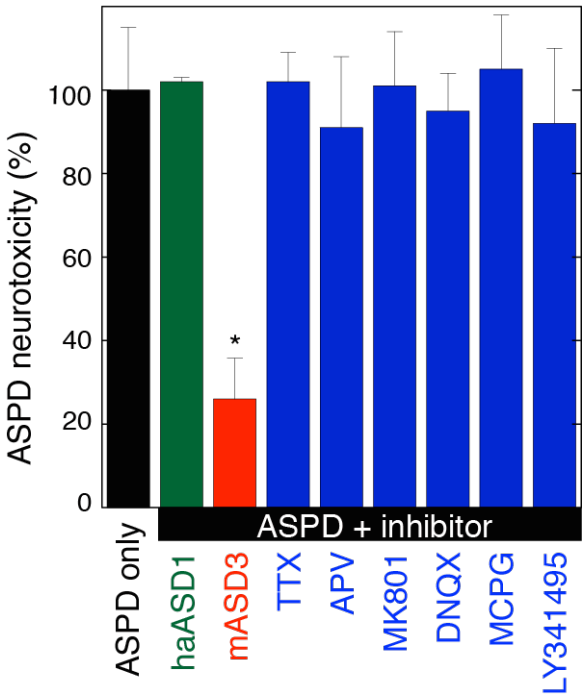
ASPD neurotoxicity (%)
100
80
60
40
20
0
*
ASPD + inhibitor
ASPD only
haASD1
mASD3
TTX
APV
MK801
DNQX
MCPG
LY341495

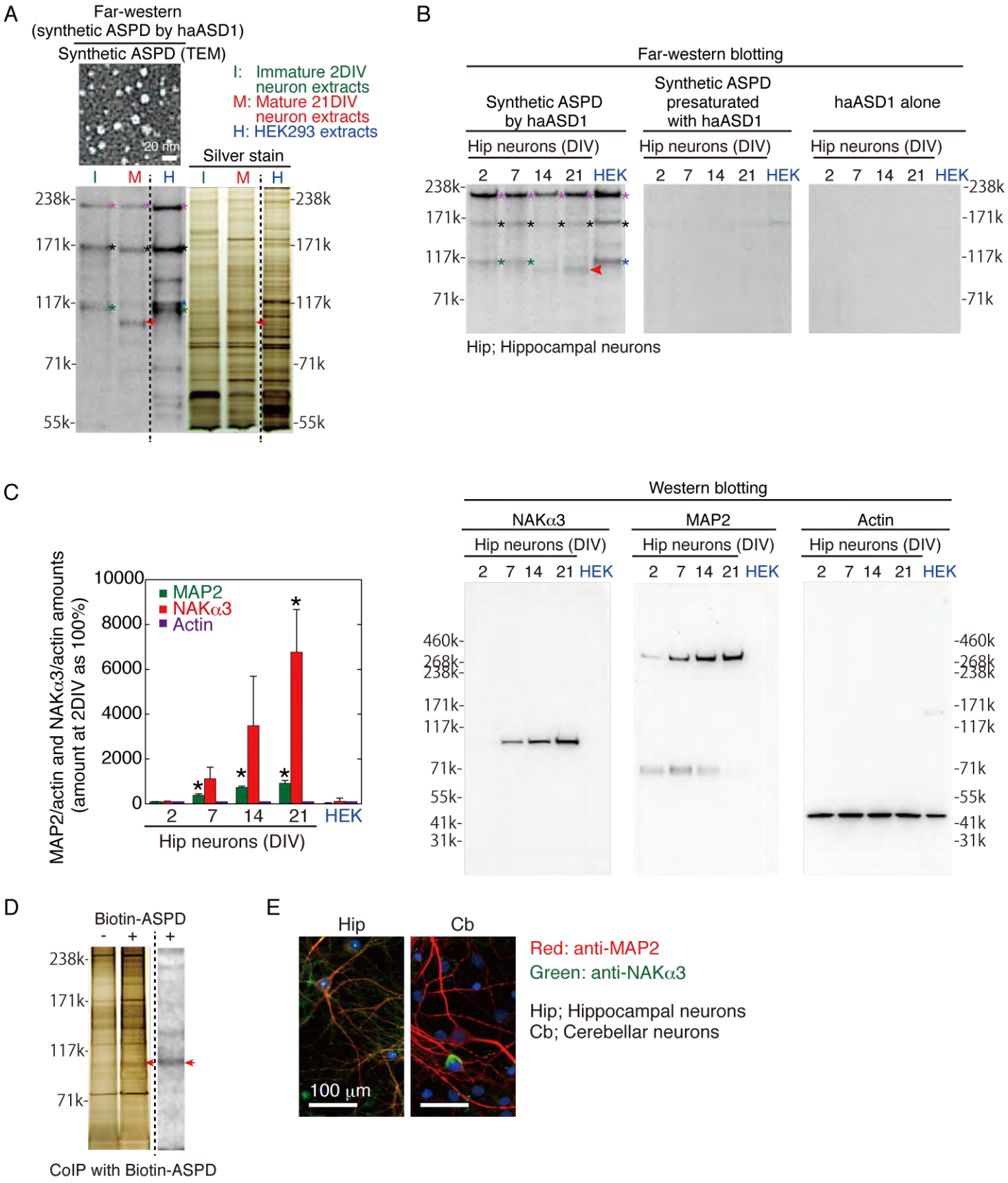
A
Far-western
(synthetic ASPD by haASD1)
Synthetic ASPD (TEM)
20 nm
I: Immature 2DIV neuron extracts
M: Mature 21DIV neuron extracts
H: HEK293 extracts
Silver stain
I M H I M H
238k-
171k-
117k-
71k-
55k-
B
Far-western blotting
Synthetic ASPD by haASD1
Synthetic ASPD presaturated with haASD1
haASD1 alone
Hip neurons (DIV)
2 7 14 21 HEK
Hip; Hippocampal neurons
C
MAP2/actin and NAKα3/actin amounts (amount at 2DIV as 100%)
MAP2
NAKα3
Actin
Hip neurons (DIV)
Western blotting
NAKα3
MAP2
Actin
460k-
268k-
238k-
171k-
117k-
71k-
55k-
41k-
31k-
D
Biotin-ASPD
CoIP with Biotin-ASPD
E
Hip
Cb
100 μm
Red: anti-MAP2
Green: anti-NAKα3
Hip; Hippocampal neurons
Cb; Cerebellar neurons

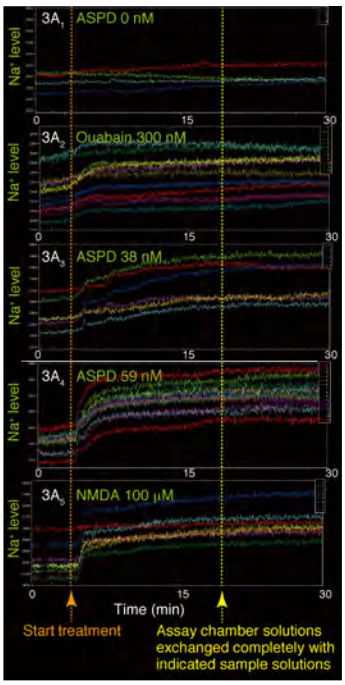
3A1 ASPD 0 nM
3A2 Ouabain 300 nM
3A3 ASPD 38 nM
3A4 ASPD 59 nM
3A5 NMDA 100 μM
Na+ level
Time (min)
Start treatment
Assay chamber solutions exchanged completely with indicated sample solutions

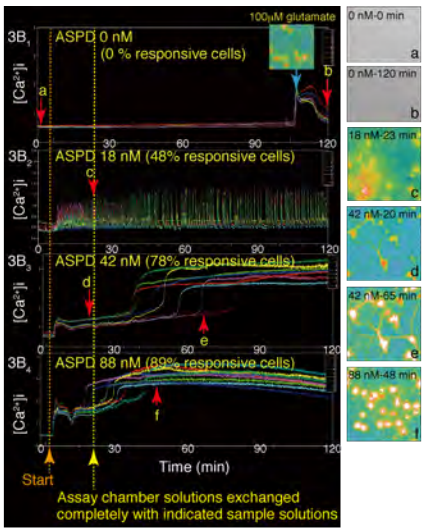
100μM glutamate
3B1 ASPD 0 nM (0 % responsive cells)
3B2 ASPD 18 nM (48% responsive cells)
3B3 ASPD 42 nM (78% responsive cells)
3B4 ASPD 88 nM (89% responsive cells)
0 nM-0 min
0 nM-120 min
18 nM-23 min
42 nM-20 min
42 nM-65 min
98 nM-48 min
[Ca2+]i
Time (min)
Start
Assay chamber solutions exchanged completely with indicated sample solutions

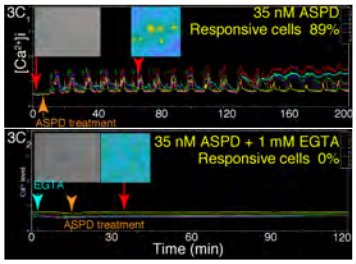
3C1 35 nM ASPD Responsive cells 89%
3C2 35 nM ASPD + 1 mM EGTA Responsive cells 0%
EGTA
ASPD treatment
Time (min)

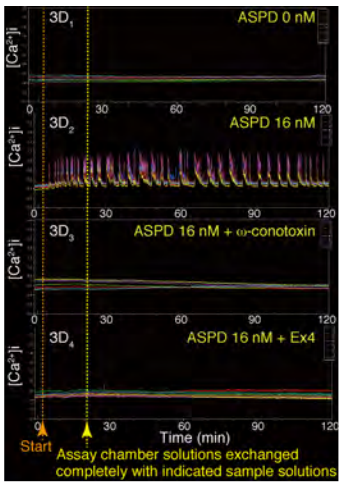
3D1 ASPD 0 nM
3D2 ASPD 16 nM
3D3 ASPD 16 nM + ω-conotoxin
3D4 ASPD 16 nM + Ex4
[Ca2+]i
Time (min)
Start
Assay chamber solutions exchanged completely with indicated sample solutions

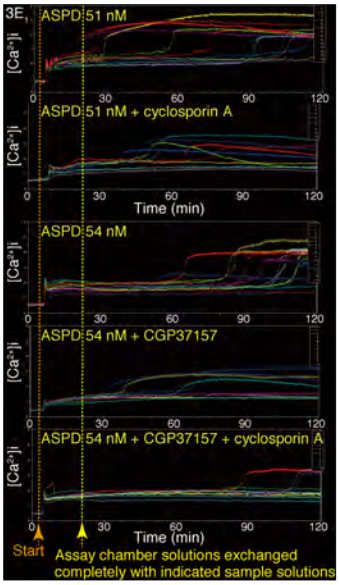
3E1 ASPD 51 nM
ASPD 51 nM + cyclosporin A
ASPD 54 nM
ASPD 54 nM + CGP37157
ASPD 54 nM + CGP37157 + cyclosporin A
[Ca2+]i
Time (min)
Start
Assay chamber solutions exchanged completely with indicated sample solutions

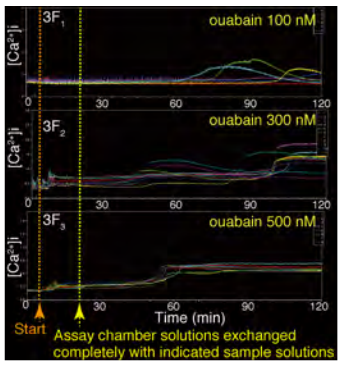
3F1 ouabain 100 nM
3F2 ouabain 300 nM
3F3 ouabain 500 nM
[Ca2+]i
Time (min)
Start
Assay chamber solutions exchanged completely with indicated sample solutions

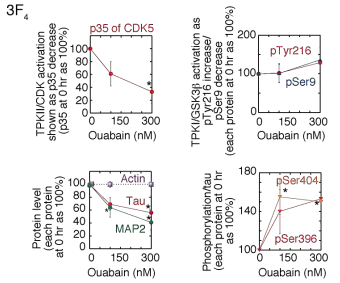
3F4
p35 of CDK5
pTyr216
pSer9
Actin
Tau
MAP2
pSer404
pSer396
Ouabain (nM)

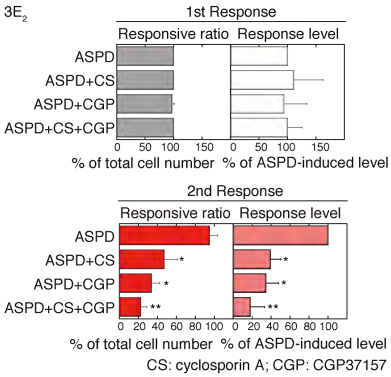
3E2
1st Response
Responsive ratio Response level
ASPD
ASPD+CS
ASPD+CGP
ASPD+CS+CGP
% of total cell number % of ASPD-induced level
2nd Response
Responsive ratio Response level
ASPD
ASPD+CS
ASPD+CGP
ASPD+CS+CGP
% of total cell number % of ASPD-induced level
CS: cyclosporin A; CGP: CGP37157

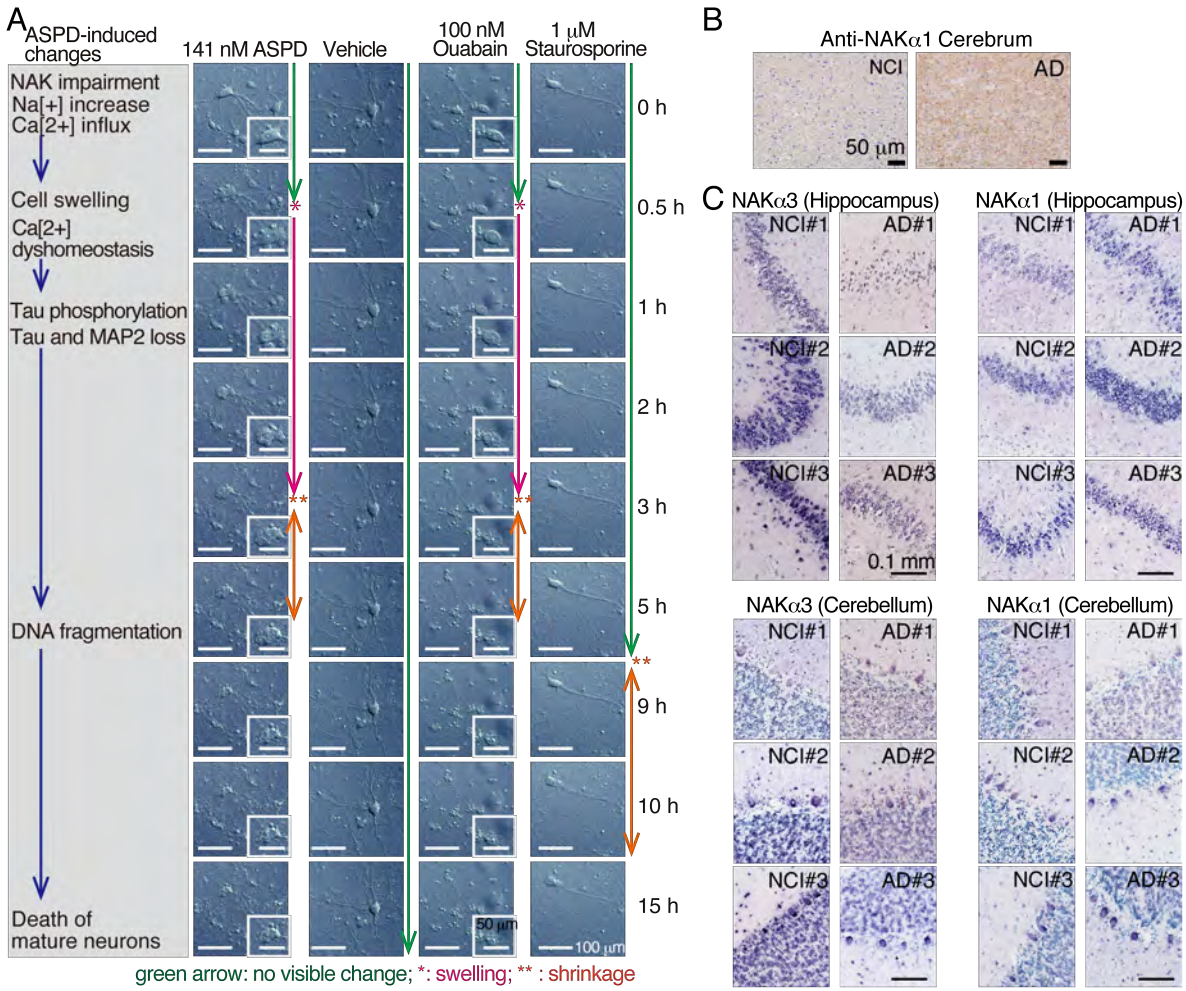
A
ASPD-induced changes
141 nM ASPD
Vehicle
100 nM Ouabain
1 μM Staurosporine
NAK impairment
Na[+] increase
Ca[2+] influx
Cell swelling
Ca[2+] dyshomeostasis
Tau phosphorylation
Tau and MAP2 loss
DNA fragmentation
Death of mature neurons
0 h
0.5 h
1 h
2 h
3 h
5 h
9 h
10 h
15 h
50 μm
100 μm
green arrow: no visible change; *: swelling; ** : shrinkage
B
Anti-NAKα1 Cerebrum
NCI
AD
50 μm
C
NAKα3 (Hippocampus)
NAKα1 (Hippocampus)
NCI#1
AD#1
NCI#2
AD#2
NCI#3
AD#3
0.1 mm
NAKα3 (Cerebellum)
NAKα1 (Cerebellum)

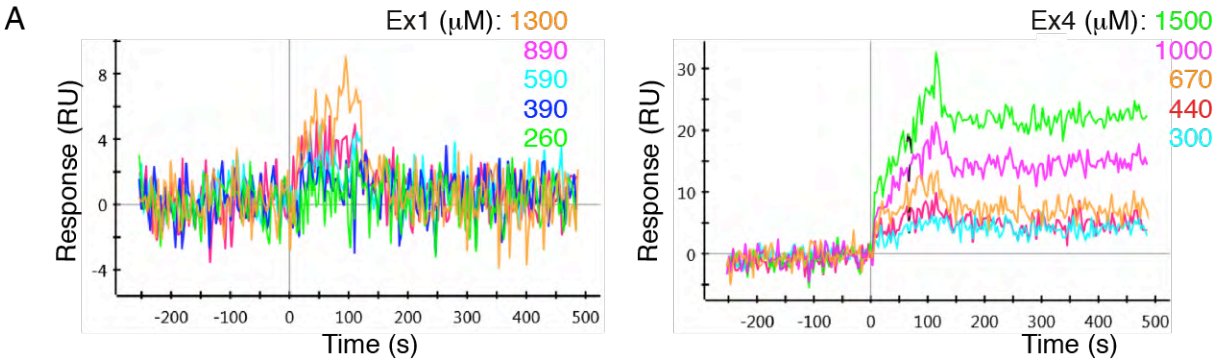
A
Ex1 (μM): 1300
890
590
390
260
Response (RU)
Time (s)
Ex4 (μM): 1500
1000
670
440
300
Response (RU)
Time (s)

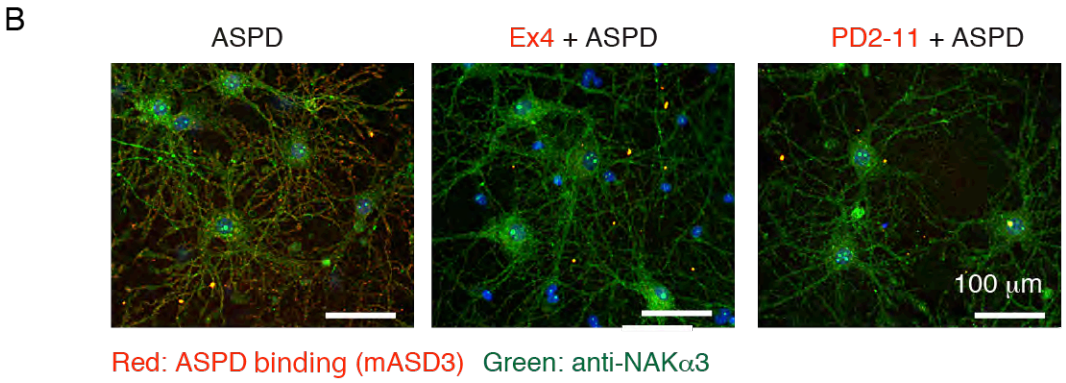
B
ASPD
Ex4 + ASPD
PD2-11 + ASPD
100 μm
Red: ASPD binding (mASD3) Green: anti-NAKα3

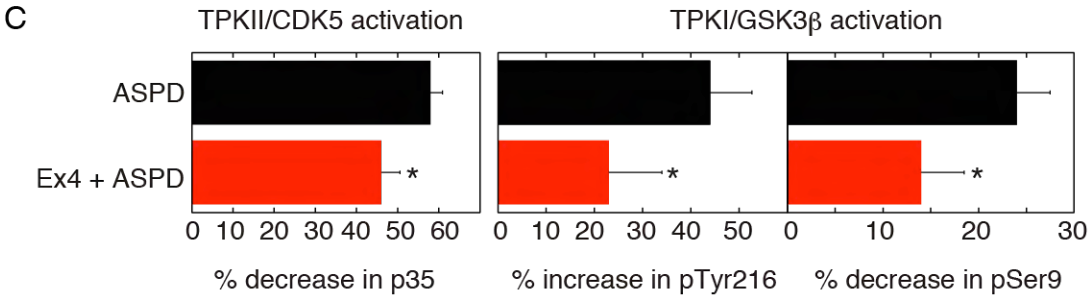
C
TPKII/CDK5 activation
TPKI/GSK3β activation
ASPD
Ex4 + ASPD
% decrease in p35
% increase in pTyr216
% decrease in pSer9

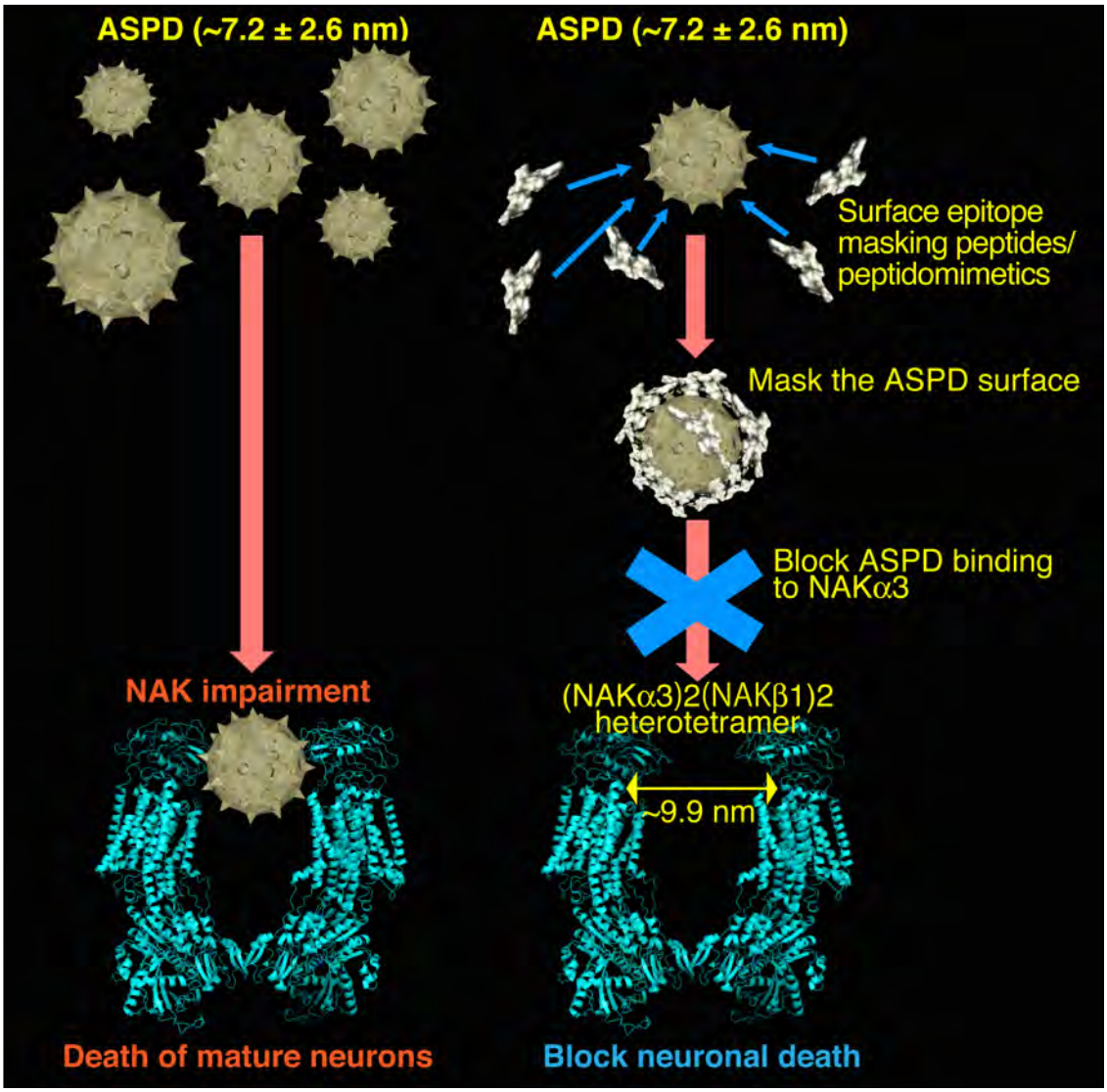
ASPD (~7.2 ± 2.6 nm)
ASPD (~7.2 ± 2.6 nm)
Surface epitope masking peptides/ peptidomimetics
Mask the ASPD surface
Block ASPD binding to NAKα3
NAK impairment
(NAKα3)2(NAKβ1)2 heterotetramer
~9.9 nm
Death of mature neurons
Block neuronal death